Establishment of a HTS amenable platform for the identification of compounds selectively targeting ABCB1 expressing multidrug resistant cancer

Doctoral dissertation

Szilárd Tóth

Molecular Medicine Doctoral School

Semmelweis University

Supervisor: Gergely Szakács, M.D. PhD

Opponents:

Antal István, PhD

Bátori Sándor, PhD

Head of the Final Examination Committee:

Sára Tóth, PhD

Members of the Final Examination Committee:

Tamás Mészáros, PhD

András Szarka, PhD

Budapest

2018.

Table of contents

Abbreviations

1,10-phen	1,10-phenanthroline
2D	2 dimensional
2-DG	2-deoxy-glucose
8-OH-Q	8-hydroxy-quinoline
ABC	ATP-binding casette
ABCB1	ATP-binding cassette sub-family B member 1
ABCC1	ATP-binding cassette sub-family C member 1
ABCG2	ATP-binding cassette sub-family G member 2
ADME-Tox	absorption, distribution, metabolism, excretion, toxicity
AI	activity index
API	active pharmaceutical ingredient
ATCC	American Type Culture Collection
CHO	chinese hamster ovary cell line
CS	collateral sensitivity
CS agent	collateral sensitivity provoking agent
DMEM	Dulbecco Modified Eagle's minimal essential medium
DTP	Developmental Therapeutics Program of NCI
eGFP	enhanced green fluorescent protein
GI_{50}	half maximal (50 %) growth inhibitory concentration
HCS	high content screening
HTS	high throughput screening
IC_{50}	half maximal (50 %) inhibitory concentration
mCh	mCherry
MDR	multidrug resistance; multidrug resistant
MDR1	multidrug resistance 1, gene of P-gp
mOr	mOrange
MTT	3-(4,5-dimethylthiazol-2-yl)-2,5-diphenyltetrazolium bromide

NAI	normalized activity index
NCE	new chemical entities
NCI	National Cancer Institute (of the United States)
P85	block copolymer Pluronic P85
PA	protoapigenone
PAIN	pan assay interference compound
PBS	phosphate buffer saline
P-gp	Permeability-glycoprotein, ABCB1
PSC833	valspodar
QY	quantum yield
RPMI-1640	Roswell Park Memorial Institute-1640; cell culture medium
RR	resistance ratio
SR	selectivity ratio
SRB	sulforhodamine B
TQ	tariquidar
TSC	thiosemicarbazone
VBL	vinblastine
VCR	vincristine

1. Introduction

Cancer is one of the leading causes of death worldwide. According to WHO, 8.8 million people died in various forms of malignant cancer in 2015. Almost half of the cancer deaths are from lung (1.69 million), liver (788 thousand), colorectal (774 thousand), stomach (754 thousand) and breast (571 thousand) cancers. Based on the factsheet of EUCAN, the most frequently diagnosed type in european countries is breast cancer, followed by colon and lung cancer for women (accounting for 48.8 % in total), and prostate cancer, followed by lung and colon cancer for men (accounting for 51.4 % in total) [1]. For females, breast cancer shows the highest death rate, while for males, lung cancer kills the most patients [2]. The mortality rate for all cancers varies from country to country, as a factor of economic level and local health care system. In Europe, based on the data collected from 2011-2013, the highest mortality rate (male and female together) was in Hungary, followed by other central european countries (Figure 1, Appendix 1) [3].

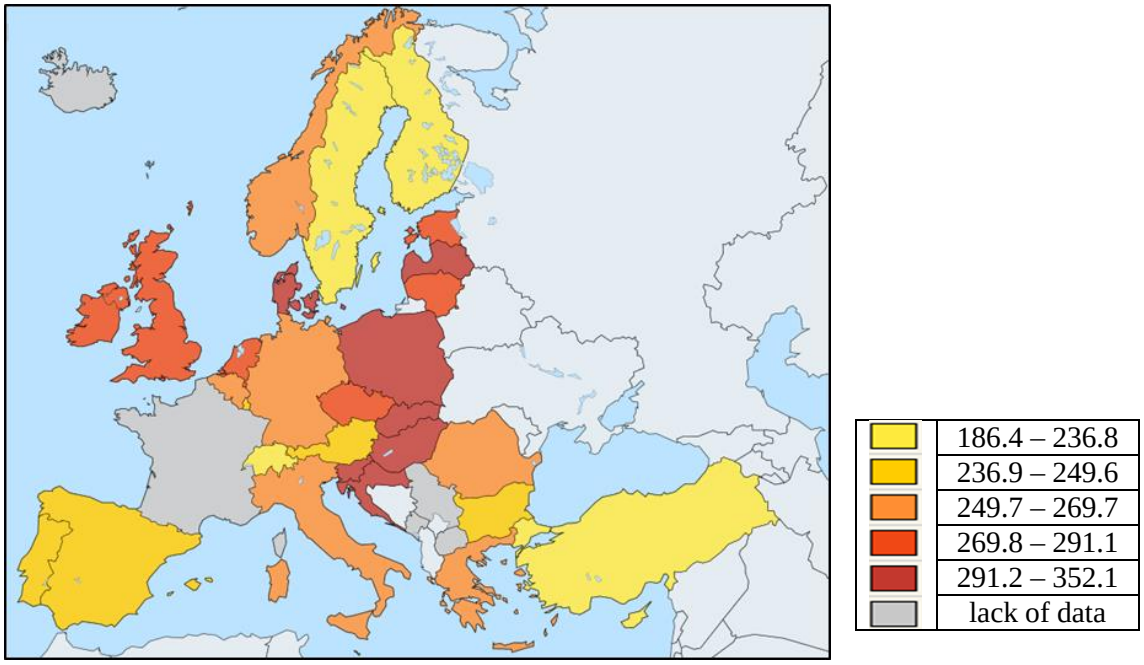

Figure 1. Mortality rate of all cancers per 100 thousand inhabitants in 2013. The highest rate was in Hungary (352.1), and the lowest rate was reported in Turkey (186.4) [3].

Cancer treatment depends on the type and the stage of the malignancy. In most cases surgical resection is needed, which is later combined by chemotherapy or radiation therapy. Another example is neoadjuvant therapy, when the usage of chemotherapeutics

precedes surgery in order to shrink the tumor [4] [5] [6]. Besides conventional therapies, targeted therapies and immunotherapies are emerging treatment possibilities.

In the last decades, survival rates have improved, especially for breast and prostate cancers, or melanoma (Figure 2). Better outcome is due to improvements in all treatment fields. In surgery, novel techniques such as keyhole surgery or lumpectomy allow more precise interventions, and further development is expected by the introduction of the iKnife [7]. Radiotherapy is performed with more focused devices, new drugs were introduced in chemotherapy regimens, and the growing field of biological therapy provides novel, cancer specific approaches (e.g. rituximab for non-Hodgin lymphoma [8], trastuzumab for HER-2 positive breast cancer [9], or combined immunotherapeutic strategies for melanoma using interferon-α, interleukin-2 and immune checkpoint inhibitors [10]). However, there are some malignancies, where only minor improvements were observed. Tumors, such as lung or pancreatic cancers continue to show poor outcome (Figure 2).

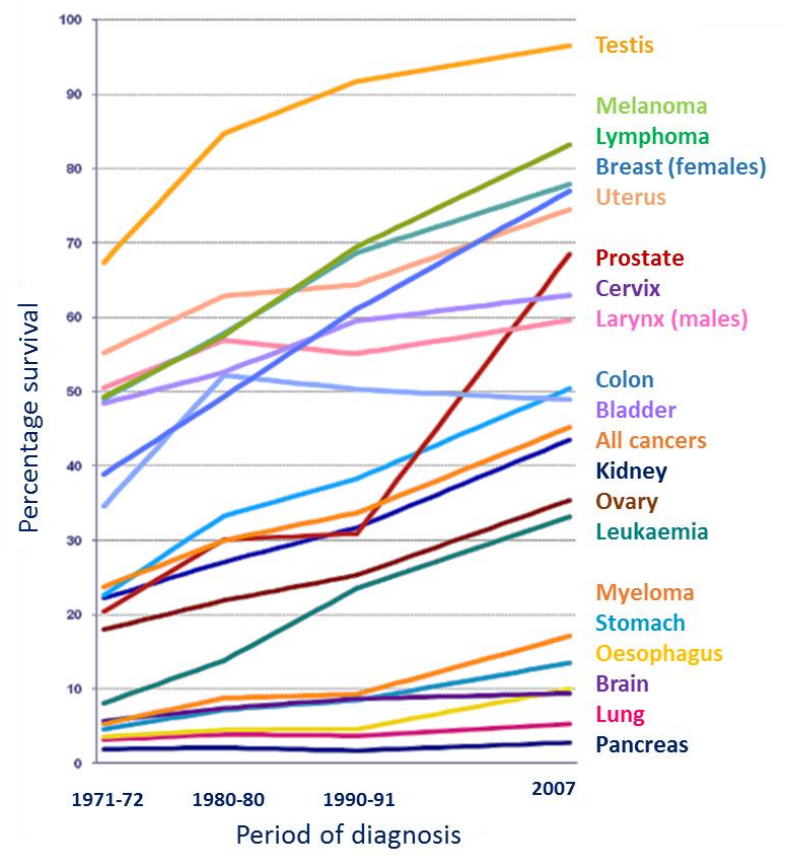

Figure 2. Ten year relative survival (%) of selected cancers for adults in England and Wales. Trends are between 1971-2007 [11].

Treatment failure is often due to the inherent or acquired resistance of the tumors, mediated by the tumor microenviroment (the stroma), or molecular changes, that can occur even in response to treatment, as tumor cells can adapt to various toxic impacts.

1.1. Hallmarks of cancer and therapy resistance

Cancer is a group of diseases consisting of over 100 different conditions. The primary distinction of cancers is based on the tissue of origin (e.g. lung cancer, breast cancer) and the cell type (e.g. carcinomas, sarcomas, adenocarcinomas) [12]. Despite the complexity of the many types of cancers, Hanahan and Weinberg defined the following 6 hallmarks that characterize all cancer types: (1) acquiring autonomous growth signals, (2) evasion of growth inhibitory signals, (3) evasion of apoptotic cell death, (4) unlimited replicative potential, (5) capability to form new blood vessels – angiogenesis – and (6) invasion and metastasis [13]. The original list of hallmarks were later completed with two enabling characteristics. Genome instability and tumor-promoting inflammation provide a permissive environment to acquire the above hallmarks. Reprogramming energy metabolism and avoiding immune destruction were defined as emerging hallmarks, as their importance in carcinogenesis is still under debate [14].

1.1.1. Role of mutations and plasticity of the tumor cells in drug resistance

Although it is not considered as a hallmark, intrinsic or acquired anticancer therapy resistance is frequently observed in all cancer types. The phenomenon of drug resistance occurs when tumor cells become insensitive to treatment. The development of cancer drug resistance is linked to DNA mutations or other metabolic changes including epigenetic events due to the plasticity of cancer cells, since these alterations serve as sources of new phenotypes during tumor progression [15] [16]. The new phenotypes emerge as a consequence of the multiple environmental pressures that compel the malignant cells to continuously change and adapt. In agreement with the Darwinian evolution model, cells, which obtained genetic mutations (or epigenetic changes) that result in growth advantage become predominant compared to neighboring cells. Clones with higher proliferation rate then expand within the tumor. Successive advantageous mutations/alterations lead to waves of clonal expansion, resulting in tumor heterogeneity [17] [18].

The consecutive mutations that accumulate and contribute to carcinogenesis are affecting

mainly proto-oncogenes, tumor supressor genes and DNA repair genes, sometimes called "drivers" of cancer [12]. According to the Cancer Genome Atlas Pan-Cancer effort, where mutation patterns of 3281 tumors from 12 cancer types were thoroughly analyzed, 2 to 6 such driver mutations are sufficient for oncogenesis [19]. The analysis also identified oncogenic mutations that can occur in any type of cancer, such as the mutations of histone modifiers, but reported several tissue specific genetic alterations as well, which affect mostly transcriptional factors and transcriptional regulators. Taken together, mutations and epigenetic plasticity of the malignant cells create a heterogeneous tumor where subclones can have different DNA alterations ranging from point mutations to large chromosomal aberrations (e.g. chromosomal translocations) [20] [21] [22] [23] and abnormal DNA methylation pattern variations [24] [25]. Tumor heterogeneity has a profound clinical impact. Therapy acts as a selective pressure, and in response, the fittest – most resistant – subclones are selected to survive, which manifests in tumor relapse [26] [27].

As an example, 5-fluorouracil (5-FU) resistance of colorectal cancer appears with the recurrence of the tumor that was initially responding well to this chemotherapeutic agent. When mRNAs were extracted from the tumor that already became resistant to 5-FU treatment, high levels of dihydropyrimidine dehydrogenase (DPD) transcripts were found. DPD is responsible for the inactivation of 5-FU before it is converted to its active form (to fluorodeoxyuridine by thymidine phosphorylase) [28]. Moreover, amplification of the TYMS locus (thymidylate synthetase, target of the activated 5-FU) was correlated with poorer survival among patients with advanced, metastatic colorectal cancer, who were treated with 5-FU previously [29] [30] [31].

Resistance derived from tumor heterogeneity is more pronounced when targeted drugs are used, due to the highly specific targeting of certain malignant alterations. As an example, when patients with chronic myelogenous leukemia (CML) are treated with imatinib, kinase-domain mutations commonly emerge, leading to clinical drug resistance and relapse [32]. A study proved that these mutations can already be present in a tumor subpopulation at the time of diagnosis, before imatinib treatment is initiated [33]. Another example is when patients with colorectal cancer are treated with cetuximab and irinotecan, a subpopulation with p.K57T missense mutation in the MAP2K1 gene will likely outgrow in the tumor, which contributes to poor response to therapy [34].

1.1.2. Mechanisms of drug resistance and multidrug resistance (MDR)

The most common mechanisms that confer drug resistance to tumor cells are the (a) increased metabolic degradation of drugs, (b) keeping molecular targets at a low level, (c) increased DNA damage repair, (d) changed apoptotic pathways, (e) mutation in the target protein, (f) trapping drugs into acidic compartments, (g) alterations in the cell cycle and checkpoints and (h) the increased efflux by energy dependent transporters [15] [35]. Besides the above conventional mechanisms, cells can 'escape' from the treatment by epithelial-mesenchymal transition (EMT) [15], and certain micro-RNAs seem to contribute to the emergence of drug resistance as well [36].

Certain mechanisms from the above list can confer resistance to a single agent (the agent with which the treatment was conducted), while other forms provide cross-resistance to additional drugs. If cross-resistance is efficient against structurally unrelated and functionally distinct drugs, the phenotype is termed "multidrug resistance" (MDR) [37]. Overexpression of the ATP-binding cassette efflux transporters (ABC-transporters) in the plasma membrane of the malignant cells is one of the most common and effective mechanisms of MDR. The main ABC-transporters related to multidrug resistance are ABCB1 (P-glycoprotein, P-gp) [38], ABCG2 (BCRP) [39] [40] [41] and ABCC1 (MRP1) [42]. These transporters have broad substrate specificity, they can recognize and extrude a wide range of xenobiotics from the (tumor) cells, keeping low intracellular drug concentrations. Many anticancer therapeutics, either conventional (e.g. vinca-alkaloids) or targeted drugs (e.g. EGFR inhibitors) that are currently in use are subjects of transport by the ABC pumps [37]. The substrate specificity of the 3 main MDR ABC-transporters are partly overlapping, nevertheless when cultured cancer cells are treated with chemotherapeutics, the major mechanism of multidrug resistance is mediated by P-glycoprotein [35]. In addition, when mice bearing *Brca1*- and *p53*-deficient mammary tumors were treated with doxorubicin (a P-gp substrate), resistance frequently occurred and was linked to the overexpression of the P-gp ortholog Mdr1a and/or Mdr1b [43] [44]. P-gp is widely expressed also in many human cancers, including cancers of the gastrointestinal tract (small and large intestine, liver cancer, and pancreatic cancer), cancers of the hematopoietic system (myeloma, lymphoma, leukemia), cancers of the genitourinary system (kidney, ovary, testicle), and childhood cancers (neuroblastoma, fibrosarcoma) [45]. In hematological malignancies, sarcomas, breast cancer and other

solid cancers, the contribution of P-gp to poor chemotherapy response was demonstrated [37]. P-gp mediated (and in general ABC-transporter mediated) MDR is still a serious obstacle in cancer therapy, as during treatment, if the fittest clones, which arise due to the selective pressures are overexpressing P-gp, the tumor will most probably stop responding to P-gp substrate chemotherapeutics.

1.1.3. Physiological role and function of ABCB1

ABC-transporters are transmembrane proteins controlling the passage of their substrates across biological membranes and barriers under normal physiological conditions. Thus, ABC-pumps play a crucial role in the distribution of their endogenous substrates (reviewed in [37]). Moreover, ABC transporters make up a complex cellular defense system responsible for the recognition and removal of environmental toxic agents [46]. Accordingly, ABCB1 [47] and ABCG2 [48] [49] proteins are expressed e.g. in the blood-brain barrier, where they protect the brain from xenobiotics. P-gp is expressed also in the liver, intestine and kidney [45] [50].

P-glycoprotein is a 170,000-dalton molecular weight phosphoglycoprotein comprised of two transmembrane domains (TMD), each containing six transmembrane helices, and two nucleotide binding domains (NBD) [51]. Extrusion of xenobiotics by P-gp from the cell is an energy-dependent action fueled by ATP hydrolysis [52].

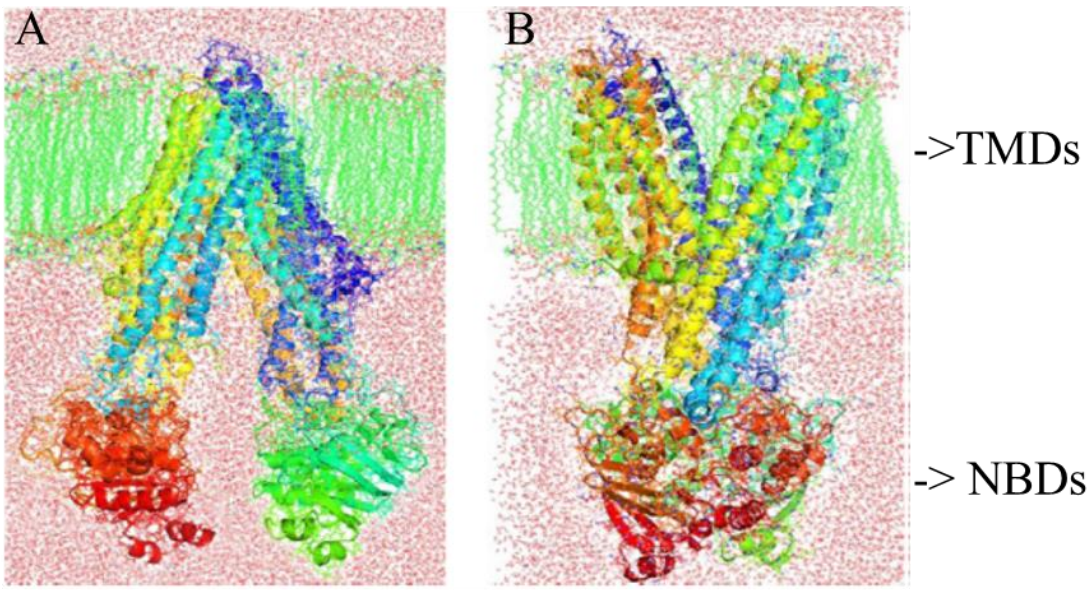

Figure 3. Structure of P-gp, based on molecular dynamics simulation [54]. Green: lipid bilayer, red: aqueous phase. A) Inward-facing state of P-gp. B) outward-facing structure of P-gp.

P-gp in its drug recognition (inward facing) state allows drug binding and asymmetric occlusion of an ATP in each NBD domains. Upon drug and ATP binding, the subsequent hydrolysis of the two ATPs triggers a conformational motion, when the transition of the inward facing state to the outward facing state takes place, resulting in the release of the captured drug into the extracellular space via the pore that is formed by the TMD helices. After drug release, P-gp returns to the inward facing state, and P-gp can start the conformational cycle again [53]. Inward-facing and outward facing states are shown in Figure 3.

1.2. Overcoming MDR by inhibition or evasion of P-gp

In vitro experiments of malignant cells showed that the relative amount of surface P-gp strongly correlates with the degree of drug resistance, and if P-gp is inhibited, MDR cancer cells regain their original sensitivity to the drugs that are subjected to transport [55] [37]. Considering that Mdr1a/b KO mice are viable and fertile [47], it was a reasonable strategy to inhibit the function of P-gp *in vivo*, and co-administer chemotherapeutics with the inhibitor to reverse MDR in tumor cells [56]. Unfortunately, the *in vitro* effectiveness of inhibitors has not translated to the clinic. Clinical trials were conducted with 3 generations of P-gp inhibitors (e.g. the first generation inhibitors cyclosporin or verapamil, PSC833 from the second generation, or tariquidar as a third generation inhibitor), but no remarkable benefit was reported, and the reasons for failure were assosiated to side effects, undesirable pharmacokinetic interactions or simply to ineffectiveness [37] [57]. Thus, novel approaches are needed to fight against MDR in cancer, which do not interfere with the role of P-gp in pharmacological barriers.

Presently, drug candidates are commonly tested to determine if there is an interaction with ABC transporters. One strategy to improve therapy response and avoid transporter mediated MDR is to design new classes of anticancer agents that simply bypass the multidrug transporters [58]. This can be achieved by modifying already existing therapeutics in a way that they are no longer recognized by the transporters (e.g. design of daunomycin [59] or camptothecin [60] analogues), or by discovering novel agents that lack MDR transporter interaction. Another advance is the encapsulation of drugs in nanoparticles or liposomes, preferably designed for targeted delivery [58]. Liposomal formulations of MDR substrate drugs have a greater potential against MDR cancer, e.g. efflux pump based MDR in allograft bearing mice occurred less frequently, and with a

delayed onset– as it was demonstrated by our research group – when the effect of doxorubicin and liposomal doxorubicin treatment was compared [61]. Moreover, both overall and relapse free survival were increased remarkably when the liposomal formulation was administered. In an earlier study, conducted by Krishna and Mayer [62], when liposomal doxorubicin and the second generation P-gp inhibitor PSC833 were co-administered in P388 ascites tumor bearing mice, the tumor volume was reduced more efficiently compared to when the combination of PSC833 and free doxorubicin was used, albeit the tumor did not diminish completely.

1.3. Exploiting the phenomenon of collateral sensitivity

There is an alternative strategy against drug resistant cancer, which is substantially different from the efforts to overcome MDR by blocking transporter function, or to avoid drug extrusion by designing molecules which are not recognized by the ABC-pumps. The novel approach relies on the phenomenon called collateral sensitivity (CS), which was originally observed and described as an interesting anomaly by Szybalski and Bryson, who found compounds that provoked induced sensitivity to resistant bacteria strains [63]. They hypothesized that during isolation of strains possessing resistance to one antibacterial substance, associated characters producing higher sensitivity (hypersensitivity) to another agent might be selected. As a conclusion, they proposed to apply such compounds as selective agents alone, or in combination with other drugs to prevent the emergence of bacterial resistance. The hypothesis they claimed became well accepted, and the definition of collateral sensitivity was soon adapted for non-bacterial cases. CS was observed in insects (since 1950s, termed enhanced susceptibility [64] [65]), yeast [66] and protozoa [67] (both since the 1970s) or weeds (first report from 1987 [68]). In cancer, the first report of collateral sensitivity is from 1951 [69], when 6-mercaptopurine resistant mouse leukemic cells were noticed to be more sensitive to methotrexate than the parental line.

Collateral sensitivity is a type of synthetic lethality, which in MDR tumor cells is linked to the cellular alterations resulting from the adaptation to cytotoxic/cytostatic drugs, and associated with vulnerabilities that were created concurrently to drug selection [70]. Accordingly, collateral sensitivity of MDR tumor cells can be exploited therapeutically in such a strategy, where multidrug resistance is considered as a trait (similarly to the

hallmarks of cancer) that might be targeted by new drugs. Theoretically, administration of collateral sensitivity provoking compounds have the potential to prevent MDR tumor formation by the preferential killing of MDR cells in a heterogeneous tumor population [71].

1.3.1. Experimental evaluation of collateral sensitivity of P-gp expressing MDR cancer cells

Several compounds demonstrating preferential hypertoxicity to P-gp positive cell lines were listed in a recent review [70], proving that application of drugs eliciting collateral sensitivity can be effective also against MDR cancer cells with pathological P-gp overexpression.

The compounds were identified in various *in vitro* cytotoxicity experiments, which served as the basis of determining their potency. A common way to evaluate the extent of collateral sensitivity is to calculate the ratio of cytotoxicity measured against the parental, P-gp negative cell line divided by the cytotoxicity measured against its multidrug resistant, P-gp positive derivative [71]. The cytotoxicity of a compound is expressed as the half-maximal inhibitory concentration (IC_{50}) value, and their ratio is termed selectivity ratio (SR) [72]. If SR > 1, the compound is killing the MDR cells preferably over the parental line, while a SR < 1 indicates that the tested compound exerts greater toxicity towards the parental cell line, e.g. because the test compound is a P-gp substrate. Correspondingly, higher SRs refer to more pronounced collateral sensitivity. However, selectivity ratio is not the only factor of a compound's potency, the cytotoxicity (IC_{50}) value is also relevant, as it can range from nanomolar to millimolar concentrations. Moreover, the P-gp expressing MDR cells can be targeted via non-transporter related and also by P-gp mediated mechanisms. Therefore the contribution of P-gp in CS has to be clarified. As explained above, drug efflux by P-gp is a frequent form of MDR, thus P-gp mediated CS might be preferable over mechanisms related to cell line specific alterations evolved during drug selection of the cell line. There are 3 common ways to address the observed hypertoxicity of an MDR targeting drug candidate to P-gp. First, by testing the compound against additional parental and P-gp positive MDR cell line pairs, the robustness of selectivity can be investigated, and collateral sensitivity has to appear across all cell pairs, if P-gp is involved. Additionally, if a compound's hypertoxicity towards P-gp expressing MDR cells is significantly abrogated when an ABCB1 inhibitor is co-

incubated in a non-toxic concentration, the observed CS is P-gp dependent (concurrently the cytotoxicity towards the parental cell line has to be unaffected). Abrogation of selectivity may be achieved also by siRNA driven P-gp knockdown [71], or by the use of a tetracycline controlled promoter, where the presence of the antibiotic suppresses the transcription of P-gp, and P-gp mediated CS of the MDR line is observed only when tetracycline is absent [73]. The third way is to apply *MDR1*-transfected cell lines, which are created from parental lines with *MDR1* gene insertion. The *MDR1* transfected resistant cell lines, in contrast to P-gp expressing MDR cell lines created with *in vitro* selection of parental lines in chemotherapeutics, lack other cellular changes that might have occurred during drug selection, thus cell line specificity of the experienced selective toxicity is minimal [71].

1.3.2. Examples of collateral sensitivity provoking agents from the literature

P-gp expressing MDR cancer cells are indeed targetable [70] [72]. Most of the collateral sensitivity provoking substances (CS agents) were found serendipitously, when the original aim of the research teams was to investigate cross resistance, or simply the lack of transporter mediated resistance of anticancer substances. In several cases, the observed hypersensitivity of MDR cells could be linked to certain cellular changes that cells acquired during drug selection in parallel to P-gp overexpression.

A good example for this kind of cell line specific hypertoxicity is the case of 2-deoxy-D-glucose (2-DG), which was found to kill the vinblastine resistant and P-gp overexpressing cell line KB-V1 more effectively than its parental (KB-3-1 cervix carcinoma) form [74]. 2-DG provoked collateral sensitivity in 2 other KB-3-1 derived MDR cell lines, the colchicine selected KB-C1 and doxorubicin selected KB-D1, but the extent of hypertoxicity was not proportional to the level of multidrug resistance. Selective toxicity of 2-DG was first associated to the decreased expression of GLUT-1 transporter found in MDR cells, but finally it was linked to altered apoptotic pathway of resistant lines. Another compound that originally was believed to be an MDR-selective agent is the natural product austocystin D [75]. A later study by Marks et al. has shown that austocystin D directly interacts with P-gp as a low affinity substrate, although this interaction is not responsible for its selective toxicity towards MDR cells [76]. As they explain, the observed hypertoxicity is linked to the elevated levels of the Cytochrome P450 enzyme, which activates and turns austocystin D into a DNA damaging agent upon

entering the cell. Thus, certain P-gp expressing MDR cells, thanks to the potential coordinated upregulation of CYP enzymes and ABC-transporters are more susceptible to austocystin D. 2-DG and austocystin D, albeit killed the investigated MDR cells preferably, are not ideal drug candidates, because their selective manner is tied to a special cellular change, which is not expected to represent resistant tumors in general.

In contrast, there are other compounds that were published to selectively kill P-gp overexpressing cells, where the selective action was mediated by the transporter. The hypertoxicity of verapamil towards MDR cells was widely studied in Chinese hamster ovary (CHO) cells. MDR cells derived either from E29 or from AuxB1 parental CHO cell lines become sensitive to verapamil after selection in vincristine or colchicine, and sensitivity was linked to the overexpression of hamster P-gp [77] [78] [79]. By using the same AuxB1 and its colchicine resistant derivative (CH^RC5) hamster cell lines, Laberge et al. proved the MDR-selective toxicity of verapamil, and discovered the MDR-selective toxicity of the electron transport chain (ETC) complex I inhibitor rotenone [80]. When verapamil and rotenone were tested in the presence of PSC833 (a 2nd generation P-gp inhibitor), the preferential toxicity against MDR cells was completely abrogated. Besides hamster cell lines, verapamil was also studied in a P-gp expressing human MDR cell line K562/ADR, but it showed only a slight, 1.78 fold selectivity compared to parental K562 [81]. Two additional compounds, TritonX-100 [82] and reversin121 [83] were identified and published as MDR-selective agents against MDR CHO cells. While the hypertoxicity of TritonX-100 was demonstrated only against MDR hamster cell lines, and was found to be equally toxic to LR73 and the mouse mdr1a transfected LR73/1A CHO cell lines, reversin121 killed the human KB-V1 cell line preferably over KB-3-1.

In search for novel anticancer compounds, Nakagawa-Goto et al. tested several unique flavonoids with desmosdumotin B skeleton, and reported a striking collateral sensitivity towards the human MDR cell line KB-VIN, which is a vincristine selected derivative of the parental KB nasopharyngeal carcinoma line [84]. The most potent compounds were 6,8,8-triethyldesmosdumotin B and its 4'-Me and 4'-Et substituents, showing 222-, 460- and 320-fold selectivity, respectively. The MDR selective effect of desmosdumotins was partly sensitive to P-gp inhibition by verapamil in KB-VIN cells (however data were not shown for KB). In a later work the same group observed selective toxicity for the 3 most potent compounds also against the vincristine selected Hep3B-VIN cells over Hep3B

[85]. Although the difference of sensitivity between parental and MDR cell lines were much smaller, P-gp knockdown with siRNA resulted in the loss of cell proliferation blockage by the flavonoids [86]. Despite the observed P-gp mediated hypertoxicity of desmosdumotin B flavonoids towards KB-VIN and Hep3B-VIN, the authors noted that the hyperactivity of the synthesized analogues was not general against every MDR cell line, but they refer only to their unpublished data, without mentioning the name of the cell lines [84]. According to the authors the activity of these compounds is linked to single-nucleotide polymorphisms (SNPs) of the *MDR1* gene, of which some can radically affect P-gp conformation, thus changing its interaction with the drugs [87].

In addition to small molecules, the block copolymer Pluronic P85 (P85) was also reported to act selectively against MDR cell lines, and the selective cell damaging effect was attributed to the function of P-gp [88] [89] [90]. P85 was proposed to be utilized to inhibit P-gp and restore the accumulation of otherwise P-gp substrate therapeutics in MDR cancer cells, but no convincing *in vitro* cytotoxicity tests were performed to clarify if P85 alone is a cytotoxic MDR-selective agent.

The above mentioned compounds can plausibly kill P-gp overexpressing cancer cells with a preference over their parental counterparts. However, in many studies the lack of systematic investigation of P-gp dependency of the observed collateral sensitivity leaves doubts about the role of the transporter, thus cell line specificity of the MDR-selective candidate compounds has to be delineated in later studies.

1.3.3. Systematic study revealed MDR-selective compounds from the NCI-60 Cell Line Screening assay database

The discovery that radically changed and boosted the research of anticancer collateral sensitivity, and when the list of known P-gp potentiated MDR-selective compounds was extended is tied to a systematic study, which originally meant to investigate ABC-transporter mediated cross-resistance, and intended to predict substrates of ABC-transporters [73]. The study used a publicly available database of the National Cancer Institute of the National Institute of Health (NCI of the NIH) that was created by the Developmental Therapeutics Program (DTP). Since its inception in 1955, DTP has supported the discovery of more than 40 US-licensed anti-cancer agents by providing services and resources to the academic and private-sector research communities

worldwide [91]. The drug discovery and development services include *in vitro* and *in vivo* screens. The so-called NCI-60 Human Tumor Cell Line Screen was initiated in 1990, and utilized 60 different human tumor cell lines to identify and characterize novel compounds with growth inhibitory effect or tumor cell line killing potency [92]. In exchange for the service, DTP collected and stored the dose response data against the 60 cell lines in a publicly available database. In 2016, the NCI announced to close the NCI-60 screen in favor of launching a new repository of cancer models that are derived from fresh patient tumor samples with known clinical history [93]. The latest database from 2016 includes the toxicity values of more than 50,000 compounds [94]. One of the great advantages of this database is that the 60 different human tumor cell lines (representing leukemia, melanoma and cancers of the lung, colon, brain, ovary, breast, prostate, and kidney cancers) are thoroughly characterized, thus toxicity patterns can be recognized and linked to specific alterations occurring in cancer types [95], such as the alterations of the quantity or quality of resistance factors.

The referred systematic study of Szakács et al. [73] analyzed a 1429 compound set whose screening data in the DTP database met a certain quality control criteria (described in [96]), including 118 compounds with known mechanism of action. To identify the compounds of the 1429 set whose toxicity was influenced by the presence of ABC-transporters, mRNA levels of all the 48 human ABC-transporters were measured and correlated to the toxicity patterns disclosed by DTP. The toxicity data is stored as growth inhibition values, thus ABC-substrates showed strong negative correlation (the higher level of mRNA of a transporter the lower grade of growth inhibition). Interestingly, when ABCB1 mRNA levels were correlated to the growth inhibition data, several compounds gave strong positive correlation coefficients, suggesting that besides conferring MDR, ABCB1 is capable to potentiate the toxicity of certain molecules. To test this paradoxical observation, which seemed to be a statistically insignificant event, the authors performed a Benjamini-Hochberg procedure [97], which estimated that only 30% of the top scoring hits were false positives, and 70 % of the compounds with strong positive coefficients are likely to be abundant of valid correlations. After consecutive *in silico* filtering and *in vitro* tests, the first compound that was validated to exert hypertoxicity in various MDR model systems was the thiosemicarbazone NSC73306 (Figure 4). Increased toxicity of NSC73306 was only observed when functional P-gp was expressed in the plasma

membrane, and when P-gp was blocked by inhibitors, hypersensitivity of MDR cells could be abrogated [73]. In a follow up study, the entire DTP dataset (approx. 43,000 substances) was systematically analyzed to find more MDR-selective compounds [98]. As a result, dozens of compounds showing collateral sensitivity against KB-V1 cell line (over KB-3-1) were successfully identified, of which 4 structurally distinct compounds were further investigated against additional cell lines pairs, and were found to exert robust P-gp potentiated hypertoxicity. The new MDR-selective compounds were NSC10580, NSC168468, NSC292408 and NSC713048 (Figure 4).

As thiosemicarbazones (TSCs) are known to possess a diverse biological activity profile, including anticancer and antiviral activity, as reviewed recently in [99], the identification of the P-gp potentiated MDR-selectivity exerted by NSC73306 inspired further investigations, and new analogues were synthesized and tested. Hall and co-workers disclosed a basic structure-activity relationship (SAR) study in 2 subsequent articles [100] [101], where residues and moieties, which increased/decreased the magnitude of the P-gp mediated hypertoxicity of NSC73306 were identified. The most effective, improved TSC was ‘compound 32’ (Figure 4) showing an increased, almost 3 times higher selective toxicity compared to NSC73306.

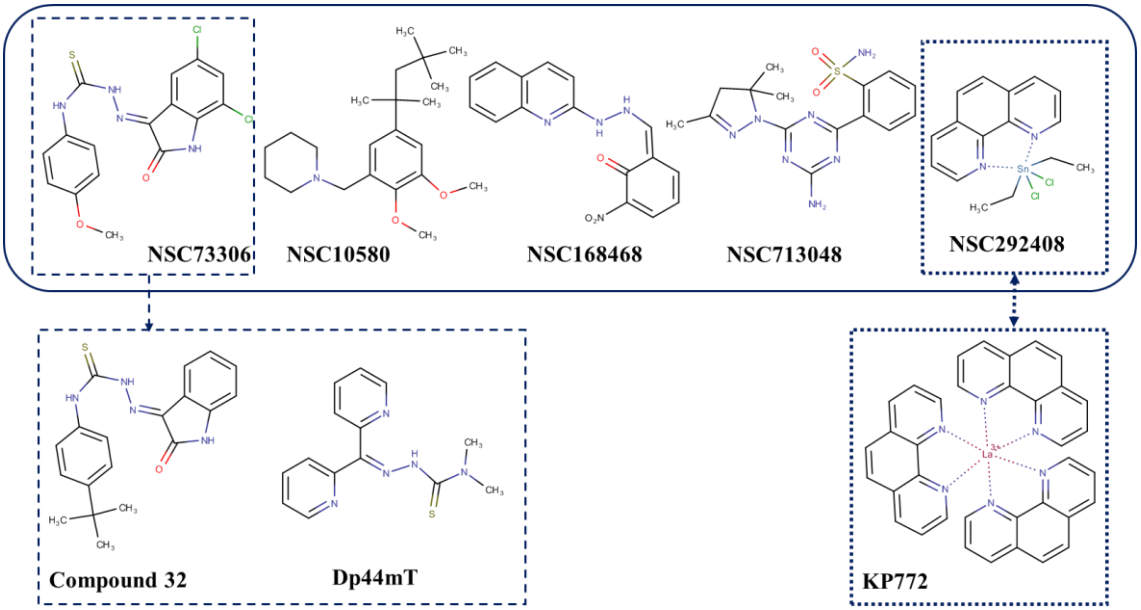

Figure 4. Verified MDR-selective compounds NSC73306, NSC10580, NSC168468, NSC713048 and NSC292408, identified by the systematic datamining approach. Compound 32 [101] and Dp44mT are analogues of NSC73306 (TSCs), and KP772 (1,10-phenanthroline lanthanum complex) is the analogue of NSC292408.

A further example of the potential of the TSC scaffold against P-gp overexpressing MDR cells is Dp44mT, described by Richardson et al., which mediated MDR-selective toxicity against the P-gp positive KB-V1 cell line [102]. As subsequent research demonstrated, Dp44mT showed a P-gp inhibitor (Elacridar and PSC833) sensitive hypertoxicity to KB-V1, and also to the P-gp expressing MDR cell lines HCT-15, DMS-53 and the paclitaxel resistant 2008/P200A [103]. The collateral sensitivity elicited by Dp44mT seemed to be P-gp dependent. However, no *MDR1* transfected cell lines were involved in the studies, thus the preferential MDR cell killing effect of Dp44mT cannot exclusively linked to the function of P-gp until further experiments are performed.

TSCs are not the only compounds that were identified in several independent laboratories as potential MDR-selective agents. In 2007, Heffeter and colleagues identified the preferential and P-gp mediated hypertoxicity of KP772 towards MDR cells [104]. KP772 is a complex of lanthanum and 1,10-phenanthroline (1,10-phen), which was capable to exploit the vulnerability derived from the maintenance of functional P-gp overexpression in the plasma membrane of the colchicine resistant KB-C1 cell line, and killed it with a small but significant preference over the parental KB-3-1 line. KP772 is very similar to a tin complex of 1,10-phen called NSC292408 (Figure 4), identified in the above referred systematic study as an MDR-selective compound. Moreover, as KP772 was submitted to the drug screening repository of DTP (renamed as NSC632737), it was identified in the same systematic study as a putative MDR-selective analogue of NSC292408 [98], supporting the relevance of 1,10-phenanthroline metal complexes.

The list of the compounds eliciting collateral sensitivity against P-gp expressing MDR cells is longer and more diverse, here I only introduced examples that were relevant milestones (and that are related to the present PhD thesis). The observed collateral sensitivity was tested in different ways for each compound. In some of the presented studies, the role of P-gp in the preferential toxicity was not properly delineated, and still remains to be elucidated. The reason is partly due to the fact that collateral sensitivity provoking compounds were identified only by retrospective observations in experiments conducted with drug selected cell lines, which possibly harbor other alterations besides P-gp overexpression. To overcome the problem of cancer cell specific activity, systematic studies are preferred, as seen in the two consecutive studies of Szakács et al. [73] [98]. To identify further, potent MDR-selective agents, well-designed high-throughput

screening of compound libraries against parental and MDR cell line pairs would be highly beneficial. Identification of novel structures and subsequent lead optimization for better candidates is still an important task.

1.4. In vitro cytotoxicity assays and HTS in drug development

1.4.1. In vitro cytotoxicity assays to identify MDR-selective compounds

In general, when the target of interest is a membrane transporter, membrane receptor, nuclear receptor or ion channel, cell-based assays are applied [105] [106]. In accordance, ABCB1-potentiated MDR-selective compounds reported in the literature so far have been identified and validated also by comparing their growth inhibitory potential against parental and MDR cell lines. This so called phenotype-based approach is required, as the exact targets of MDR-selective compounds are not known, only the function of P-gp is proven to be responsible for the observed effect (phenotype- versus target-based approaches are explained later in 1.4.2.). *In vivo* effects of a test compound can be predicted based on *in vitro* cytotoxicity assays. Thus, the cell-based approach is an important and integral step in drug discovery both for academic research and for the pharmaceutical industry. Validated compounds can be ranked based on their toxicity and/or MDR-selectivity, keeping in mind that the *in vivo*/clinical efficacy depends also on the 'drug-likeness' of the compounds [107].

There are general requirements for cytotoxicity assays. The established assay has to be pharmacologically relevant, which means, it has to be capable of identifying compounds that provoke the desired effect. It has to be reproducible across assay plates or across testing days. The assay must be robust: the quality of the assay has to be uninfluenced by the variability derived from assay methodology or perturbation introduced by the instruments. It is also important that solvents should not interfere with the assay output [108] [109]. Cost-effectiveness and safety (and the related waste management) are also taken into consideration during planning larger experiments [110].

An additional relevant feature of a cytotoxicity assay in general if it is 'robot friendly' [111]. When larger compound libraries are intended to be tested in a relatively short time, automated liquid handling is beneficial, and 384- or 1536-well microplates are preferred. Thus, the assay has to be suitable for the scale down of the reaction volume to 384- or 1536-well formats without detrimental effects on the above mentioned properties, and the statistical significance of the results.

1.4.2. Main principles of high-throughput cytotoxicity screening

The main goal of high throughput screening (HTS) technique is to accelerate drug discovery by screening large compound libraries. HTS originates from the 1980s when automation, preparative chemistry, analytics and overall compound management reached a certain technical level allowing robust screening campaigns of good quality compound libraries [112]. Nowadays, the number of compounds tested in HTS campaigns are usually narrowed down with cheminformatics prior to in vitro tests. The *in silico* filtering step can be applied to remove problematic functionalities, to predict solubility and ADME-Tox properties, or to run uniqueness analysis if intellectual property issues have to be considered [107] [113].

Today HTS is a mature and validated approach to identify the chemical starting points. There are 2 main screening types, phenotypic and target-based approaches (Figure 5).

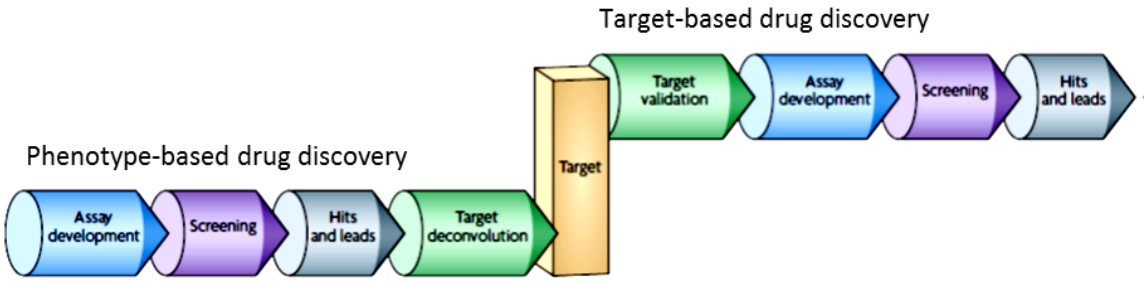

Figure 5. Flow chart of phenotype-based and target-based drug discovery [116]. The aim of early phase drug discovery is to identify the target and the lead molecules. In the phenotype-based approach, lead molecules are obtained first, followed by target deconvolution to identify the molecular targets that underlie the observed phenotypic effects. In the target-based approach, molecular targets are identified and validated before lead discovery starts.

Analysis of 259 new FDA approved drugs from 1999 to 2008 suggested that phenotypic screening strategies were more productive in the discovery of first-in-class small-molecule drugs [114]. However, another analysis using 113 first-in-class drugs, which were FDA approved between 1999 and 2013, reported that target-based approaches yielded more drugs [115]. The apparent contradiction, as it is explained in the latter article, is partly due to the different categorization of certain screens, and the conclusion could be biased also by the chosen drug sets, e.g. the second analysis contains many kinase inhibitors, which were typically discovered by target based approaches. Whichever

article is closer to the answer, both screening types are important and contribute to the discovery of new therapeutics.

Selection of compounds for HTS campaigns should be well designed. Based on the source, chemical libraries can consist of natural products, semi-synthetic and synthetic compounds. If there is no known structure preference before the compound screening, researchers tend to use diversity sets with a high variety of chemical scaffolds and structures. Fragment library is used to determine biologically active compound fragments that can be fused to obtain more effective compounds (thus, second round of screening is often needed with the compounds synthesized as the combinations of the fragments). If there is already a promising chemotype, a focused library can be designed, that is well suitable also for SAR purposes and lead optimization. Historically, and for practical reasons, a compound library can be also 'off-the-shelf' relating to compounds that are already existing active pharmaceutical ingredients (APIs), thus compound synthesis is not necessary, and repositioning is possible [113].

There are numerous therapeutics in use that were identified through HTS. Tyrosine kinase inhibitors (e.g. gefitinib, erlotinib, sorafenib, dasatinib or lapatinib) are common examples, HTS was run in the 1990s and it took approx. 10 years for each drug to obtain FDA approval [117].

1.4.3. Role of reagent-based cytotoxicity assays in HTS

There are a plenty of reagent-based methods to determine the cytotoxicity (growth inhibition) of a compound in a 96-well plate format. However, only a part of these are sufficiently sensitive and applicable in HTS [118]. In the practice, avoiding the usage of radioactively labelled materials is highly preferred due to the extra safety risks and disposal costs. Furthermore, the simple 'mix and measure' liquid handling principle is preferred, while filtration, separation and washing steps are to be avoided, as they are time consuming and difficult to automate [119]. Accordingly, cell component staining dyes, such as crystal violet or sulphorhodamine B (SRB) [120] are not favorable and limited to manual or semiautomatic screening due to the multiple washing steps and volatile liquid pipetting in their protocols. Similarly, the conventional MTT assay [121] that is probably the most broadly used viability assay, can be only augmented by automation with inevitable manual steps. Nevertheless, there are examples, when these

cytotoxicity assays were utilized in compound screening, for instance the NCI-60 Human Cancer Cell Line Screen (see in 1.3.3.) used the SRB assay for the identification of anticancer compounds [122].

The need for HTS facilitated the development of less laborious reagent based assays with minimized liquid handling and incubation time. For such purposes, viability reagents (measuring the activity that is attributable to cellular maintenance) proved to be the most convenient. The MTT analogue MTS [123] provides an absorbance-based assay and indicates the mitochondrial reductive capacity of the cells, as the tetrazolium salt reagent is converted to a light absorbing formazan by living cells. Alamar Blue [124] is another popular viability reagent, offering fluorescent read-out. Its fluorophore called resazurin is converted to the highly fluorescent resorufin, mostly through mitochondrial reductases, similarly to MTT. Another common technique is the bioluminescent detection of ATP using the firefly luciferase enzyme [125], which provides a sensitive way of live cell (cellular energy) measurement [110] [111]. Although all these assays are assessing cell viability, they have relevant differences, which has to be considered in cytotoxicity testing.

If reagent conversion is low (due to the small amount of viable cells), absorbance-based measurements are inherently less sensitive than the fluorescence- or luminescence-based measurements. This is because absorbance is the difference between the intensities of the emitted light and the light passing through the sample, which may be both very strong for the low concentration reagent sample and also for the control (no reagent) sample, while the emitted light – derived either from fluorescence or luminescence – can be distinguished easier from background by the detector even if the signal (reagent concentration) is low [126]. Another difference between the assays is in their deteriorative effect to cells. ATP quantification involves lysis of the cells with detergents, thus it is destructive and is considered as a typical end point assay. In contrast, MTS has minor toxicity on the cells, while resazurin based assays are not considered cytotoxic, and cells might be used later for additional measurements [110] [111]. However, longer exposure to Alamar Blue assay can hinder cell growth, as it was shown for the cisplatin resistant A2780 ovarian carcinoma cell line [127].

1.4.4. Examples of novel, fluorescent protein based cytotoxicity assays

The right choice of the in vitro screening assay is of paramount importance in the drug-discovery process. Reagent-based assays are popular and commonly used in research, as they are well characterized, and protocols are available and easy. However, the attractiveness of reagent-free and label-free approaches, and the technical improvement of spectrophotometers and fluorescence imaging created the possibility to quantify cytotoxicity in novel ways. Also, techniques that provide more information are preferred (e.g. high content screening) [109]. One of the novel approaches to measure cell mass is to exploit the light emitting nature of fluorescent proteins. Gene constructs of the fluorescent proteins can be inserted to host cells, allowing the establishment of fluorescent cell lines. Examples of fluorescent protein based, non-conventional cytotoxicity measurements are demonstrated in this chapter.

In a study by Steff et al. in 2001 [128] eGFP-expressing mammalian cell lines were created and cytotoxicity was determined based on the decay of the eGFP signal by flow cytometer and also by fluorescent microplate reading, as cell death was accompanied with degradation of the fluorescent protein. In the same year, a more comprehensive study was carried out. Torrance et al. [129] used 2 isogenic DLD-1 cell lines (of which one cell line had a mutant K-Ras allele) transfected with either YFP or BFP, co-cultured them, and followed their growth for 6 days by a microplate reader via daily fluorescent intensity detections. They screened the effect for the growth curves of almost 30,000 compounds, and identified a lead compound against mutant K-Ras cell line, then confirmed its effect in a xenograft tumor model. High content screening (HCS) devices are also capable to count fluorescent protein expressing cells. In 2008 Rosado et al. [130] transfected two immortalized lymphoblastic murine cell line variants with either eCFP or eYFP, co-cultured them, and tested a dozen of molecules to find selective Akt signaling inhibitors. The measurement of differential cell survival was performed by an automated high-content microscopy system. In 2011 another dual-fluorescent based HCS study was performed, 3119 chemicals were screened against ovarian cancer cell lines [131]. One cell line of a pair was marked only with eGFP whilst the other was co-transfected with mCherry and a truncated form of the MUC16 tumor marker. After compound incubation, nucleus of the cells were stained with Hoechst, then plates were imaged and analyzed by a cellular imaging system to find MUC16 selective agents.

In 2009, Brimacombe et al. [132] set up a dual-fluorescent system for probing multidrug resistance in cancer. They used the OVCAR-8 (parental) and NCI/ADR-RES (MDR phenotype) cell line pair from the NCI-60 cell panel, transfected with DsRed2 and eGFP, respectively. To avoid the extra nucleus staining steps, required for image based evaluations, co-cultured cells were investigated with a fluorescent laser scanning microplate cytometer, and evaluation was based on eGFP and DsRed2 intensities only. The same type of device was used in 2015 in the study of Kenny et al. [133] to screen the Prestwick Chemical Library (1140 compounds) and the Library of Pharmacologically Active Compounds (LOPAC^{1280}) to identify drugs preventing adhesion, invasion and growth of ovarium carcinoma cell lines. Tumor cells expressing eGFP were seeded (simultaneously with test compounds) in a well where a multilayered culture containing primary human fibroblasts, mesothelial cells and extracellular matrix were already present. After 16 h incubation, consecutive cell fixation and washing steps, fluorescent cell counting was carried out, then hits were identified and taken for subsequent investigations. The most promising compounds were validated against ovarium cancer cells also in 4 different *in vivo* models.

These examples show how fluorescent proteins can be used in hit and lead validation by cytotoxicity measurements in various ways, as appropriate alternatives to reagent based assays. Moreover, as apparent from some of the above examples, screening of larger compound libraries can be designed to rely on the fluorescent protein expression as a measure of growth inhibition. Cell fixation and consecutive nuclear staining had to be performed in some of the studies, because imaging software programs usually require it to distinguish (and count) cells. Therefore, washing steps could not be avoided in all cases, while other studies could perform a reagent-free assay procedure, which was beneficial in the aspect of automation. The utilization of fluorescent proteins provides additional benefits. Co-culturing of isogenic cell line pairs, which are different only in their fluorescent color can reduce the cost of culturing materials by multiplexing techniques, moreover cell lines in a well grow (obviously) under the same conditions.

1.4.5. Evaluating the robustness and reproducibility of assays – Z'-factor

Standardization is important in every part of the screening assay set-up, starting from the supply and maintenance of cells and other aspects of the tissue culture procedure, the quality of the tissue culture/detection plates used, the hardware, software and data

management [110]. During assay development and optimization, statistical analysis of the measured data is monitored to track the assay quality. The analysis is based on statistical parameters such as the mean or deviation of the measured signals. Developers can use for instance the coefficient of variation (CV, which is the standard deviation normalized by the mean value) or the signal to noise ratio (SNR) to amend the assay performance. In addition, there is a more complex quality metrics, that is often used for small-molecule high throughput screens, called the screening window coefficient or Z'-factor [134]. Z'-analysis, which determines the robustness of the assay integrates a number of external and internal impacts. It measures the assay resolution, which is influenced by many factors, e.g. by the assay procedure, or by the instrumentation that was used. By definition Z'-factor is a number that is ≤ 1 and the intervals of Z'-factor designate the usability of the investigated assay (Table 1).

Table 1. Assay quality regarding to Z'-factor values [134].

Z'-factor value	Related to screening	Assay type
1	An ideal assay	Dose-response acquisition is possible
$1 > Z \geq 0.5$	An excellent assay	Dose-response acquisition is possible
$0.5 > Z > 0$	A double assay	More suitable for primary screening
0	A "yes/no" type assay	Primary screening
< 0	Screening essentially impossible	

Formula of Z'-factor:

$$Z'\text{-factor} = [|\mu_{neg} - \mu_{pos}| - 3(\sigma_{neg} + \sigma_{pos})]/|\mu_{neg} - \mu_{pos}| = 1 - [3(\sigma_{neg} + \sigma_{pos})/|\mu_{neg} - \mu_{pos}|],$$

where μ_{pos}/μ_{neg} are the mean of positive/negative controls and $\sigma_{pos}/\sigma_{neg}$ are the standard deviation of positive/negative controls. Components of the formula of Z'-factor are visualized on Figure 6.

Based on Table 1, screens with a simple yes/no answer as an output are acceptable if the Z'-factor is above 0. To be able to obtain dose-response curves, better quality assays have to be used, where the Z'-factor is above 0.5. As apparent from the formula and from Figure 6, Z'-factor reports the proportion of the assay dynamic range that is not overlapping with either the positive or negative controls' data variability band (which

cover 99.7 % of all the possible positive and negative control signals if normal distribution is assumed). For example a Z'-factor of 0.6 reports from an assay where 60 % of the assay dynamic range is not overlapping with the data variability bands. Accordingly, robust measurements have wider separation band size, while overlapping data variability bands of positive and negative controls would refer to unreliable assays. Nevertheless, if there are a few extreme values (outliers) in either the positive or negative controls, standard deviation will increase and it can affect the Z'-factor, potentially leading to an apparently unfavorable Z'-value, even when the assay would perform well [135].

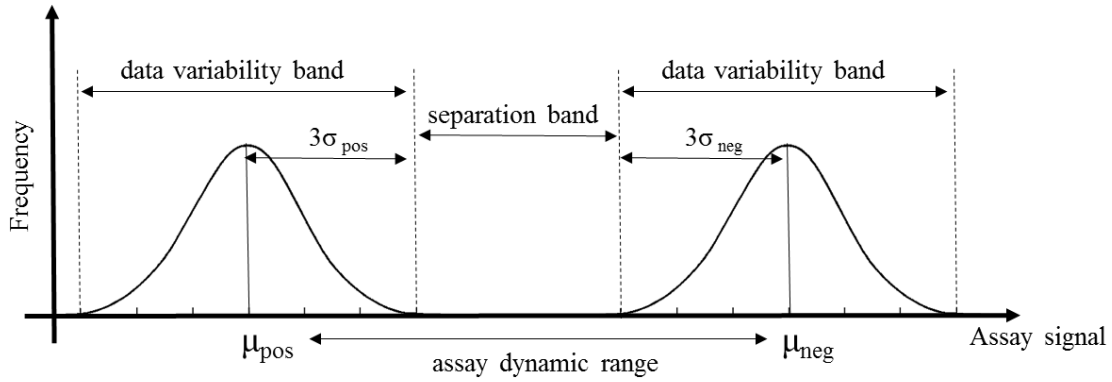

Figure 6. Graphical definition of Z'-factor. Z'-factor calculation is based on the measured mean and deviation of the positive and negative controls, which return the lowest and highest values that can possibly be measured. Z'-factor is the ratio of the separation band and the assay dynamic range. (The formula consist the assay dynamic range in an absolute value as depending on the assay type, either positive or negative controls can return the highest/lowest possible signal.)

1.4.6. Hit identification by assays based on fluorescent protein expression

Besides finding the active substances from a screen, exclusion of false positive hits (not truly active substances) and false negative hits (missed active substances) are also part of the hit identification process. While with an appropriate Z'-factor it is possible to keep the number of false hits low, there are assay specific factors, which can disturb the integrity of the data. In the case of fluorescent protein expressing cell lines, disturbance of compound screening might derive from unspecific gene expression change due to the applied DNA transfection procedures, or from the usage of inherently fluorescent compounds. Thus, it is advisable to use a counter assay in the follow-up studies for at least the best hit compounds, and when possible, to use repeats during the screen [136] [137] [138].

2. Objectives

Overcoming P-gp-mediated cancer multidrug resistance is still a serious obstacle. A possible solution could be the application of so called MDR-selective agents, which target P-gp overexpressing tumor cells. However, proof-of-concept *in vivo* studies are still missing, the attempts reported inactivity of compounds, which is plausibly due to the unfavorable pharmacokinetics and the low MDR-selectivity of the tested agents. Thus, our overall aim was to establish a screening platform for the robust and high throughput identification of MDR-selective compounds at the scale of an academic research group, to find drug-like candidates for iterative lead optimization. Identification of novel MDR-selective compounds would broaden our knowledge on the nature of the P-gp potentiated MDR-selective mechanism, which would supply SAR models intended to predict even more potent, pharmacologically active candidates.

Objective #1. Establishment of a standardized cytotoxicity testing system amenable for high throughput screening of compound libraries

#1A. Design of a 3-step compound screening system including primary, confirmatory and secondary screening.

#1B. Introduction of a reagent free, fluorescent protein based cytotoxicity assay measuring growth inhibition.

#1C. Robotization of the screening procedure and automated data evaluation implemented for both 96 well and 384 well plate experiments to increase compound throughput.

Objective #2. Identification and validation of MDR-selective compounds guided by literature data

#2A. Verifying the putative MDR-selective toxicity of compounds reported to preferentially kill P-gp overexpressing MDR cell lines.

#2B. Systematic identification of novel MDR-selective compounds from the NCI DTP drug repository database.

#2C. Defining chemotypes linked to MDR-selective cytotoxicity, based on #2A and #2B.

Objective #3. Screening of focused libraries designed to investigate the chemical space around MDR-selective chemotypes

3. Materials and Methods

3.1. NCI DTP database and *in silico* data mining

The *in silico* data mining was performed using the NCI-60 Cell Line Screen database released in December, 2010, which is available at the DTP website [94]. The algorithm we used was the same that our group used before on an earlier release [73] [98]. Briefly, we determined the Pearson's coefficient between the pGI_{50} values of each DTP chemical entity measured against the NCI-60 cell line panel and the mRNA expression of ABCB1 of the NCI-60 cell lines. We filtered out uninformative drug profiles, where >50% of the 60 possible values were either missing or indicated inactivity, and collected the *in silico* hits with a coefficient higher than 0.4, thus when high drug sensitivity was accompanied with high ABCB1 expression, which is characteristic of the P-gp mediated MDR-selective compounds.

3.2. Compounds and chemicals

Unless otherwise stated, chemicals were purchased from Sigma Aldrich (Merck). NSC compounds were acquired from DTP's drug repository, except NSC733435, which was purchased from ChemBridge Corp. Desmosdumotin analogues were synthesized by Szintekon Ltd. Pluronic P85 was a kind gift from Dr. R. Mészáros (ELTE University, Hungary). Tariquidar was a kind gift from Dr. S. Bates (NCI, NIH). KP772 was synthesized by our colleague, Veronika F.S. Pape as described by Hart and Laming with slight modifications [139]. Compounds of the protoflavone library was synthesized and provided by the group of Dr. Attila Hunyadi (SZTE, GYTK, Szeged). Compounds of the library containing flavonoids and thiosemicarbazones were synthesized and provided by Ahcène Boumendjel (Univ. Grenoble Alpes, Département de Pharmacochimie Moléculaire, France). Library of the thiosemicarbazones and their analogues was designed by Veronika F.S. Pape, who also synthesized several substances of the library, while other compounds were either obtained from DTP or were purchased from commercial sources.

Dissolved compounds of the liquid library were stored in 1.1 ml tubes in 96 position racks, where tubes could be collected for the experiments individually, while mother plates (96 well polypropylene trays) had fixed layouts with 36 compounds in 2 concentrations per plate in 100 µl.

Structure of compounds were sketched by Marvin (ChemAxon Ltd.). 2D structural clustering was performed with PubChem's Chemical Structure Clustering Tool [140], which uses the Single Linkage algorithm, and draws the dendograms based on the 2D Tanimoto similarity index.

3.3. Cell lines and culture conditions

The following cell lines were used in the experiments:

- MES-SA uterine sarcoma cell line and its doxorubicin selected derivative MES-SA/Dx5 (referred only as Dx5 from here) were purchased from ATCC. MES-SA mCherry and Dx5 mCherry cell lines were created using lentiviral transduction by Creative Cell Ltd., Budapest. Cells that were expressing mCherry stably were sorted with a Beckton Dickinson FACS Aria cell sorter.
- A431 human skin-derived, epidermoid carcinoma cell line was purchased from ATCC. The retrovirally transduced A431-B1 and A431-G2 cells were established earlier [141] [142].
- OVCAR-8 (OVC-8) DsRed2 and NCI/ADR-RES eGFP ovarium carcinoma cell lines were a kind gift from Dr. Michael M. Gottesman (National Institutes of Health, US). The respective expression vectors encoding the fluorescent proteins DsRed2 and eGFP were transfected by Lipofectamin2000 reagent.
- KB-3-1 cervix carcinoma cell line and its vinblastine selected derivative KB-V1 were a gift from Dr. Michael M. Gottesman (National Institutes of Health, US).
- MDCK II (Madin-Darby canine kidney cell line) was obtained from ATCC. MDCK II B1 cell line stably expressing the human wild-type ABCB1 was created by the Sleeping Beauty transposon-based gene delivery system, using the 100 × hyperactive SB transposase [143].
- HCT-15 cell line was obtained from DTP (DCTD Tumor Repository, National Cancer Institute at Frederick, US).
- KB (nasopharyngeal carcinoma) and KB-VIN (vincristine-resistant KB subline) cell lines were a generous gift of Dr. Y.-C. Cheng, Yale University, US.
- DMS 114 small cell lung carcinoma and the nintedanib resistant DMS 114-NIN cells were granted by Dr. Walter Berger (Medical University of Vienna) for the experiments.

Cell lines were maintained either in DMEM (Mes-Sa, KB-3-1, A431, MDCK II and DMS 114, and their derivative cell lines) or in RPMI (OVC-8 DsRed2, NCI-ADR/RES eGFP and HCT-15) completed with 10% FBS, 5 mM glutamine and 50 units/ml penicillin and streptomycin (Life Technologies). KB and KB-VIN cell lines were maintained in RPMI medium completed with 10% FBS, 25mM HEPES and 100 μg/ml kanamycin as it was indicated in the literature [85]. Cells were periodically tested and resulted negative for mycoplasma contamination with the MycoAlert mycoplasma detection Kit (Lonza).

Drug selected cell lines Dx5 and Dx5 mCherry were treated with 500 nM doxorubicin prior to the experiments, while KB-V1 and KB-VIN cell lines were selected in 300 nM vinblastine and 100 nM vincristine, respectively.

3.4. Cytotoxicity assays using MTT, PrestoBlue or SRB reagents

Cells were seeded in a 5000 cells/well density on 96-well plates in 100 μl, except for MDCK II cells that were seeded in 2500 cells/well density due to their high proliferation rate. After cell attachment, serially diluted compounds were added to the wells in a final volume of 200 μl, then plates were incubated until measured. When inhibitors (TQ: 1 μM, PSC833: 2 μM) were used to block P-gp, 4-times concentrated solutions were added to the 100 μl cells in a volume of 50 μl, few minutes before adding 50 μl of the test compound.

When viability was measured by MTT, the medium was removed before adding the tetrazolium salt dissolved in PBS (0.5 mg/ml). Plates were incubated for 4 hours, then formazan crystals were dissolved in isopropanol-HCl (9:1) using 1 M HCl, and absorbance was obtained at 540 nm. When PrestoBlue cell viability reagent was applied, we diluted the dye in PBS (5-10 %) and exchanged the medium in the wells to it, and incubated the plates for 1 hour. The fluorescence of the dye was obtained with $555_{ex}/585_{em}$ wavelengths. SRB assay was carried out by following the manufacturer's instruction, using a 0.4 w/v % solution. We used the 540 nm filter to measure absorbance and the 660 nm filter to measure background absorbance. For negative controls, we used the wells with untreated cells. For positive controls, we used cell-free wells in the case of MTT and PrestoBlue, while for SRB, we used the wells, where devastating concentrations of drugs were applied, to exclude the error deriving from cell debris.

MTT and SRB assays presented in this thesis were measured by a filter based Victor X3

Multilabel plate reader, while PrestoBlue assay was detected by a monochromator based EnSpire Multimode plate reader (both readers are the product of Perkin Elmer). As solutions were homogenous, all the 3 assay types were read with top reading mode and with single point measurements.

3.5. Fluorescent protein based cytotoxicity assays

OVCAR-8 DsRed2 and NCI/ADR-RES eGFP cell lines were tested in 96 well plates, seeded in a density of 5000 cells/well. After cell attachment and drug addition, plates were incubated for 144 hours, which was interrupted only for short times, when the plates were measured at certain days prior to the final measurement at day 6 (144 h). Based on literature data [132], we applied a 540 nm – 579 nm filter set (excitation and emission, respectively) to measure the fluorescence of the wells where DsRed2 expressing cells were seeded, and 485 nm - 535 nm filter set to measure eGFP by a Victor X3 Multilabel plate reader.

On the purpose of cytotoxicity testing, Mes-Sa mCherry and Dx5 mCherry cell lines were seeded in a density of 5000 cells/well on 96 well plates, and 2500 cells/well on 384 well plates in 100 µl and 20 µl of medium, respectively. The following day, the liquid handling machine (Hamilton Microlab StarLet workstation) prepared serial dilutions, and dispensed the test compounds on the plates according to the plate maps. The final volume of the assay was 200 µl in a 96 well plate and 60 µl in a 384 well plate. Microplates were incubated, and the fluorescence was measured at $585_{ex}/610_{em}$ wavelengths on certain days, most frequently at 72 h and at 144 h by the EnSpire Multimode plate reader, where the excitation wavelength is produced by a monochromator. When eGFP or mOrange expressing cells were measured, we used protocols with $545_{ex}/567_{em}$ and $485_{ex}/510_{ex}$ wavelengths, respectively. Values - obtained from bottom reading mode - were normalized to the untreated (negative) control and to wells, where all cells were killed (similarly to SRB assay), as the relative fluorescent value of this positive control was different from values of cell-free wells containing only medium.

As for culture plates, we used clear walled polystyrene microplates in the cytotoxicity experiments, both when 96 or when 384 well formats were applied. The 96 well plates were purchased from various sources (e.g. from TPP Techno Plastic Products AG, Eppendorf AG, Thermo Fisher Scientific, Orange Scientific), considering that each

compound set/focused library was assayed on plates from a single vendor, while 384 well plates were all obtained from Greiner Bio One International GmbH.

Cytotoxicity (IC_{50} or GI_{50} values) were obtained by sigmoidal curve fitting by the GraphPad Prism software using the four parameter logistic equation with automatic top (cf. negative control) and bottom (cf. positive control) plateau determination:

Y = Bottom + (Top-Bottom)/(1+10^((LogIC_{50}-X)*HillSlope)),

where Y: measured values

X: corresponding concentration

Bottom: value of the bottom plateau of the curve

Top: value of the top plateau of the curve.

Alternatively, automated data evaluation was performed by our custom program, which was written by Judit Sessler in C#, and half-maximal growth inhibition was calculated based on nonlinear least square regression (nls) of the logistic function:

nls (y = 1/ (1 + exp (-b * (x -c))))

where y: measured values

x: corresponding concentration

b: Hill slope

c: log IC_{50}.

The source of the automatic data processing was the raw plate reader output file which is in a text (.txt) or in a comma separated values (.csv) format. To visualize the results for quality check, the program is using the graphical surface of the 'R' software environment.

3.6. Flow cytometry

3.6.1. Analysis of mCherry expressing cell line populations

The expression level of the mCherry fluorescent protein in cells and the proportion of the fluorescent protein containing population were analyzed by an Attune Acoustic Focusing Cytometer (Thermo Fisher Scientific) in cell culture medium. Cell lines expressing mCherry were excited with a violet laser at 405 nm, and detected in the Violet Laser 3 (VL-3; 579-627 nm) channel.

3.6.2. Calcein-AM efflux assay

After detachment with trypsin 250,000 cells were collected in serum free medium in test tubes, and incubated with 0.25 mM Calcein-AM (Dojindo Molecular Technologies) with or without 50 μM verapamil for 10 minutes at 37°C. The uptake was stopped by adding ice-cold PBS, tubes were centrifuged, then cells were re-suspended in ice-cold PBS and stored on ice until measured by the Attune Acoustic Focusing Cytometer. The forward and side scatter density plot (FSC-SSC plot) was used to discriminate cell debris, and cells without intact membrane were excluded based on staining with Zombie Violet Dye, which was excited at 405 nm and detected in the Violet Laser 1 channel (VL-1; 430-470 nm). To measure the calcein accumulation of cells, the samples were excited at 488 nm with a blue laser, and the signal of calcein was detected by using the Blue Laser 1 emission filter (BL-1; 515-545 nm).

4. Results

First, I describe the introduction, automation and characterization of the fluorescent protein based cytotoxicity assay system (4.1). The assay development is followed by the verification of reported MDR-selective agents and a systematic datamining from a publicly available database, all in order to identify structures related to P-gp potentiated hypertoxicity (4.2). In the third part (4.3), results of focused library screening are presented.

4.1. Establishing an automated cytotoxicity testing platform capable of HTS, combined with a fluorescent protein based cytotoxicity assay development

In this chapter, I describe the development of the screening algorithm together with the fluorescent protein based cytotoxicity assay. Results of the drug screens will be shown in chapters 4.2 and 4.3.

4.1.1. Establishing a 3-step screen to for the identification of MDR-selective compounds

One of our primary goals (objective #1A) was to introduce a compound screening system, which has a higher throughput in order to be able to test larger compound libraries, and to discover potent MDR-selective agents. Accordingly, to achieve our aim, we designed a 3-step small molecule screening system that is suitable for HTS purposes, and facilitates lead selection for further optimization. The 3 steps to be accomplished were: (1) primary screen, (2) confirmatory screen and (3) secondary screen (Figure 7).

The goal of the primary screen was to identify and exclude nontoxic or low activity compounds. The primary screen we developed was probing the unknown compounds in 2 concentrations (10 μM and 100 μM) against 2 cell lines (a parental and MDR derivative). The results were interpreted simply as growth inhibition normalized to the live and dead controls, ranging ideally between 0 and 100 %. The 2 concentrations per cell line allowed us to classify and prioritize the compounds. The 9 classes provided some degree of flexibility in determining the set of interesting compounds, which were chosen by considering both cytotoxicity and cell line selectivity (Table 2).

Table 2. Cytotoxicity classes derived from the primary screen. A compound was considered toxic if its growth inhibition was higher than 50 %. CS: collateral sensitivity.

		P-gp expressing MDR cell line (e.g. Dx5)		
		toxic at 10 μM	toxic only at 100 μM	not toxic at any concentrations
Parental line (e.g. Mes-Sa)	toxic at 10 μM	toxic	substrate category II	substrate category I
	toxic only at 100 μM	CS category II	intermediately toxic	substrate category III
	not toxic at any concentrations	CS category I	CS category III	not toxic

For both substrates and collateral sensitivity provoking agents, category I possessed compounds, which were not toxic to one of the cell lines at 100 μM but killed the other already at 10 μM. Category II possessed compounds killing one cell line at 10 μM, while killing the other only at 100 μM. Category III possessed compounds, which killed a cell line only at 100 μM and was inactive against the other line. Intermediately toxic compounds killed both cell lines only at 100 μM. In the primary screen, every compound that was toxic at 100 μM in at least one of the cell lines was considered as a hit. The prioritization of the hits based on the categories shown in Table 2 (cytotoxicity classes) was not needed when smaller compound libraries were tested – in that case non-toxic compounds were excluded from further investigations. In the case of larger compound libraries, cytotoxicity classes were used to control the amount of compounds to be probed in multiple concentrations, thus beyond the non-toxic substances, some hits might have been excluded as well.

We used the two-point growth inhibition data derived from the primary screen to estimate the concentration interval to be used in the second step, the confirmatory screening, where the primary hit compounds were probed against the same cell lines, but in a serial dilution in DMSO, consisting of 7-9 concentration points, depending on the plate layout. To minimize the error of missing the full dose response curves, broader concentration intervals were used for the confirmatory screening. The hits that were interesting also in the second step, e.g. compounds whose dose-dependent MDR-selective toxicity was confirmed, were then tested in the third step, the secondary screening. In the secondary

screening step we planned to utilize cytotoxicity assays that work by a different principle than the assay in the primary and confirmatory steps (a counter assay), and to involve additional cell line pairs in order to test the robustness of the observed cytotoxic effect. In the secondary assay step, drugs were diluted in cell culture medium. The workflow of the 3-step process is shown on Figure 7.

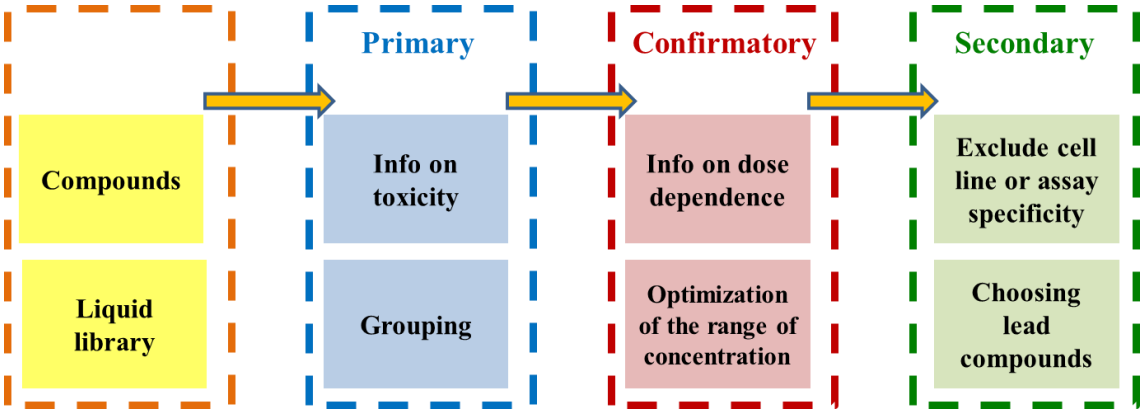

Figure 7. Scheme of the multistep screening process we developed to identify potent MDR-selective compounds. The potency (cytotoxicity and cell line selectivity) of the tested drugs were investigated after each step, based on the information (info) shown in the respective boxes to choose lead (or lead-like) compounds.

4.1.2. Utilization of fluorescent protein expressing cells in cytotoxicity testing

The next task was to choose a cytotoxicity assay for the primary and confirmatory screens, keeping in mind that it has to be suitable for HTS. Thus, the main aspects we considered was the simplicity of the assay procedure and long term cost effectiveness. We used genetically engineered cell lines that express fluorescent proteins (under a constitutive promoter) to introduce a reagent free method. Fluorescent cells were seeded in microplates, and cell numbers were estimated based on fluorescent intensity. To establish and validate such a fluorescent protein based cytotoxicity assay (objective #1B), we used the OVCAR-8 DsRed2 and NCI-ADR/RES eGFP cell lines, which were engineered and characterized by the research group of Michael M. Gottesman [132]. These two cell lines stably express the fluorescent proteins and their growth characteristics are identical to the corresponding non-fluorescent cells in the period of a cytotoxicity assay.

The first criterion was to find a linear correlation between the cell number and the fluorescent intensity measured by the plate reader. By using the appropriate filter combinations for the fluorescent proteins DsRed2 and eGFP, and a cell number range that

is relevant in the cytotoxicity assays, we defined a proportional relation between the actual cell number and the fluorescence of a well on the microplate (Figure 8). Thus, the mere presence of the intracellular fluorescent proteins was sufficient for measuring the amount of cells reliably.

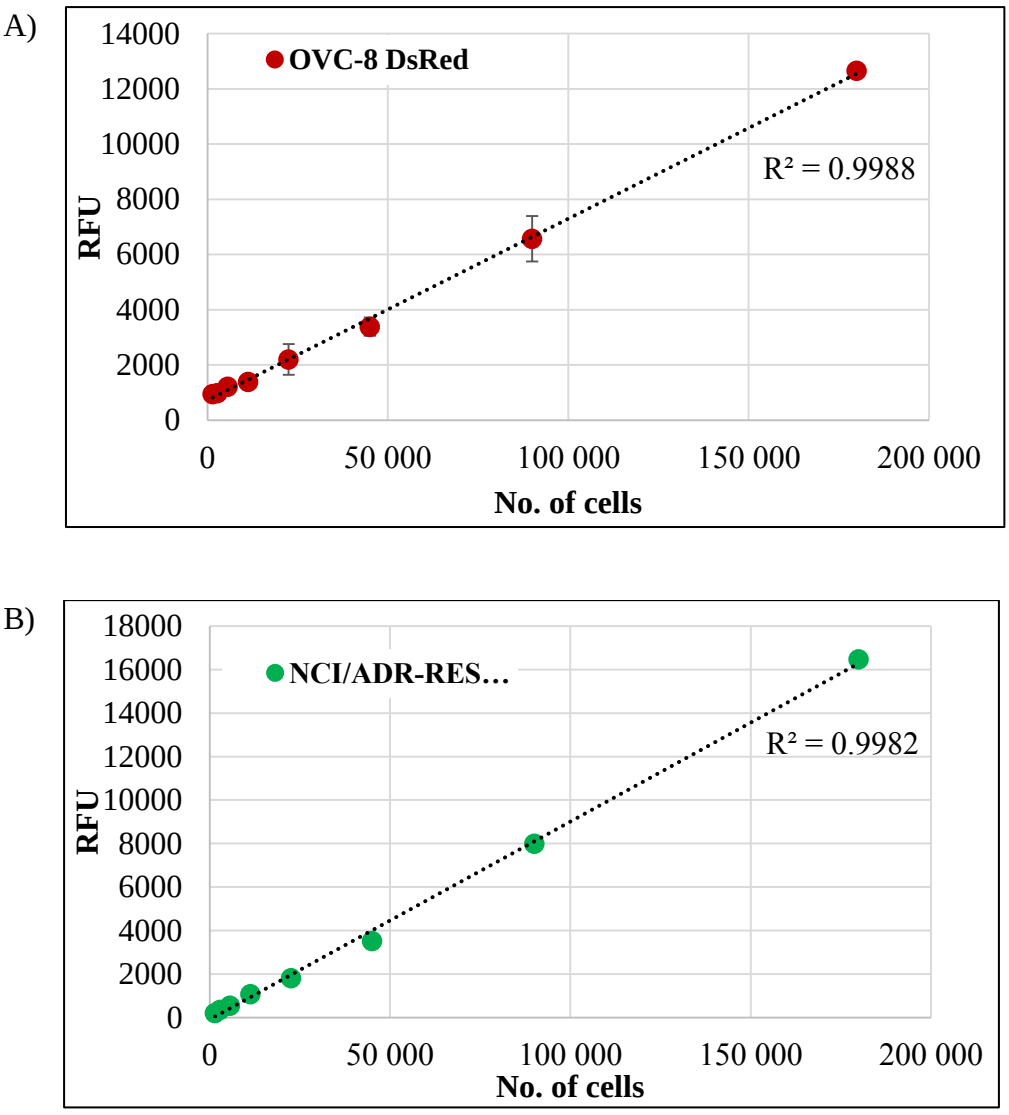

Figure 8. Fluorescent intensity (relative fluorescent unit, RFU) as the function of the number of OVC-8 DsRed2 and NCI/ADR-RES eGFP cells (panel A and B, respectively). Dotted lines represent the linear fit with a coefficient of R^2.

As a next step, we checked the growth rate of the cell lines. In contrast to end-point assays, the fluorescent protein based measurement is not harmful to the cells (it is 'quasi label-free'), thus we measured the same plate each day. The fluorescent signals of DsRed2 and eGFP were increasing in the whole duration of the experiment, and the growth profile of

the cells followed the logistic curve that is the common model of population growth (Figure 9).

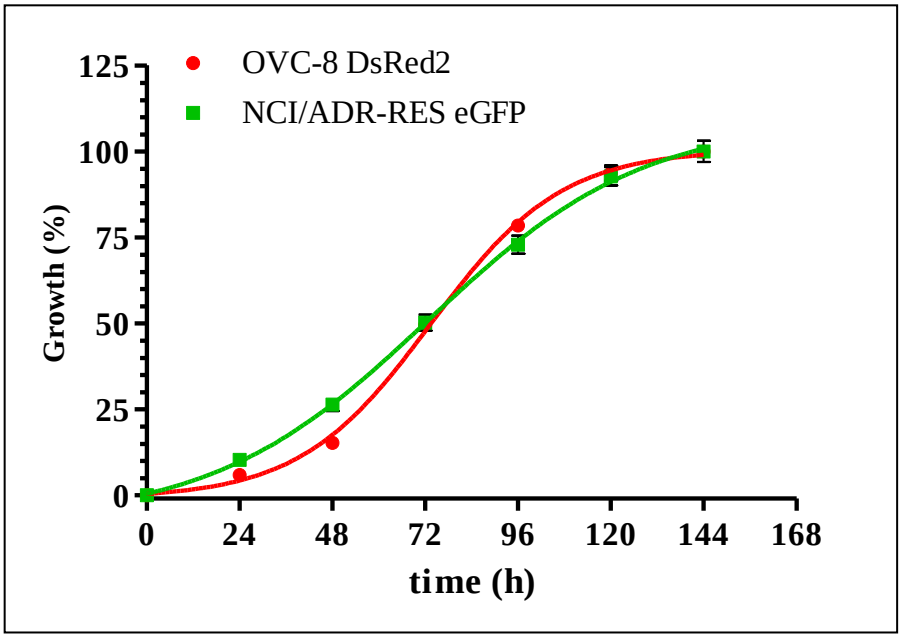

Figure 9. Normalized growth kinetics of the fluorescent cell lines OVC-8 DsRed2 (red line) and NCI/ADR-RES eGFP (green line) in a 144 h long experiment.

Based on the above experiments, we can reliably measure and follow the number of cells in time. Thus, we have to be able to measure if growth is hindered or inhibited by a given test compound. To see how growth inhibition changes over time, we conducted a cytotoxicity assay, where each day the same plate was measured for DsRed2 and eGFP fluorescence (Figure 10). As a test compound NSC73306 was chosen because of its known MDR-selective cytotoxic effect [73]. NSC73306 showed concentration dependent growth inhibition of OVC-8 DsRed2 and NCI/ADR-RES eGFP cells. For both cell lines 100 μM of the compound caused complete inhibition of growth, and fluorescence signal was slightly decreased by 144 h referring plausibly to the degradation of the fluorescent proteins as a consequence of cell death. At 3.13 μM NSC73306 hindered both cell lines in their growth, and this effect was much more pronounced in the MDR cells, proving the MDR-selective toxicity of this compound. The untreated cells had identical growth rates as cells seeded in wells where NSC73306 were present in non-toxic concentrations.

A)

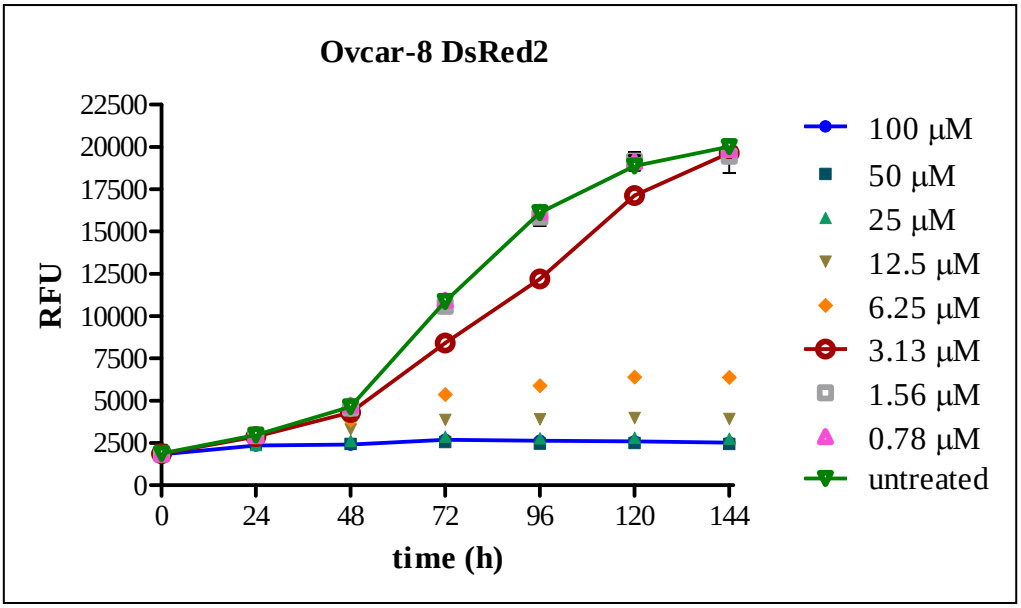

B)

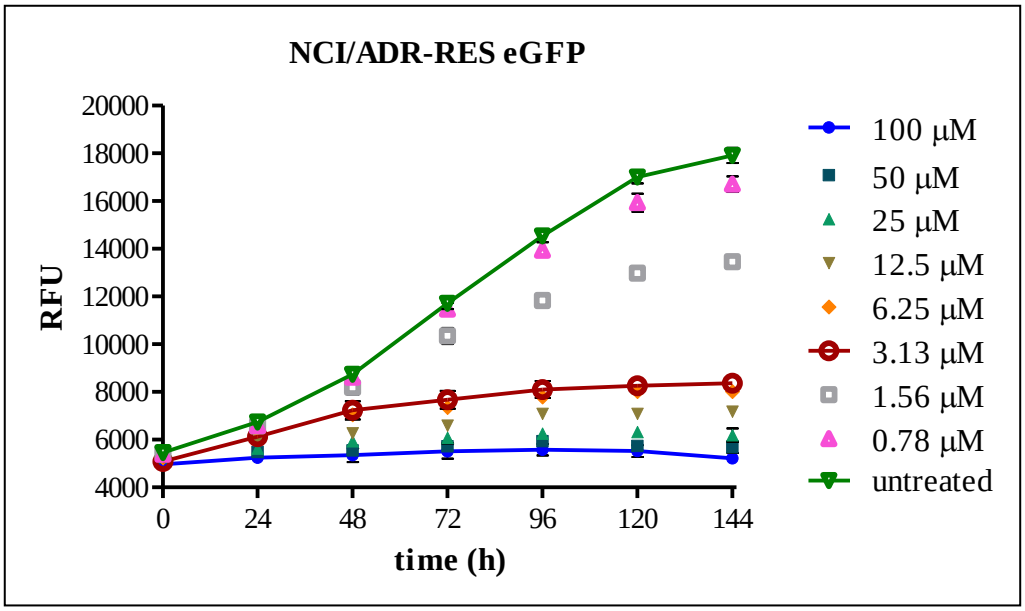

Figure 10. Growth curves for (A) OVC-8 DsRed2 and (B) NCI/ADR-RES eGFP treated with various concentrations of NSC73306 for 144 h. RFU values of the untreated control and two concentrations of the NSC73306 are connected with a line to highlight the change in cell number.

When we normalized the raw fluorescent values of each day separately, where 0 % referred to the complete growth inhibition (when 100 µM NSC73306 was applied) and 100 % referred to the untreated control, we could draw dose-response curves (Figure 11), and determined the cytotoxicity by calculating the half maximal growth inhibition (GI_{50}) values (Figure 12/B).

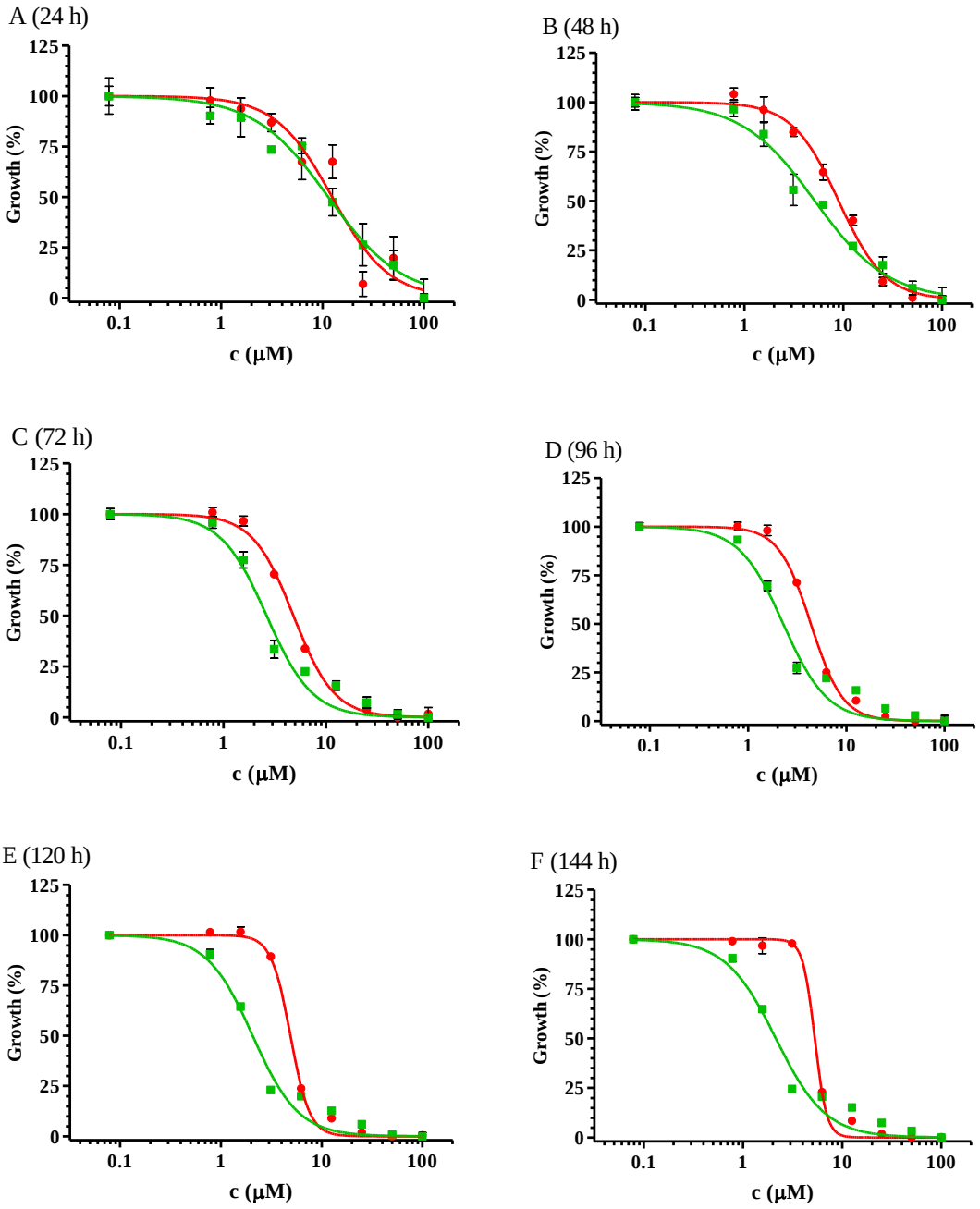

Figure 11. Dose-response curves with sigmoidal fit for NSC73306 obtained over 6 days (at 24-48-72-96-120-144 h in figures A-B-C-D-E-F, respectively. Red curves: OVC-8 DsRed2, green curves: NCI/ADR-RES eGFP.

The toxicity of NSC73306 was increasing till 96 h for OVC-8 DsRed2 cells, when toxicity apparently started to slightly decrease. For NCI/ADR-RES eGFP cells cytotoxicity was increasing in the whole period of the experiment. As a consequence, the highest MDR-selective toxicity of NSC73306 was observed at the last day at 144 h.

As the fluorescent protein based assay was not harmful to the cells, we were able to perform a conventional MTT assay after the 144 h fluorescent measurement. The obtained half maximal inhibitory concentration (IC_{50}) values and also the selectivity ratio (SR) were a bit lower than that of the corresponding fluorescent measurements (Figure 12).

A)

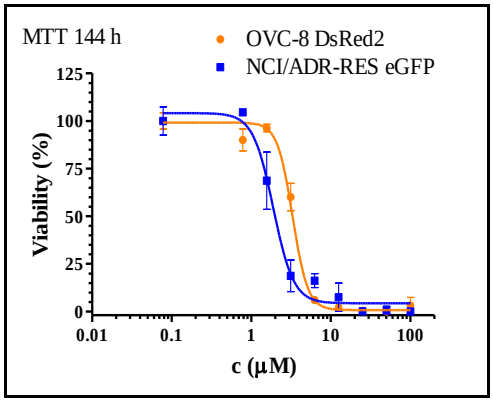

B)

time of measurement	OVC-8 DsRed2	NCI/ADR-RES eGFP	Selectivity Ratio
24 h	12.4	11.4	1.1
48 h	9.0	5.2	1.7
72 h	4.8	2.6	1.8
96 h	4.3	2.3	1.9
120 h	4.9	2.1	2.4
144 h	5.3	2.1	2.5
144 h MTT	3.3	1.9	1.7

Figure 12. A) Dose response curves for NSC73306 measured with MTT assay after 144 h drug incubation. B) Table of GI_{50} (and IC_{50} for MTT) values of NSC73306 in µM, and selectivity ratio (OVC-8 DsRed2 divided by NCI/ADR-RES eGFP).

To avoid daily measurements for 144 h in the further use of the fluorescent protein based assay (which would include weekends) and to reduce measuring time, normalization of the data and drawing dose-response curves at certain time points seemed a better solution to find selectively toxic agents than comparing growth curves for each concentration points (which was the case in [129], where 6-days growth kinetics were compared). The separate GI_{50} values are clear interpretations of the grade of inhibition, which is easier to quantify and handle, while for growth kinetics, raw data collected on different days must be linked, making the evaluation more complex and more prone to mistakes. As common cytotoxicity procedures deal with 72 h incubation time of drugs on cells, we decided to measure plates at this customary time as well as at 144 h where selectivity of NSC73306 was the highest. In this way, we decreased the number of measurements to 2 instead of 7 that would be necessary to obtain growth kinetics in a 144 h measurement.

We investigated two ABCB1 substrates, vinblastine and morpholino-adriamycin, and another MDR-selective compound NSC693871 [98] to support the utility of this novel microplate based cytotoxicity assay. Both ABCB1 substrates killed the parental OVC-8

DsRed2 cell line in low concentrations of the drugs, but killed the MDR-cell line only at extremely high concentrations (Figure 13 and 14). In contrast, NSC693871 conferred a well apparent MDR-selectivity at 72 h and 144 h time points (Figure 15). Our results suggest that the fluorescent protein based assay that we adapted is suitable to test the cytotoxicity of compounds via growth inhibition, and we are able to identify the resistance of MDR cells to ABCB1 substrates and also the MDR-selective toxicity of certain compounds.

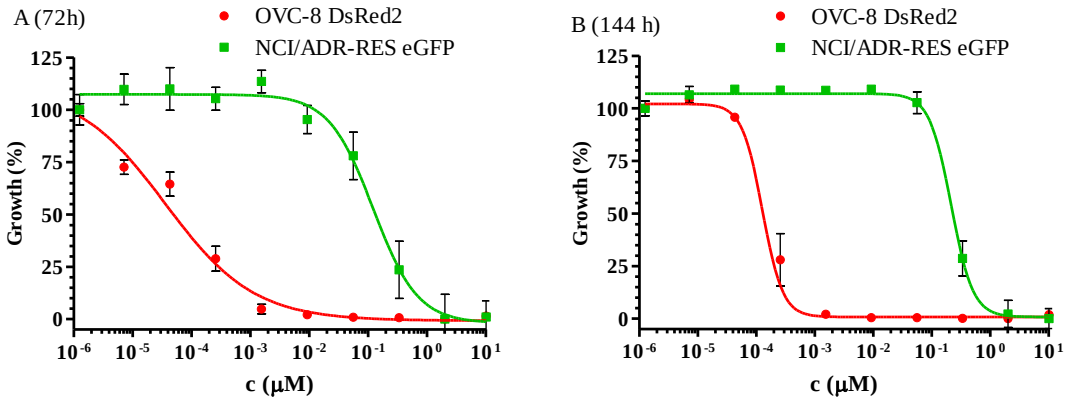

Figure 13. Cytotoxicity of vinblastine measured with the fluorescent protein based assay (A) at 72 h and (B) at 144 h.

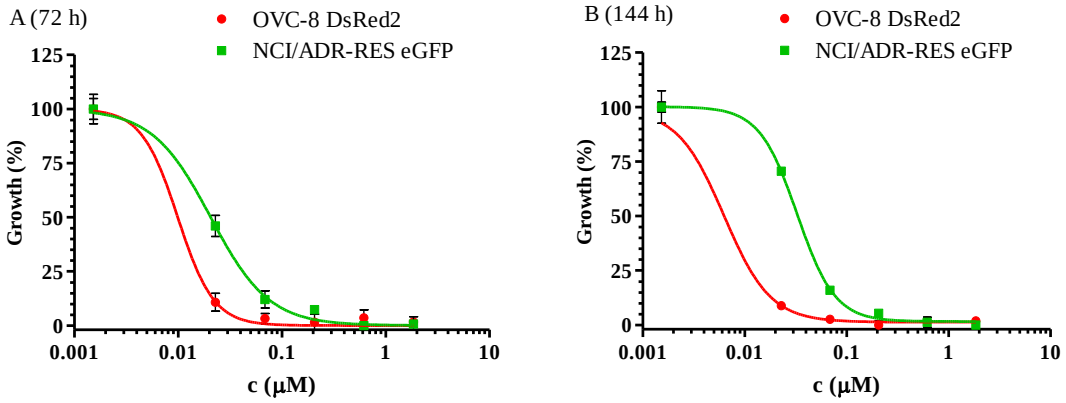

Figure 14. Cytotoxicity of morpholino-adriamycin (NSC354646) measured with the fluorescent protein based assay (A) at 72 h and (B) at 144 h.

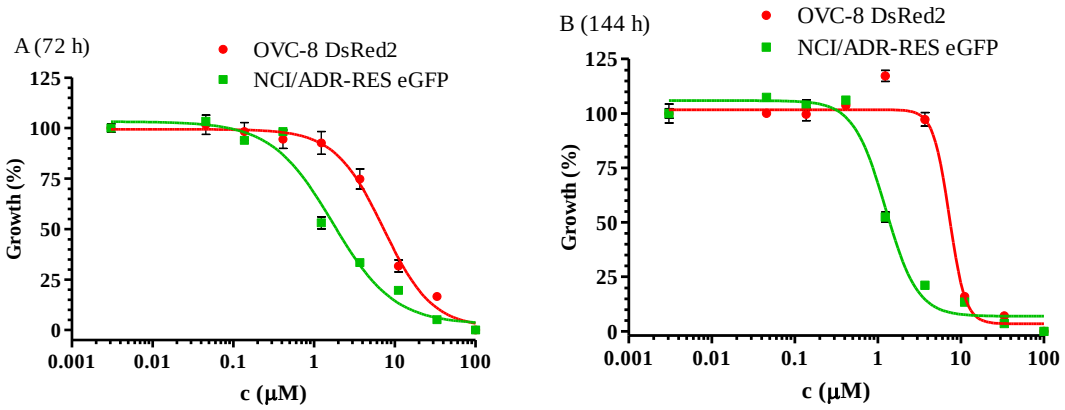

Figure 15. Cytotoxicity of NSC693871 measured with the fluorescent protein based assay (A) at 72 h and (B) at 144 h.

Following validation of the fluorescent protein based assay, we tested several compounds with unknown cytotoxic activity against the OVC-8 DsRed2 and NCI/ADR-RES eGFP cell lines. The assay development is demonstrated prior to the results of compound library testing (according to Objective #1 and #2-#3), and the respective growth inhibition values are shown in Table 12 (4.2.2.1).

4.1.2.1. Statistical approach to qualify the fluorescent protein based assay

The next step was to decide if the established fluorescent protein based assay is amenable to be utilized in high throughput screening (HTS). In general, an assay can be automated for HTS if the Z'-factors (calculated from positive and negative controls from each assay plate) is above zero. The higher Z'-factor the more reliable the assay is. Accordingly, an assay with a Z'-factor over 0.5 allows already to investigate dose dependency instead of a yes/no type of assay (Table 1; [134]).

The data from all the cytotoxicity assays performed with OVC-8 DsRed2 and NCI/ADR-RES eGFP cell lines measured at 72 h and/or at 144 h were collected, and Z'-factors were retrieved. These Z'-factors, depicted on Figure 16, were calculated from the controls of each cytotoxicity plate, and represent the reliability of the individual measurements.

Based on the Z'-values, the fluorescent protein based cytotoxicity assay conducted on 96 well plates performed well, both when DsRed2 and when eGFP was measured. Some individual assay plates although returned a Z'-factor of smaller than 0.5, thus in those certain cases the dose-dependence data had to be checked, and the experiments were repeated. If individual Z'-factors fell below zero, those measurements were excluded

from data evaluation. As the average Z'-factor was above 0.5, which is the category of an excellent assay based on Table 1, the cytotoxicity data we obtained was reliable at both time points (Table 3).

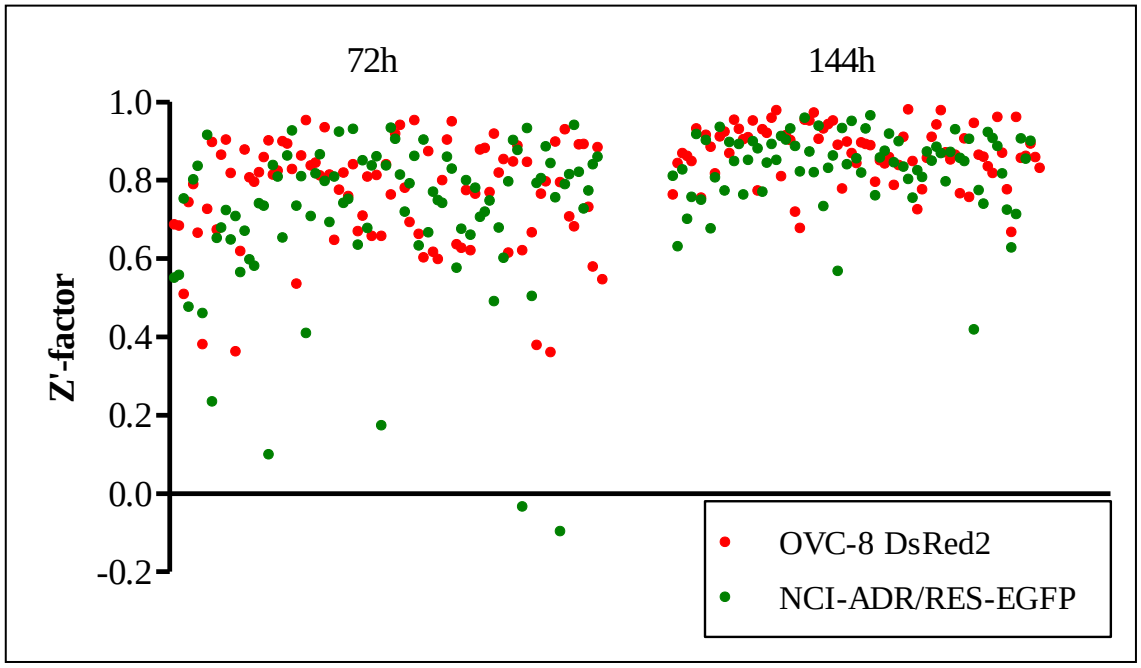

Figure 16. Z'-factors per experiment for OVC-8 DsRed2 (red dots) and NCI/ADR-RES eGFP (green dots) measured at 72 h and at 144 h. Each dot represents the reliability of the measurement from a single 96 well plate.

Table 3. Average and standard deviation of Z'-factors calculated from the fluorescent protein based measurement performed on 96-well plates.

Cell line	72 h	144 h
OVCAR-8 DsRed2	0.76 ± 0.16	0.87 ± 0.12
NCI/ADR-RES eGFP	0.72 ± 0.21	0.84 ± 0.13

4.1.3. Installation of an automated screening platform to perform fluorescent protein based cytotoxicity assays on 96 and 384 well plates

The fluorescent protein based cytotoxicity assays against OVC-8 DsRed2 and NCI/ADR-RES eGFP cell lines were all performed manually. The throughput (no. of tested compounds in a given time) of manual testing was relatively low, and the possibility of unnoticed pipetting errors was present.

Our aim (objective #1C) was to reach an advanced level in cytotoxicity testing by the robotization of the assay procedure combined with automatic data evaluation.

4.1.3.1. Items of the screening platform

In order to increase the throughput and test larger compound libraries in search for potent MDR-selective agents, automation of liquid handling was indispensable. Therefore we installed a Hamilton StarLet automated liquid handling machine and wrote various methods (programs in the Venus2 software) to seed cells on culture plates, to perform serial dilutions and to perform liquid transfer of the dissolved drugs for primary, for the confirmatory and for the secondary screening steps. As the methods operate with fix deck layouts, all plate maps had to be standardized and pre-defined by considering also the possible robot specific pipetting channel movements. Example plate maps are shown in the supplement (Appendix 2).

As a part of the screening platform, we purchased also a Perkin Elmer EnSpire multimode plate reader that was dedicated mostly for our screening purposes. The EnSpire protocols were created according to the pre-defined plate layouts that were used for the Hamilton methods. After the desired incubation time of the cytotoxicity tests, microplates were measured by the plate reader. Plates could be loaded either manually or automatically, as the robot and the reader were connected and capable of information exchange.

4.1.3.2. Creation of a fluorescent cell line deposit

We validated the fluorescent protein based cytotoxicity assay for OVC-8 DsRed2 and NCI-ADR/RES eGFP cell lines. However, for compound screening we intended to use other cell lines as well. In cooperation with the research group of Dr. Katalin Német (Creative Cell Ltd.) and with the help of my colleagues, especially of Nóra Kucsma, we created a fluorescent cell line deposit, which we still continuously expand. The deposit consists of cancer cell lines from different tissues of origin. Lentiviral transduction of a pRRl-EF1 plasmid containing the gene of the fluorescent protein was followed by sorting for fluorescence (at least twice) by a flow cytometer (BD FACS ARIA). Examples of fluorescent cell lines in the deposit are introduced in Table 4.

Table 4. Fluorescent cell line deposit with the respective virus titer for 3*10^4 cells. Parental and MDR variants of the cell lines were grouped together.

Cell line	eGFP	mOrange	mCherry
A431	25 µl		
A431 B1			25 µl
A431 G2		5 µl	25 µl
Mes-Sa	25 µl; 50 µl	10 µl	25 µl; 100 µl
Mes-Sa B1	25 µl	25 µl	100 µl
Dx5	25 µl	10 µl	25 µl; 100 µl
KB-3-1	5 µl; 25 µl		
KB-V1			5 µl; 25 µl
MDCK II	5 µl		
MDCK II B1			5 µl

4.1.3.3. Compound registry

To conduct the HTS fluently, incoming compounds were registered in a systematic way. We created a database, where the amount of compounds, disposition of powders/solutions, etc. were stored, to make them easily accessible for testing. Structural information was also entered, which was connected to the Instant JChem software (ChemAxon Ltd.), allowing structural search for uniqueness identification of new molecules (Figure 17).

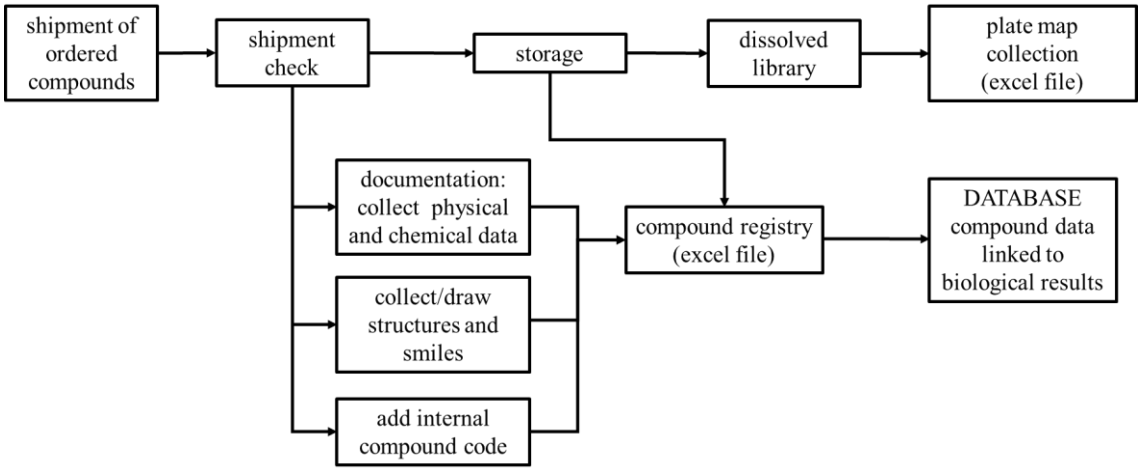

Figure 17. Flow chart of compound registry. Upon compound arrival, all physical and chemical data (e.g. amount of compounds, or structures as smiles) were collected and entered to an excel file, where an internal code was assigned to each compound. The compound registry was uploaded to a database, which stored and matched the corresponding biological data. The plate map collection stores the data of the dissolved compounds (e.g. place of storage or concentration).

4.1.3.4. Automated raw data processing

The automation of liquid handling in primary, confirmatory and secondary screening, and the throughput increment lead to an increasing amount of raw data to process. The solution for the "data boom" relied on our custom made *in house* software that read and processed the raw data files from the microplate reader (written by Judit Sessler). When the automated GI_{50} calculations were compared to the individual curve fitting by GraphPad Prism with a compound set of 80, the differences were negligible (Appendix 3), thus we considered the automated technique reliable. The growth inhibition values were stored in the same database where the compounds were registered, thus linking biological data to chemical features were also available.

4.1.3.5. Optimization of fluorescent protein based cytotoxicity screening with mCherry expressing uterine sarcoma cell lines

For compound screening we worked predominantly with the uterine sarcoma cell line pair Mes-Sa and Dx5, both transfected with mCherry fluorescent protein. Mes-Sa and Dx5 cells are easier to handle compared to other cell line pairs we used, and the fluorescence of mCherry did not interfere with the fluorescence of the calcein dye, that is commonly used to check the distribution of P-gp expression in a cell population [144].

In the preparatory phase, several cell lines were created with different levels of fluorescent protein expression, partly as a consequence of lentiviral transfection optimization, as the virus titer (based on the efficiency of transfection) can be different for each cell lines, and partly because the sufficient fluorescent protein level in the cytoplasm that is required for reliable detection of cell mass with the EnSpire plate reader was unknown. Thus, we characterized initially 3 mCherry expressing cell lines, Mes-Sa mCherry, and 2 variants of Dx5 mCherry, one with low and one with higher fluorescent protein expression, in order to choose the appropriate fluorescent protein level. (Dx5 cells with low and high expression profile were created by 4-fold difference in the amount of viruses used for transfection; Table 4). All the 3 cell lines were expressing mCherry stably and homogenously (Figure 18/A). We investigated if the lentiviral transduction of mCherry induced any change in the P-gp expression of the cell lines. Therefore, we performed a calcein uptake assay [144]. Mes-Sa mCherry accumulated the calcein dye, which was unaffected when verapamil was present, showing that Mes-Sa remained P-gp negative (Figure 18/B). Dx5 mCherry variants were extruding most of the non-fluorescent

calcein-AM, preventing its intracellular cleavage to the fluorescent calcein form, while in the presence of verapamil, calcein-AM accumulation was restored (Figure 18/C and D).

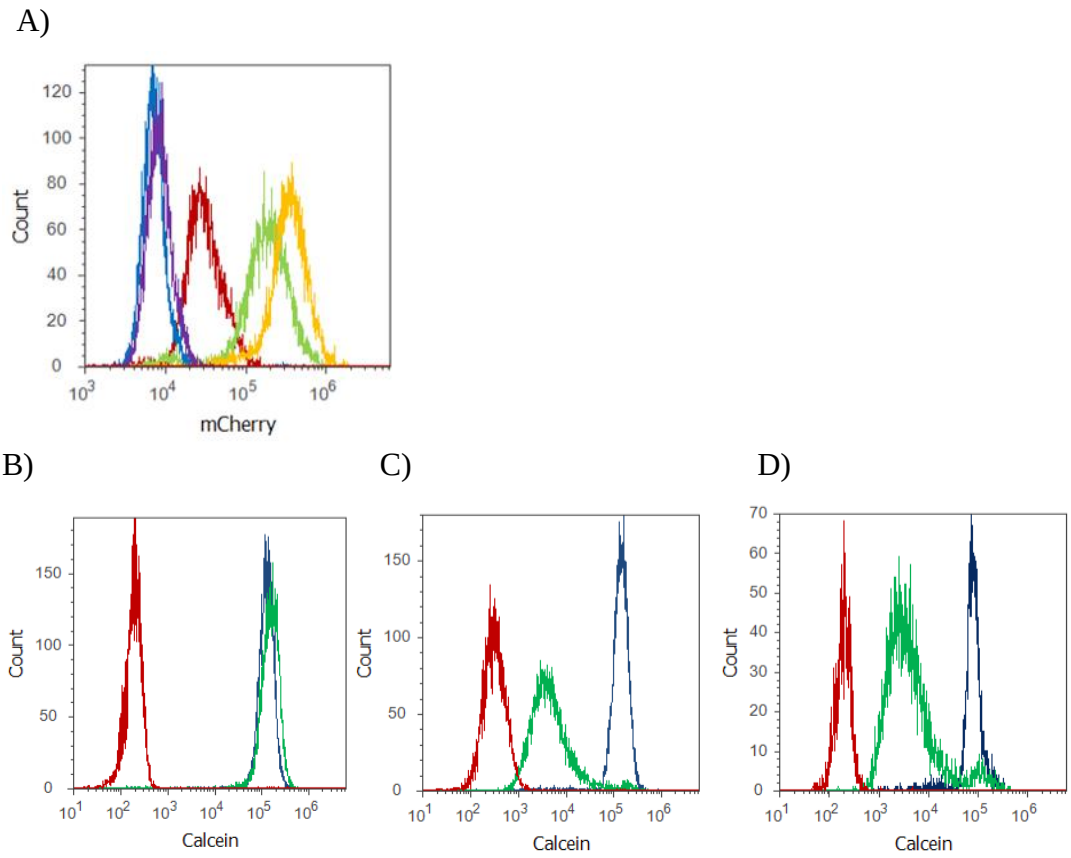

Figure 18. A) Fluorescent intensity of mCherry expressing Mes-Sa (yellow) and two variants of Dx5 mCh (green and red). Control cells were non-fluorescent Mes-Sa (purple) and Dx5 (blue). Calcein-AM efflux assay of (B) Mes-Sa mCh and (C, D) Dx5 mCh cells (higher mCherry expressing variant on panel C and the faint variant on panel D), graphs show unstained cells (red), calcein-AM treated cells (green) and calcein-AM treated cells pre-incubated with verapamil (blue).

After proving that the automated pipetting did not do any harm to the cell lines (Appendix 5), we had to optimize the plate reading protocols regarding to the special characteristics of the fluorescent proteins and of the cell lines expressing them. The first set of the fluorescent based cytotoxicity experiments - such as the first screening - were conducted on 96 well plates. During the fluorescent assay development measuring mCherry we created 3 different plate reader protocols for the 96 well plate layouts.

In the beginning, we used two microplate reader protocols, where flash number, which refers to the duration of the measurement, was set to 1000 or 1250 flashes to see the effect

of measuring time. Albeit the measurement with 1250 flash number showed better performance (Z'-factors), the coherence of data derived from these measurements were far from what we expected and what we observed previously during the adaption of this assay type, when DsRed2 and eGFP expressing cell lines were measured with another, filter based plate reader. Thus, after the first set of experiments, we started to examine the effect of the uneven 2D distribution of the cells on the bottom of the well, and its influence on assay reliability.

4.1.3.6. Uneven distribution of cells

When cells are seeded in 96 well plates, their distribution can change over time. For certain cell lines, uneven distribution occurs soon after attachment, and cells tend to migrate closer to the wall of the wells, which is even more pronounced in the case of outer wells. If cells proliferate during incubation time, they occupy the middle of the well only if the sides around are already confluent or even overgrown. This effect is well observed in the case of the uterine sarcoma cell lines we used (Figure 19).

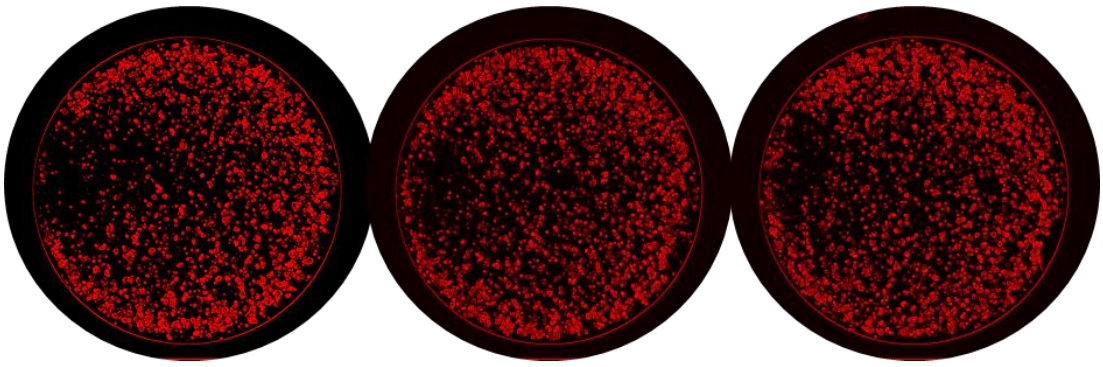

Figure 19. Distribution of Dx5 mCherry cells in a 96 well plate after 72h incubation. Images were taken with the JuLi Stage real-time fluorescent microscope (NanoEntek) by Veronika Nagy.

Because of the uneven distribution of the cells, single point measurement protocols (with 1000 or 1250 flashes), which focused the exciting light beam in the middle of the well could not measure the cell mass appropriately. By using the 'well area scan mode' available in the EnSpire reader, we could tailor our measurement protocol by choosing the scanned area and considering the special growth feature of the cell lines. Accordingly, we divided the 1250 flashes into a 5 scan points per well protocol (5x250 flashes). Four points measured cells on the side of the well and one point in the middle. The location of the 5 points and the uneven distribution of cells as a reader output is shown in Figure 20.

Distance between the points were set to 2 mm based on the morphology of the cell cultures.

A) B)

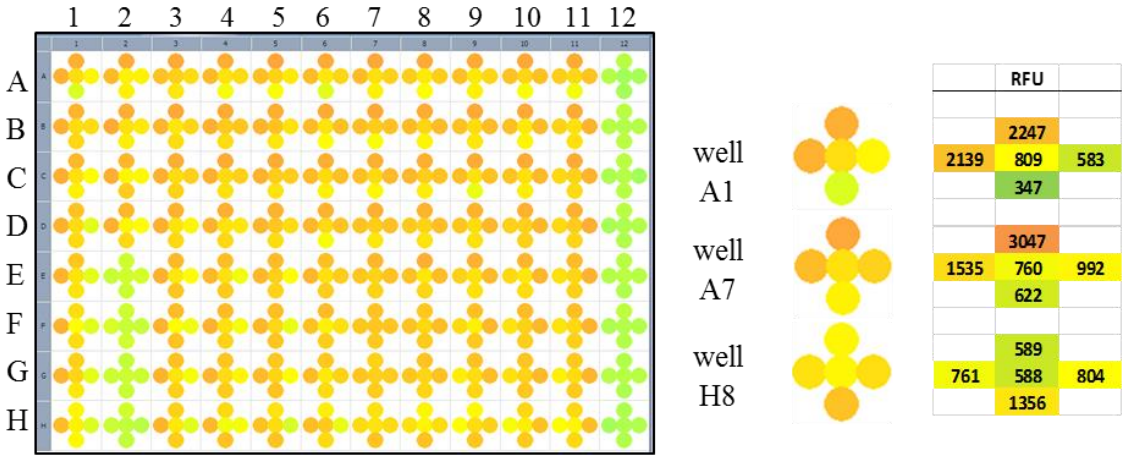

Figure 20. A) Heat map showing the distribution of Mes-Sa mCherry cells in the wells of a 96 well plate measured by the plate reader in scan mode (5 points/well) after 72h incubation time. Column 2 from well E to H and the whole column 12 is the background (dead cells). Green refers to lower fluorescence (lower cell numbers), and the more orange refers to higher fluorescence, thus higher cell density. B) Individual relative fluorescent intensity units (RFU) of the scanned points demonstrate the 2D cell distribution within wells A1, A7 and H8. Each of the 5 RFU values were measured with 250 flash numbers.

4.1.3.7. Measuring growth and growth inhibition based on mCherry detection

The technical developments of the protocol had an impact on the sensitivity of the fluorescent intensity measurements. When cell numbers of Mes-Sa mCherry and the 2 Dx5 mCherry lines were correlated to the measured intensity, better linearity was achieved with the well area scan mode (Figure 21/A; B; C). In every case, especially for Mes-Sa mCh, the coefficient of determination (R^2) was better for well area scan mode. For the low mCherry expressing Dx5 cells, the correlation was good only above 20 000 cells, which limits its usability in cytotoxicity measurements.

As the cell number correlated well with fluorescent intensity, we measured both growth and growth inhibition of the mCherry expressing cells, but we used now only the well area scan mode with 5x250 flashes. The daily mCherry measurements to acquire growth curves were performed for all the 3 mCherry expressing uterine sarcoma cell lines for 144 h. The fluorescence signal of Mes-Sa mCh and the brighter Dx5 mCh was

A) Mes-Sa mCherry

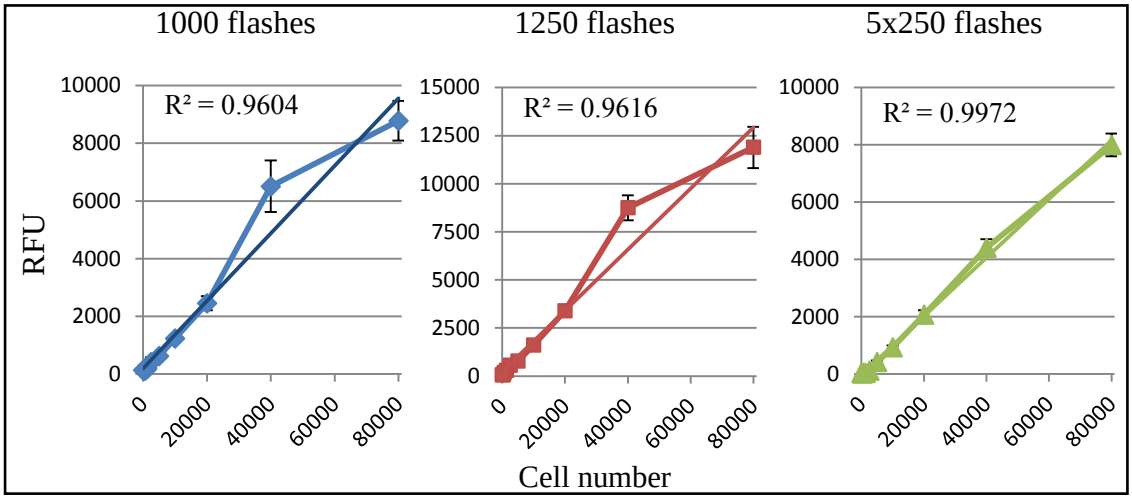

B) Dx5 mCherry (high level of mCherry)

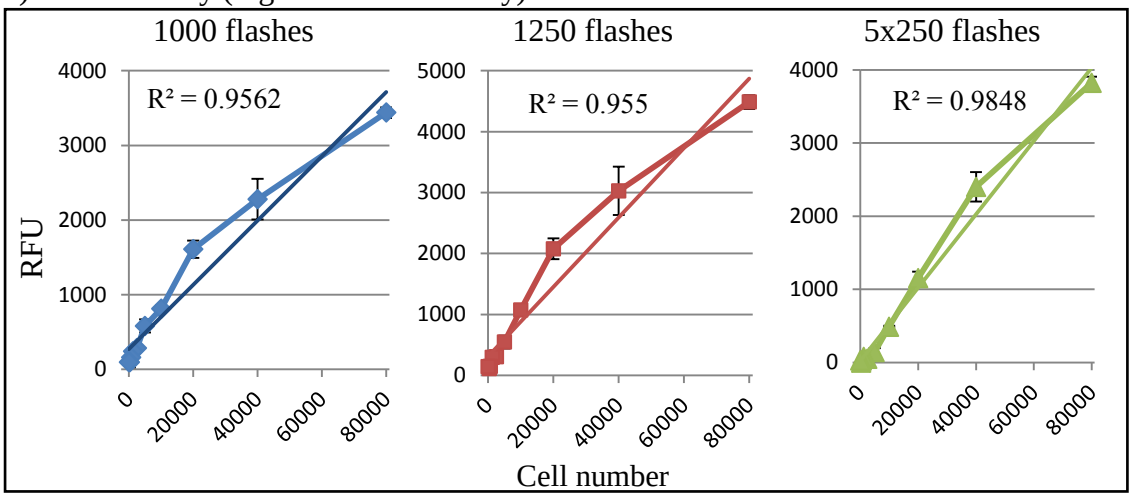

C) Dx5 mCherry (low level of mCherry)

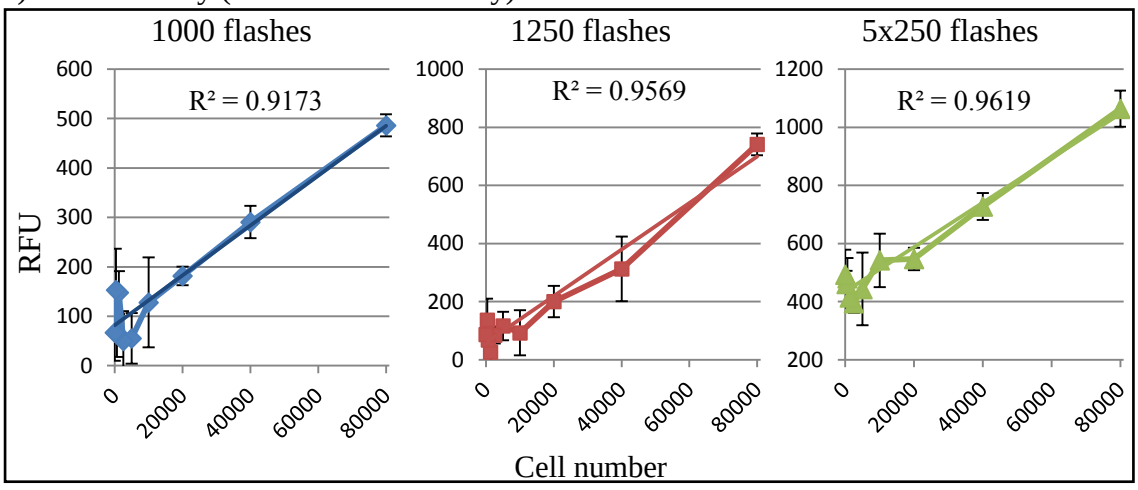

Figure 21. Correlation of the cell number to the measured fluorescent intensity and the coefficient of determination (R-squared) for A) Mes-Sa mCherry for B) highly fluorescent Dx5 mCherry and for C) faint Dx5 mCherry expressing low level of fluorescent protein. 1000, 1250 and 5x250 refers to the flash no.

continuously increasing, while the plate reader could not detect the faint Dx5 mCh cell line reliably before 72 h (Figure 22/A). (Assuming one cell division per day, cell number exceeded 20 000 cells/well only after 48 h incubation time, which is in concordance with the correlation shown in Figure 21/C). Therefore the faint Dx5 cell line with low amount of mCherry was excluded from further experiments due to our inability to follow its full growth kinetics. To compare the growth rate of mCherry positive cells to their non-fluorescent counterparts, we followed the growth also by the PrestoBlue viability reagent (Figure 22/B). For this purpose we used identically seeded plates, and each were assayed at a different day to obtain the growth curves. The proliferation of the cells were not affected by the mCherry expression, as fluorescent cell lines had identical growth rates to the 'colorless' cells. The PrestoBlue assay procedure we used was optimized for 72 h assays, and accordingly, the conversion of PrestoBlue to a highly fluorescent substrate during the 1 h incubation time saturated between 72-96 h.

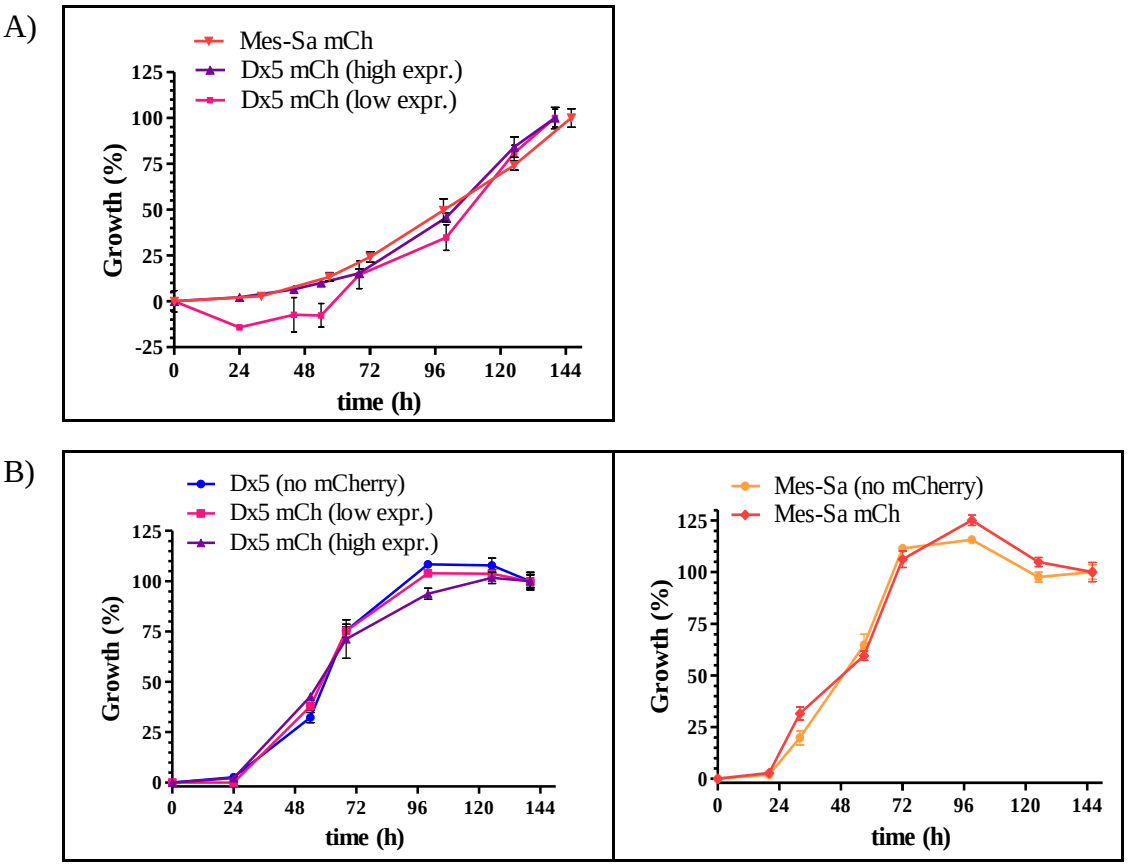

Figure 22. Following cell growth A) with the fluorescent protein based assay of mCherry expressing Mes-Sa and two Dx5 cell lines with a well area scan protocol (5x250 flashes); B) with PrestoBlue viability reagent of Dx5 and Mes-Sa cell lines. Initial cell number at 0 h was 5000 cells/well.

To investigate growth inhibition, we used both non-fluorescent and mCherry expressing cell lines, and we measured the cytotoxicity based on the fluorescent protein intensity, and also by PrestoBlue viability reagent. As test compound, we used the MDR-selective NSC693871 [98]. When after 72 h drug incubation we measured the mCherry intensity of the cells, we observed the MDR-selective behavior of the NSC693871 (Figure 23/A). The same plate was then assayed with PrestoBlue, and compared to another plate, where the same drug dilution was performed against non-fluorescent cells. The fitted dose-response curves were almost identical of the non-fluorescent cells to their fluorescent versions (Figure 23/B).

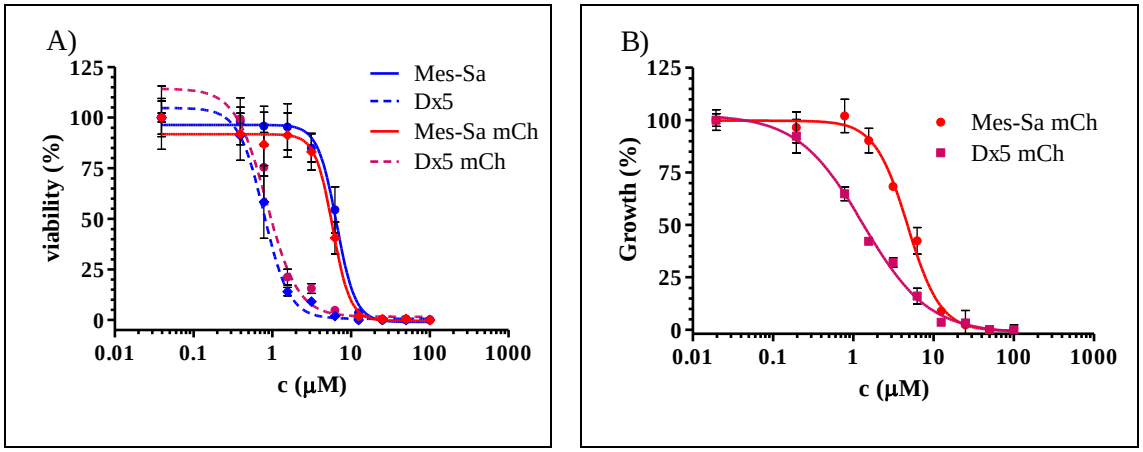

Figure 23. Cytotoxicity of NSC693871 measured after 72 h incubation A) by PrestoBlue and B) by fluorescent protein based assay (well area scan mode with 5x250 flashes).

Based on these result we concluded that the mCherry expressing uterine sarcoma cell lines fulfilled the criteria of being utilized in cytotoxicity (growth inhibition) determination of test compounds. Thus, we successfully optimized the mCherry based cytotoxicity measurements performed on 96 well plates.

4.1.3.8. Robustness of 96 well plate fluorescent assays of mCherry expressing cells

The 3 EnSpire protocol variants with 1000, 1250 or 5x250 flash numbers were consecutively developed for Mes-Sa mCh and Dx5 mCh cell mass measurements, which was based on the continuous checking of the assay robustness via the Z'-factor. Moreover, the 5x250 well area scan protocol was used twice to measure each plate: first after 72 h and then after 144 h drug incubation. As it is apparent from Figure 24 and Table 4, average Z'-factors were remarkably increasing due to the optimization steps. When 1000 flash no. was applied as a single point measurement, the average Z'-factors were above 0

for both cell lines, but interplate differences were extremely high (Z'-factors were ranging from - 0.5 to 0.84), producing many uninterpretable experiments, which needed to be repeated. Increasing the flash number, the number of scanning points and the incubation time all improved our fluorescent protein based cytotoxicity assay (Figure 24).

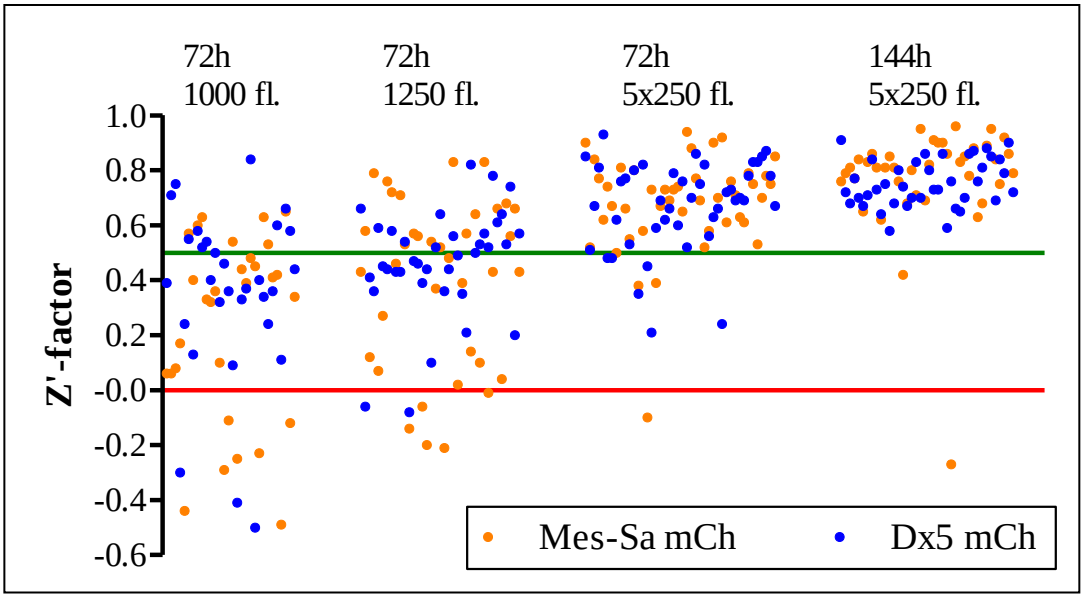

Figure 24. Individual Z'-factor values for the fluorescent protein based assay measuring mCherry. Single point detection (1000 and 1250 flashes) and well area scan (5x250 flashes) are plotted under the headings. Red line stands for the threshold of acceptable data, green line represents the preferable threshold of screening window coefficient for dose-response measurements (confirmatory and secondary steps). Tests were carried out on 96-well plates.

Table 5. Average and standard deviation of Z'-factors calculated from the fluorescent protein based measurement performed on 96-well plates.

Incubation time	Flash no.	Mes-Sa mCh	Dx5 mCh	Usability
72 h	1000	0.23 ± 0.33	0.35 ± 0.31	-
	1250	0.40 ± 0.30	0.46 ± 0.19	primary
	5x250	0.68 ± 0.18	0.67 ± 0.16	primary, (confirmatory)
144h	5x250	0.77 ± 0.20	0.75 ± 0.08	primary, confirmatory

The protocol with 1000 flash no. would not be suitable for a cytotoxicity measurement, as too many assay plates returned a Z'-factor below zero. However, a 25 % increase in measurement time (to 1250 flashes) seems to be already suitable for primary screening, as only a few individual measurements has failed to reach the acceptable level of reliability. When the same flash numbers were distributed to 5 different points within a

well, beyond an excellent yes/no type assay measurement, dose response acquisition became available. To perform the confirmatory screening with the fluorescent protein based assay on 96-well plates, 72 h measurement is reasonably reliable, but 144 h measurement is preferred, as Z'-factors keep increasing with longer incubation time, exceeding the threshold of 0.5 more securely.

As a conclusion of the optimization steps, we learned that 2D spatial distribution of the cells can influence the accuracy of fluorescent protein based assay immensely. As wells on the side of the microplate had more pronounced uneven distribution, it is recommended to avoid using them. Other factors such as the sensitivity of instruments (e.g. the sensitivity of the plate reader at certain wavelengths) or liquid handling accuracy can influence the robustness also.

4.1.3.9. Scale down of the cytotoxicity assay volume to increase compound screening throughput

We designed, optimized and successfully automated the fluorescent protein based cytotoxicity assay for 96 well plates, which was followed by primary and confirmatory compound screening of a small compound library (for the statistical characterization of the assay in 4.1.3.8, we used the control wells of the plates from the experiments presented later in point 4.3.4). In order to increase the assay throughput to screen larger compound libraries, we implemented the miniaturization of the cytotoxicity assay for 384 well plates. Preliminary experiments during optimization was carried out by using the mCherry expressing Mes-Sa cell line.

Learning from the previous optimization procedure, we checked firstly the 2D distribution of cells. The wells on a 384 well plate have a different geometry: in contrast to the circular wells of a 96 well plate, wells of the 384 well plate are square shaped with rounded corners. Not surprisingly, also on the 384 well plates cells tend to migrate and grow close to the wall of the wells after attachment. We observed also intraplate differences. Cells in wells that are in the middle of the plate proliferated by the well's wall in equal distribution (the gradient of cell mass was increasing to every direction from the middle of the well equally), while cells that were seeded in a side well (that is by the edge of a plate) migrated more likely to that wall or corner of the well, which is not in connection with other wells (Figure 25). As the middle of the wells were almost

unpopulated in every part of the plate, we set a 4 point scanning protocol (4x250 flashes) with 1.75 mm distance between the points, where the highest cell density was expected (the diameter of the well is 3 mm).

A)

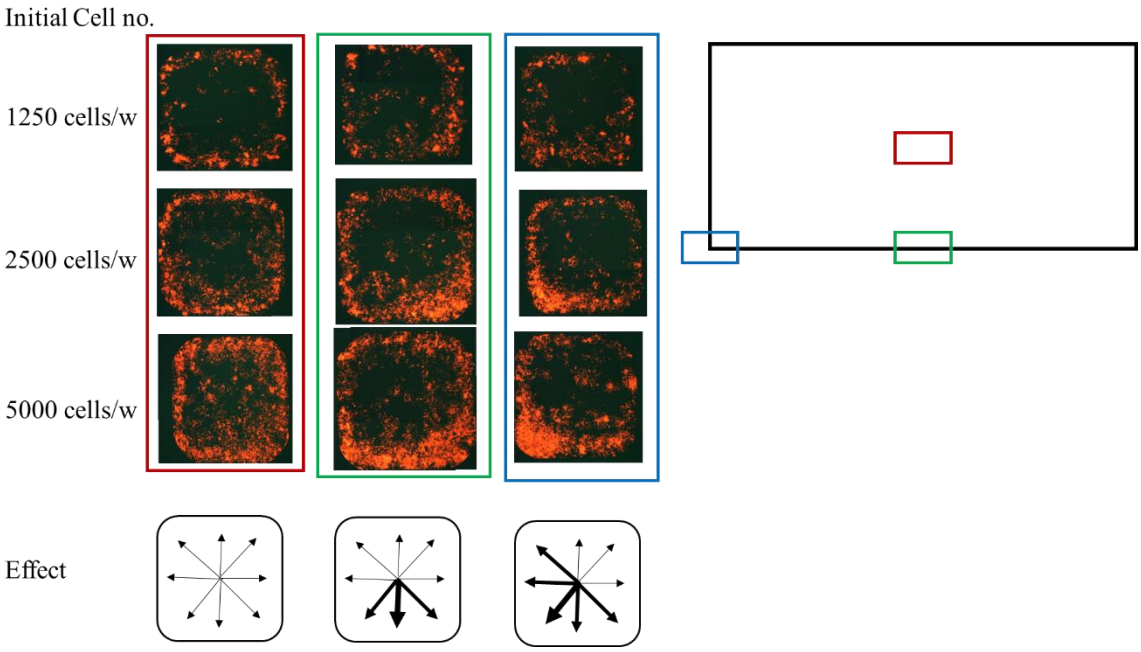

B)

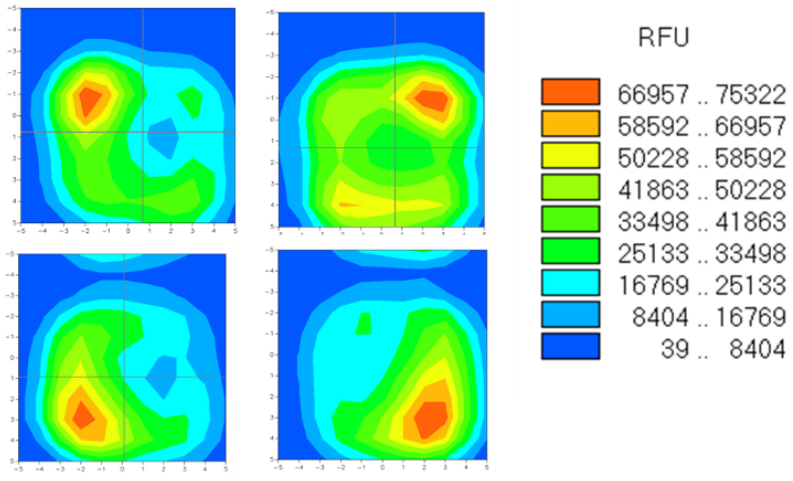

Figure 25. A) Mes-Sa mCherry cells with various initial cell no. imaged by a fluorescent microscope after 72 h incubation. Red, green and blue rectangles refer to the intraplate position of the imaged wells. Effect refers to the observed gradient of cell mass. B) Heat map of Mes-Sa mCherry cells in the 4 corner wells (marked with blue in panel A), scanned and visualized by the Perkin EnSpire microplate reader.

In the next step, we optimized the initial cell number. Theoretically, the optimal initial cell number for Mes-Sa mCherry would be 1250 cells/well, as the area of one well on the 384 well plate is approx. ¼ of the area of a well on a 96 well plate, where we seeded 5000 cells/well. Thus, we examined the growth characteristic of 3 different initial cell numbers, 625-, 1250-, and 2500 cells/well. When half amount of the expected initial cell number was seeded (625 cells/well), the confluency of the well after 120 h was still very poor, that is apparent also from the RFU values (Figure 26/A). Interestingly, when 1250 cells/well were seeded, cell density was still not sufficient, as seen at 72 h, and the growth did not start to saturate until 120 h. The 2500 cells/well setting returned a better confluency after 72 h, and we observed that the growth followed the well-known logistic equation.

For the initial cell number optimization, cells were seeded and followed in 60 µl of medium. We investigated also, if the change in the final volume is influencing cell growth. Thus, we designed a plate layout, where 2500 cells/well (Mes-Sa mCherry) were kept in 40-, 60-, or 80 µl of medium. By following cell growth for 120 h, we didn't notice any difference in the proliferation rates (Figure 26/B). For practical reasons, we decided to keep using the 60 µl of final volume.

However, what we observed during these preliminary experiments was the non-negligible effect of the evaporation of medium from the 384 well plate, especially from the outer rows and columns of wells, which was visible also by eye. Thus, we compared cell growth also by dividing the microplate into 3 parts: (1) the outer wells, which are on the edge of the plate, (2) the wells in the second rows/columns and (3) inner wells (the rectangle defined by the wells C3-N3-C22-N22). The growth rate was influenced by the extent of evaporation, as both the outer and the second row/column wells suffered variable levels of decrease in growth rates compared to the inner wells (Figure 26/C). As both medium evaporation and uneven distribution of the cells were more prominent in the outer wells, we excluded the outer and second line wells from further experiments, in favor of smaller interplate differences, and better assay robustness. However, as a positive control (dead cells), we used the second line wells in certain plate layouts (see in Appendix 2).

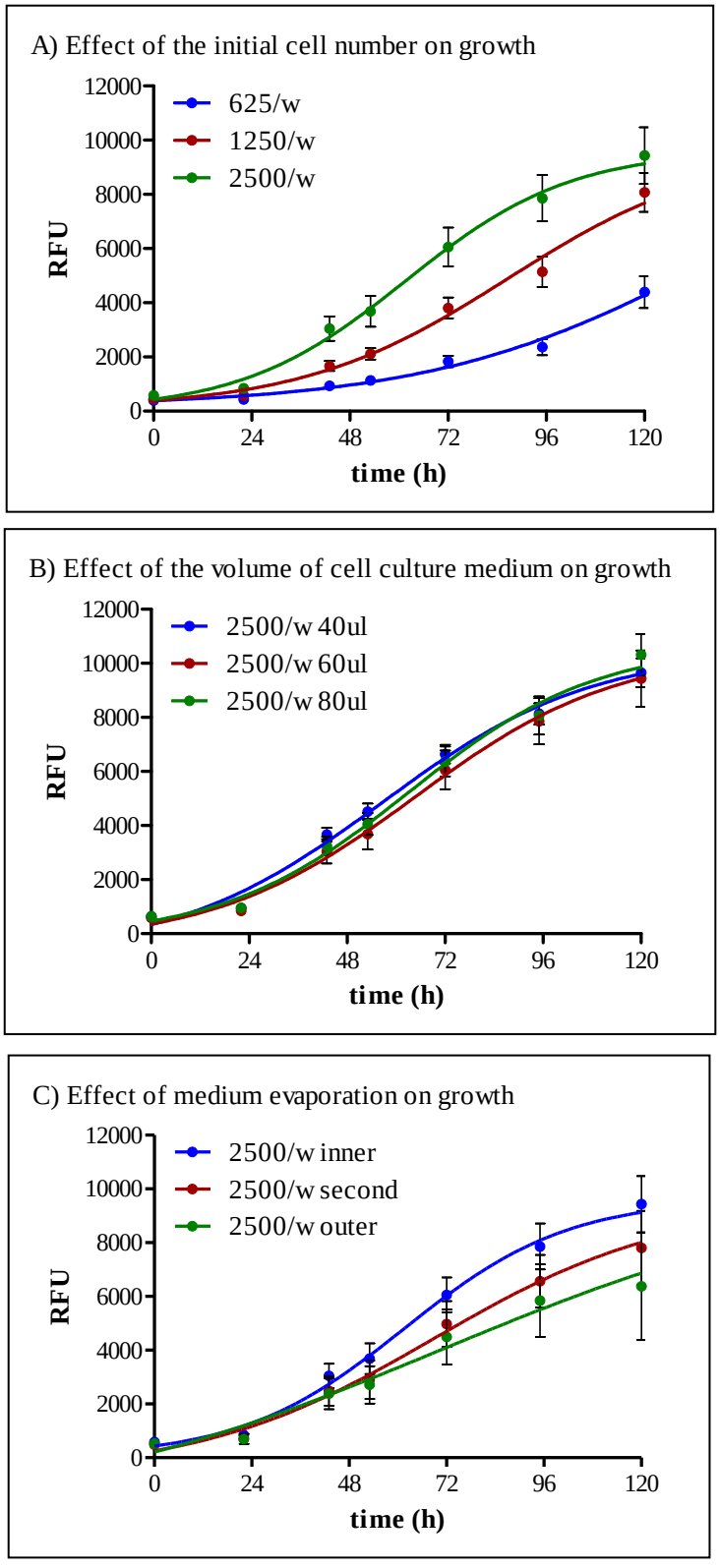

Figure 26. Growth kinetics of Mes-Sa mCherry cell line under different conditions in 384 well ('w') plates. A) Influence of the initial cell number to cell growth kinetics. B) Cell growth in different volumes of medium. C) Effect of the evaporation of medium to the growth.

After cell growth measurements, we followed the same logic as earlier, and checked the growth inhibition of the test compound NSC693871. The growth inhibition was followed daily for 144 h. At each day, the fluorescent intensity values were normalized to the control wells (complete inhibition and untreated control), and GI_{50} values were obtained (Figure 27).

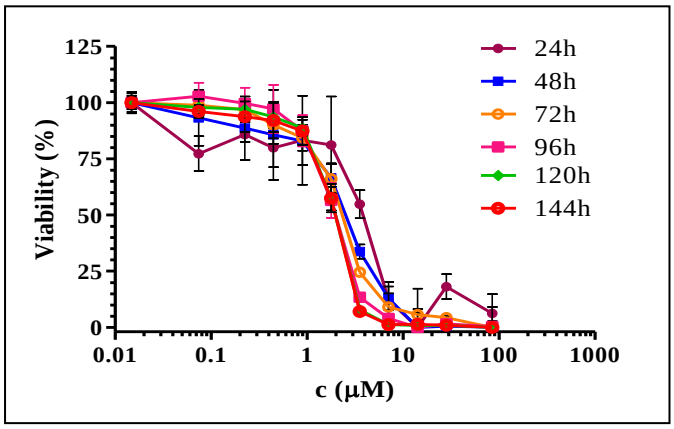

	GI_{50}	sd
24h	4.92	0.72
48h	3.59	0.40
72h	2.64	0.12
96h	2.18	0.08
120h	2.35	0.12
144h	2.29	0.11

Figure 27. Cytotoxicity of a test compound (NSC693871) against Mes-Sa mCherry on a 384 well plate, measured daily for 144 h. GI_{50} values (in μM) were obtained based on sigmoidal curve fitting, standard deviations (sd) were calculated from 8 parallel experiments.

As a conclusion, we were able to demonstrate the dose-dependent cytotoxicity of NSC693871, thus mCherry fluorescence based assay was successfully optimized for 384 well plates.

4.1.3.10. Robustnes of the fluorescent protein based assay on 384 well plates

In contrast to 96 well plate experiments, where compound testing was performed in packages concurrently to the optimization of mCherry detection (via flash number adjustments), screening of compound libraries on 384 well plates was carried out always with the same scan mode and measuring time. Thus, we examined only the incubation time dependence of the robustness. Despite the miniaturization, Z'-factor values remained acceptable (Figure 28). Measurements after 72 h incubation time returned a few individual vales below zero for Dx5 mCherry cells, while at 96 h and 144 h most of the values exceeded even the Z'-factor of 0.5. When the robustness of Mes-Sa mCherry experiments were quantified, all individual Z'-factors were above zero, regardless of the drug incubation time. Moreover, at 144 h, all the individual values calculated from Mes-Sa mCherry fluorescence intensity were above 0.5.

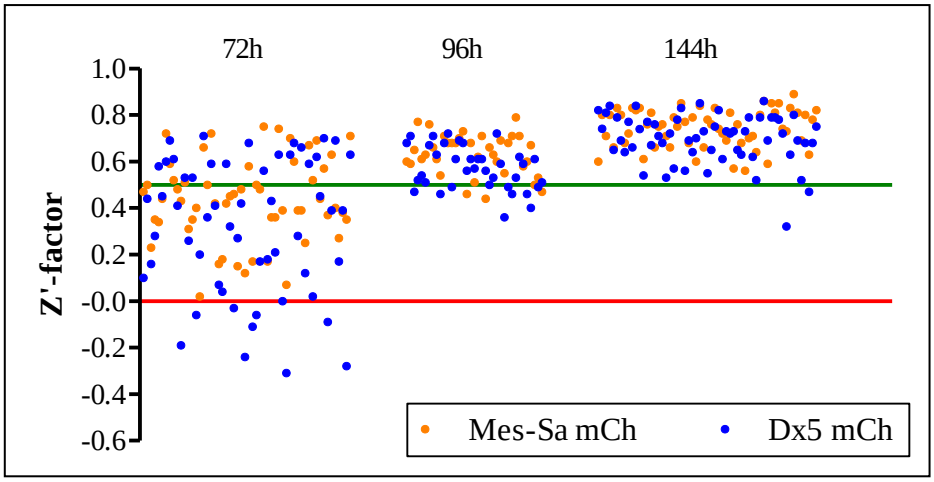

Figure 28. Individual Z'-factors calculated from the positive and negative control wells of the measured 384 well plates. Red line stands for the threshold of acceptable data, green line represents the preferable threshold of screening window coefficient for dose-response measurements (confirmatory and secondary steps); mCherry measurement was carried out by a well area scan protocol with 4x250 flashes. Data was obtained from the same plates at the different time points.

For primary screening, the toxicity against Mes-Sa mCherry cells can be measured already after 72 h, while for Dx5 mCherry cells, growth inhibitory data is better to be measured only after 96 h incubation time. For dose-dependent cytotoxicity data, 144 h incubation time is preferred prior to detection for both cell lines. Average Z'-factor values for 72-, 96-, and 144 h measurements with the corresponding standard deviations are compiled in Table 6.

Table 6. Average Z'-factors from 384w plates, and the possible usability of the assay.

Incubation time	Mes-Sa mCh	Dx5 mCh	Usability
72 h	0.43 ± 0.18	0.32 ± 0.29	(primary)
96 h	0.64 ± 0.09	0.57 ± 0.09	primary, (confirmatory)
144 h	0.75 ± 0.08	0.70 ± 0.10	primary, confirmatory

4.1.3.11. Probing other fluorescent proteins in the cytotoxicity assay

In a set of experiments (not included in this thesis), we measured cytotoxicity data against 3 fluorescent cell lines. Each cell line expressed a different fluorescent protein in their cytoplasm, which was either mCherry, mOrange or eGFP (Table 7). The detection of

fluorescence strongly depends on the level of the fluorescent proteins in the cytoplasm, although other factors also play an important role. Such factors are the brightness and quantum yield of the fluorescent proteins. The quantum yield (QY) indicates the proportion of the energy that is emitted by the fluorophore after absorption. Brightness is the product of QY and the molar extinction coefficient, where the coefficient is defined as the quantity of light (at a given wavelength) that can be absorbed. Additionally, excitation energy is also a determinant factor of the fluorescence detection. Albeit the lamp power is not adjustable for the measurements with the EnSpire reader, due to an unfortunate event, the xenon flash broke, and had to be replaced. The new lamp performed with higher energy, whereupon the Z'-factor values of mCherry detections changed, and dose-response acquisition became available already after 72 h incubation (Table 7). The Z'-factors of mOrange and eGFP measurements were also considerably above 0.5 at each measured time point, thus were suitable for confirmatory screening of compounds.

Table 7. Z'-factors of the fluorescent protein based assays after 72-, 96-, and 144 h drug incubation time. Flash no. refers to the measurement time in the well area scan mode. Brightness and QY (quantum yield) are quality metrics of the fluorescent proteins, and were taken from [145] [146] [147].

Cell line		Mes-Sa	Mes-Sa B1	Dx5
Fluorescent protein		mCherry	mOrange	eGFP
Flash no.		4x250	4x200	4x100
Brightness		15.8	34.8	33.6
QY		0.22	0.6	0.6
Z'-fact. at	72h	0.69 ± 0.12	0.72 ± 0.12	0.75 ± 0.11
	96h	0.78 ± 0.11	0.78 ± 0.11	0.84 ± 0.11
	144h	0.85 ± 0.09	0.77 ± 0.12	0.87 ± 0.10

As a summary of the results introduced in 4.1, we were able to adapt a fluorescent protein based cytotoxicity assay, which is based on the linear correlation of the cell number and the measured fluorescent intensity. We successfully involved various cell lines with different fluorescent protein expressions, and investigated the impact of mCherry expression levels to the detection of fluorescent cells in the case of Dx5 mCherry cell

line. The cytotoxicity assay was automated for both 96 and 384 well plates, and the primary and confirmatory steps from the 3 step screening algorithm was designed to rely on this assay type. As a main conclusion of the optimization of the fluorescent protein based assay, we learned the importance to follow assay robustness via the Z'-factor during the series of experiments. As demonstrated, the robustness of the cytotoxicity assay is the function of the 2D distribution of the cells, the incubation time and the duration of measurements (flash no.), which all need to be considered and set before actual compound screening campaigns start.

4.2. Identification and validation of MDR-selective compounds

As a major aim (objective #2 and #3), we wanted to increase the number and the potency of MDR-selective compounds. To reach the goals, our strategy required the identification of chemotypes, which are associated to MDR-selectivity, and which can be the basis of focused library design, assembled by structural congeners.

As the introduction/development of the fluorescent protein based assay and the implementation of the screening system went in parallel to cytotoxicity testing, several experiments, conducted in an earlier phase, were performed only manually, and in some cases, non-fluorescent cell lines were used predominantly. These experiments can be considered as secondary screening without prior primary or confirmatory steps.

4.2.1. Delineating cell line specificity of compounds reported to show collateral sensitivity

Our #2A objective was to catalogue, test and verify the MDR-selective toxicity of several reported substances, and identify the structures, which are associated to robust P-gp potentiated hypertoxicity. Therefore, we compiled a diverse cell line panel to probe these putative MDR-selective agents that were reported to kill P-gp overexpressing cancer cells in a preferential manner. The cell line set was comprised of two drug selected lines, the vinblastine treated KB-V1 cell line and the doxorubicin resistant Dx5 with their parental counterparts KB-3-1 and Mes-Sa, respectively. KB-3-1- and its P-gp expressing resistant derivatives were commonly used in studies dealing with collateral sensitivity in cancer (see in 1.3.2 and in 1.3.3), while Mes-Sa and Dx5 constitute a good model cell line pair to investigate MDR modulations [148]. Thus, the contribution of functional P-gp to the provoked hypertoxicity was investigated also by using Mes-Sa and Dx5 cells, when compounds were co-incubated with the specific P-gp inhibitors tariquidar or PSC833.

Additionally, we used an MDCK II cell line transfected with human P-gp to determine, if the transporter expression itself is sufficient to convey the hypertoxic effect compared to the parental MDCK II. The list of the compounds that we tested and their respective IC_{50} values are listed in Table 8 and Table 9. Average selectivity ratios (SR, $IC_{50\ parental}$ / $IC_{50\ MDR}$) are also shown in the tables.

Table 8. Cytotoxicity (IC_{50} in μM) against KB-3-1, KB-V1 and MDCK II cell lines of compounds that were identified previously to elicit collateral sensitivity. Viability was assessed by PrestoBlue reagent. *, P < 0.05; **, P < 0.01. SR stands for selectivity ratio; TEDB is the abbreviation of 6,8,8-triethyldesmosdumotin B.

Compound	KB-3-1	KB-V1	SR	MDCK II	MDCK II B1	SR
Verapamil	55.2	69.5	0.8	52.6	43.6	1.2
Reversin121	>>150	>>150	-	>>150	>>150	-
TritonX-100	55.4	47.8	1.2	73.7	97.6	0.8
TEDB	198	100	2.0**	>>200	>>200	-
4'-Me-TEDB	26.4	14.6	2.1*	97.4	96.6	1.0
4'-Et-TEDB	13.0	7.7	1.7*	>>200	>200	-
Pluronic P85	126	129	1.0	80.7	93.4	0.9
Dp44mT	0.071	0.055	1.4	0.0035	0.0026	1.3
Rotenone	0.136	0.136	1.1	0.150	0.115	1.4
KP772	64.0	12.2	7.0**	6.6	4.0	1.6*

Table 9. Cytotoxicity (IC_{50} in μM) against Mes-Sa and Dx5 cell lines of compounds that were identified previously to elicit collateral sensitivity. Viability was assessed by PrestoBlue reagent. (i): P-gp inhibitor tariquidar (t) or PSC833 (p).*, P < 0.05; **, P < 0.01. SR stands for selectivity ratio; TEDB is the abbreviation of 6,8,8-triethyldesmosdumotin B.

Compound	Mes-Sa	Dx5	SR	Mes-Sa (i)	Dx5 (i)	SR (i)
Verapamil	49.4	33.2	1.5**	30.2	17.7	1.7**$^{(t)}$
Reversin121	131.0	13.0	10.8**	95.4	12.3	7.6**$^{(t)}$
TritonX-100	29.9	9.3	3.4**	24.2	9.9	2.6*$^{(p)}$
TEDB	91.7	67.2	1.4	-	-	-
4'-Me-TEDB	36.3	29.1	1.3	-	-	-
4'-Et-TEDB	41.5	19.9	1.9	-	-	-
Pluronic P85	45.9	49.1	1.0	-	-	-
Dp44mT	0.045	0.019	2.7*	0.046	0.010	4.8**$^{(p)}$
Rotenone	0.090	0.078	1.2	-	-	-
KP772	4.7	1.5	3.0**	4.9	4.3	1.2$^{(t)}$

Pluronic P85 and rotenone, the two compounds that were reported to act selectively on the mitochondrial electron transport chain of MDR cells [80] [88] were equally toxic to all parental – MDR pairs. Verapamil, reversin121 and TritonX-100 were selectively toxic only to the Dx5 cell line, moreover this selectivity remained significant when the function of P-gp was blocked by inhibitors. Interestingly, these 3 agents were all reported to interact with P-gp by stimulating its ATPase activity in low (non-toxic) concentrations, and inhibiting the transport activity at higher doses [80] [82] [83]. We have found that the compounds Dp44mT and the desmosdumotin B analogues also possessed cell line specific activity in the panel we used. Dp44mT was not hypertoxic to KB-V1 cell line, which contradicts the literature data [103], and its selective toxicity to Dx5 cells has increased rather than decreased in the presence of TQ. Desmosdumotins, proposed to confer an extreme level of collateral sensitivity due to special cellular changes acquired in response to vincristine selection [84] exerted a slight but preferential toxicity only to the vinblastine selected cell line KB-V1. Only KP772, the compound that was identified by Heffeter et al. [104] and also later by the systematic study of Türk et al. [98] has shown hypertoxicity against MDR cells in the entire panel, which was P-gp-dependent, as its selective manner has vanquished in the presence of a P-gp inhibitor.

The results were unexpected, especially in the case of Dp44mT and desmosdumotins, which prompted us to investigate their selective toxicity in an extended cell line panel.

4.2.1.1. Results of the additional experiments with the thiosemicarbazone Dp44mT

In the cell panel we used for the verification of drugs having robust P-gp-mediated MDR-selectivity we included additional in vitro MDR models: the retrovirally transduced A431 and A431-B1 cells, and a cell line expressing high levels of endogenous P-gp (HCT-15), which was tested against Dp44mT also in the presence of tariquidar (Figure 29/A). Regrettably, we failed to confirm the P-gp-dependent MDR-selective toxicity of Dp44mT also with the extended panel. The collateral sensitivity that KB-V1 cells shown to Dp44mT was reported to happen through a P-gp-mediated lysosomal accumulation of the copper complex of Dp44mT, which harbors redox-activity, leading to lysosomal-membrane permeabilization and apoptosis [149]. However, as demonstrated in the literature [150], P-gp is localized primarily in the plasma membrane, and absent in the lysosomes (unless being degraded). Accordingly, when we stained the lysosomes and the P-gp of KB-V1 cells, we were unable to detect any lysosomal P-gp (Figure 29/B). The

lack of lysosomal P-gp in our cell line (and presumably in all of our MDR lines) explains why we could not reproduce the published results. Irreproducibility was probably due to the different way of vinblastine (VBL) selection of KB-V1 lines, as we used 300 nM VBL prior to the experiments, while Richardson and co-workers used 1000 nM VBL concentration [103], which resulted in such an extreme P-gp overexpression, that it appeared also in the lysosomal membrane.

A)

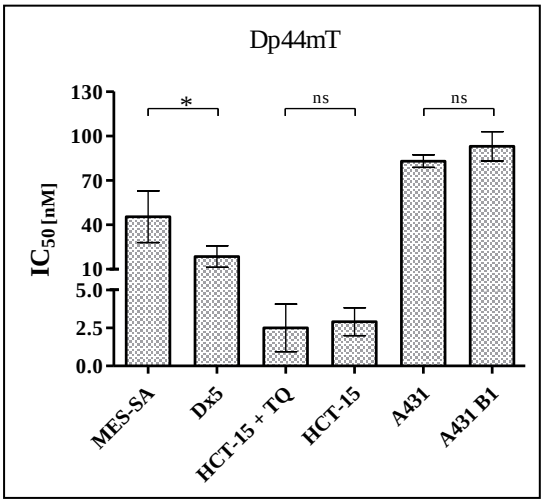

B)

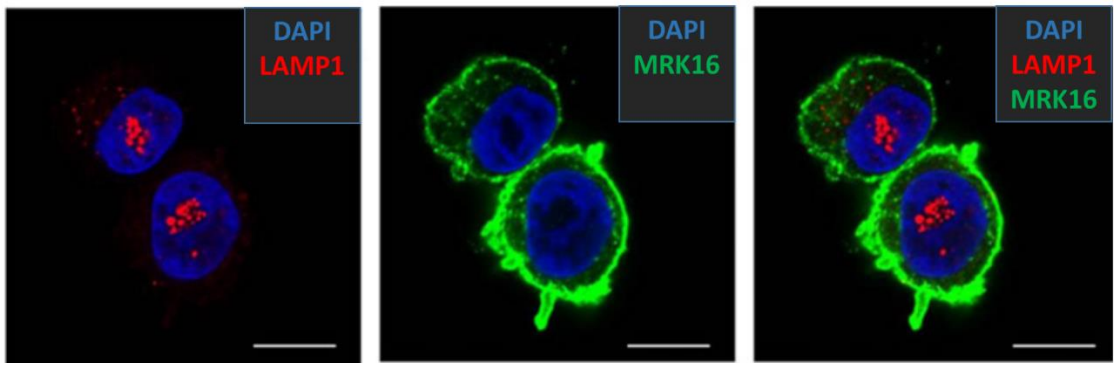

Figure 29. Additional experiments in relation with Dp44mT. A) Cytotoxicity of Dp44mT against additional cell lines. B) Confocal microscopy image of KB-V1 cells to determine the subcellular localization of P-gp (marked with the antibody MRK16, green), lysosomes (LAMP1, red) and nuclei (DAPI, blue). Scale bar, 10 μM. Figures were taken from [151].

4.2.1.2. Results of the additional experiments with the flavonoid desmosdumotin B analogues

In the case of desmosdumotins, additional cell lines were also involved to assess the extent of collateral sensitivity. We included the cell line pair that were used to identify

the selective manner of desmosdumotins, namely KB and the vincristine selected KB-VIN (Table 10). We used also the fluorescent OVC-8 and its resistant phenotype, the doxorubicin resistant NCI/ADR-RES cell line pair to test desmosdumotins (Table 11).

Table 10. IC_{50} values (in μM) of vincristine (VCR) and desmosdumotin B analogues against KB and KB-VIN cells measured by SRB assay. SR: selectivity ratio, RR: resistance ratio. ** $P < 0.01$; ns: not significant. (I) refers to P-gp inhibitor tariquidar or verapamil. TEDB: 6,8,8-triethyldesmosdumotin B.

	Nakagawa-Goto [84]				Our data						
	KB	KB-VIN	SR	RR	KB	KB-VIN	SR	RR	KB-VIN(I)	SR(I)	RR(I)
TEDB	>236	1.07	>221	-	391	230	1.7^{ns}	-	211	1.9^{ns}	-
4'-Met-TEDB	39.2	0.08	460	-	23.1	10.5	2.2^{ns}	-	11.5	2.0^{ns}	-
4'-Et-TEDB	21.9	0.07	320	-	18.2	7.75	2.3**	-	6.4	2.9**	-
VCR	0.018	8.5	-	467	0.004	0.57	-	128**	0.003	-	0.7^{ns}

The cytotoxicity of the 3 desmosdumotin analogues showed a selective tendency against KB-VIN cells, although significant selectivity was observed only in the case of 4'-Et-TEDB. Nevertheless, the selectivity ratio was much lower than expected based on the available literature data, moreover the selective manner was not sensitive to P-gp inhibition. Furthermore, the MDR cell line NCI/ADR-RES has tolerated the toxicity of desmosdumotin flavonoids significantly better than the parental OVC-8 (Table 11), resistance was approx. 2-fold, further indicating that P-gp was not inducing a general sensitivity when desmosdumotins were applied.

Table 11. IC_{50} values of vinblastine (VBL) and desmosdumotin B analogues against OVC-8 DsRed2 and NCI/ADR-RES eGFP cells measured by the fluorescent protein based assay. *$P < 0.05$; **$P < 0.01$.

		OVC-8 DsRed2	NCI/ADR-RES eGFP	SR	RR
TEDB	[μM]	15.6	36.1	0.4**	-
4'-Me-TEDB	[μM]	3.86	6.75	0.6*	-
4'-Et-TEDB	[μM]	1.86	3.4	0.5*	-
VBL	[nM]	0.0093	190.4	-	20563**

Based on the results, it is clear that the function of P-gp cannot exclusively account for the collateral sensitivity of MDR cells to desmosdumotin B analogues. In our hands, only the vinca-alkaloid resistant cells lines (KB-V1 and KB-VIN) were killed preferentially, but the effect was marginal, and was not abolished by P-gp inhibitors.

By testing the compounds reported in the literature to provoke collateral sensitivity, our aim was to identify potent MDR-selective structures, which could be further optimized by testing their congeners. Strikingly, the majority of the data published in the literature could not be reproduced. With the exception of the 1,10-phenanthroline - metal complex KP772, none of the compounds exerted a robust MDR-selective toxicity, showing increased potency only in a subset of selected MDR cells.

4.2.2. Identification of MDR-selective compounds from the DTP drug repository

In search for additional MDR-selective candidate molecules we intended to repeat the *in silico* data mining followed by *in vitro* cytotoxicity validation from the NCI DTP drug repository database. This aim (objective #2B) was based on the good hit validation ratio of a former systematic analysis by our research group [98], when several previously unknown MDR-selective agents were identified from a former (shorter) version of the database.

The DTP's database in 2010 contained the pGI_{50} values of 49169 compounds, which was a 13 % increase to 2007, when the previous data mining took place [98]. Due to the extension of the database (by retesting already existing entries and inserting new compounds), the number of missing data (NA) per compound had slightly decreased, in 2007 there were 9.2 NA/compound, while in 2010 it was reduced to 7.8 NA/compound (from the maximum of 60 data). By performing the Pearson's correlation, 224 hits returned a strong positive association between drug activity and (mRNA)*MDR1* level (r_p > 0.4). The consecutive filters (see algorithm in 3.1.), that removed hits with unreliable correlation coefficient reduced the number of candidate compounds to 80, of which 61 compounds were already identified and published from the data mining from the release of 2007. Of the 19 newly identified in silico hits, only 14 were made available by DTP, and we could purchase an additional hit from commercial sources. There were 4 remaining compounds, that neither DTP nor vendors could provide to us, thus were termed 'not available' compounds. Pearson correlation of the 19 hits are shown in Appendix 6.

4.2.2.1. Systematic in vitro cytotoxicity testing of the newly identified MDR-selective candidates

To characterize the in vitro cytotoxicity profile of the available, newly identified in silico hits, we used the same compilation of cell line pairs, which we used for characterizing the collateral sensitivity of reported substances (see 4.2.1), as it proved to be a useful cell panel in the validation of MDR-selectivity. As we already had approximate pGI_{50} values for each compounds from the database, no primary screening experiments were necessary. Cytotoxicity was assessed either by the conventional MTT assay or by PrestoBlue assay. Additionally, it was the first time that we applied the fluorescent protein based cytotoxicity measurements with OVC-8 DsRed2 and NCI/ADR-RES eGFP cell lines to test a compound set (and the usability of this novel kind of assay at the same time).

Not available compounds (NSC609800, NSC748494, NSC726708 and NSC740464) were excluded from the following cytotoxicity tables (Table 12-13-14). NSC716771 was also not available, results for KB-3-1 and KB-V1 cell lines – measured by MTT assay – were taken from [100], and were inserted to Table 13. The compounds NSC627452 and NSC733435 did not show cytotoxic effect (up to 100 μM) to any of the cell lines, thus they do not appear in the tables either. The obtained MDR-selective candidate compound set was supplemented with the control compounds NSC73306 and NSC693871, which were reported earlier [98].

Results against OVC-8 DsRed2 and NCI/ADR-RES eGFP cell lines, performed with manual pipetting on 96 well plates, are shown in Table 12. NSC79544 had a strong fluorescence, which interfered with both DsRed2 and eGFP measurements, thus we were unable to detect its cell growth inhibitory potential. The control compounds NSC73306 and NSC693871 were significantly more toxic to the MDR phenotype both at 72 h and at 144 h, as expected. Of the newly returned hit compounds (hits from the 2010R but not from the 2007R), a greater part (7 compounds) was selectively toxic to the MDR-subline NCI/ADR-RES eGFP both after 72 h and after 144 h incubation time. Four compounds killed the MDR cell line preferentially with a significant selectivity only at 144 h but not at 72 h. There was only one compound (NSC67090) that was not significantly more toxic to the drug resistant line.

Table 12. Half maximal growth inhibition values (GI_{50} in μM) and selectivity ratios (SR) measured against OVC-8 DsRed2 and NCI/ADR-RES eGFP cells at 72 h and at 144 h. All values were derived from at least 3 independent experiments. SRs were significant if the GI_{50} values between the cell lines were significantly different (unpaired t-test; $P < 0.05$:*; $P < 0.01$:**). The NSC substances in bold are previously identified, robust MDR-selective compounds.

	Measured at 72 h			Measured at 144 h		
NSC code	OVC-8 DsRed2	NCI/ADR-RES eGFP	SR	OVC-8 DsRed2	NCI/ADR-RES eGFP	SR
NSC15372	38.1	9.9	3.8**	33.6	11.2	3.0**
NSC72881	3.1	2.4	1.3	6.3	3.7	1.7**
NSC297366	1.7	0.4	4.4**	1.5	0.2	8.2**
NSC1014	7.9	3.8	2.1**	8.7	3.5	2.5**
NSC57969	3.7	0.9	4.0**	4.2	0.6	6.7**
NSC693871	8.3	2.6	3.2**	9.8	1.9	5.3**
NSC48892	1.3	0.7	1.8*	1.2	0.7	1.7*
NSC79544	Fluorescent compound			Fluorescent compound		
NSC67090	1.9	1.5	1.2	1.9	1.0	1.9
NSC676735	4.2	1.8	2.3	2.9	1.2	2.4*
NSC608465	2.0	1.3	1.5**	2.6	0.9	2.8**
NSC13977	5.2	3.5	1.5**	5.7	2.7	2.1*
NSC672035	88.5	69.8	1.3	90.8	37.4	2.4**
NSC73306	4.6	2.5	1.8**	5.6	2.2	2.6**
NSC17551	9.2	5.9	1.6	9.8	3.4	2.8**

We used the MTT assay to measure cytotoxicity against KB-3-1 and KB-V1 cell lines, and when compounds were tested against MDCK II and MDCK II B1 cell lines. Results are presented in Table 13. The control compounds NSC73306 and NSC693871 exerted hypertoxicity against the MDR cell lines as expected, as so 7 of the hit compounds. All of these MDR-selective compounds were selectively toxic also to NCI/ADR-RES eGFP cell line. Cell line specific MDR-selectivity was also observed, NSC79544 killed only KB-V1 preferably, but not MDCK II B1. On the other hand, compounds NSC1014 and NSC67090 showed only MDCK II B1 selectivity. Three compounds (NSC15372, NSC72881, NSC672035) were equally toxic to KB and to MDCK cell lines, when parental cells were compared to the MDR derivative lines.

Table 13. Results of MTT assay (IC_{50} in μM and selectivity ratio-SR) of the MDR-selective candidates. Data for NSC716771 were taken from [100]. NSC compounds in bold are known MDR-selective, control agents. SRs are significant if the difference between the IC_{50} values are significant (unpaired t-test, $P < 0.05$:*; $P < 0.01$:**).

NSC code	KB-3-1	KB-V1	SR	MDCK II	MDCK II B1	SR
NSC15372	12.8	13.5	0.9	40.3	38.0	1.1
NSC72881	15.8	10.2	1.5	18.1	13.5	1.3
NSC297366	2.1	0.1	16.4**	2.8	0.3	10.0**
NSC1014	5.8	4.3	1.3	10.8	5.6	1.9**
NSC57969	8.6	0.6	14.4*	4.4	0.8	5.5**
NSC693871	13.6	2.1	6.6**	14.5	2.9	4.9**
NSC48892	3.2	1.9	1.7**	3.6	2.3	1.6**
NSC79544	2.2	0.7	3.0**	1.3	1.0	1.2
NSC67090	3.8	2.8	1.4	3.8	1.8	2.2**
NSC676735	7.2	3.4	2.1*	12.9	9.2	1.4**
NSC608465	2.6	1.0	2.5*	2.5	1.3	2.0*
NSC13977	10.5	4.3	2.4**	9.1	4.4	2.1**
NSC672035	67.7	56.8	1.2	31.4	54	0.6
NSC73306	7.5	3.7	2.2**	6.7	2.8	2.4**
NSC17551	8.7	4.5	1.9**	14.4	4.5	3.2**
NSC716771	13.1	5.8	2.3			

We tested the newly identified candidates also against Mes-Sa and Dx5 cell lines, using PrestoBlue viability reagent. To assess the contribution of functional P-glycoprotein to MDR-selectivity, we performed the experiments in the presence/absence of the 3rd generation P-gp inhibitor tariquidar (TQ). Results are presented in Table 14. The control compounds NSC73306 and NSC693871 were hypertoxic to the MDR cell line Dx5, and this toxicity decreased significantly, when drugs were co-incubated with TQ. 6 of the 7 compounds that conferred selective toxicity to the other 3 MDR cell lines (NCI/ADR-RES, KB-V1, MDCK II B1) were more toxic to Dx5 cells as well compared to its parental from. Moreover, all of these compounds lost (at least partly) their ability to kill MDR cells preferably when TQ was present and inhibited the function of ABCB1. NSC48892, the 7th compound, had a selectivity of 1.8 against the Dx5 cell line, which was just not significant at $P < 0.05$ (its probability value was 0.062 calculated from 3 independent experiments), although SR decreased to 1.3 in the presence of TQ. NSC72881 and NSC67090 exerted TQ-sensitive MDR-selectivity also. However, NSC72881 seems to

act cell line specifically, as besides Dx5 it was hypertoxic only to NCI/ADR-RES eGFP cell line, with low selectivity. Interestingly, NSC67090 acted controversially, when TQ was present, its toxicity against Dx5 remained unaffected, while it became more toxic against Mes-Sa. Two candidates (NSC15372 and NSC672035) were equally toxic to Mes-Sa and Dx5 cells (thus were not tested in the presence of TQ). NSC1014 and NSC79544 had a slight but not significant selective toxicity against Dx5 cells.

Table 14. Results of the in silico hits measured by PrestoBlue viability reagent. IC_{50} values are presented in μM. The SRs were considered significant if the IC_{50} values were statistically different (unpaired t-test, $P < 0.05$:*; $P < 0.01$:**). TQ (tariquidar): 1 μM.

NSC code	Mes-Sa	Dx5	SR	Mes-Sa(TQ)	Dx5(TQ)	SR(TQ)
NSC15372	28.3	32.8	0.8	-	-	
NSC72881	34.3	12.5	2.7**	31.4	29.7	1.1
NSC297366	2.0	0.11	17.8**	1.6	1.5	1.1
NSC1014	17.6	10.6	1.7	16.7	11.8	1.4
NSC57969	4.4	0.6	7.6**	4.6	3.5	1.3
NSC693871	4.9	1.3	3.9**	4.8	3.4	1.4
NSC48892	3.6	2.0	1.8	3.7	2.7	1.3
NSC79544	2.6	1.7	1.5	2.2	1.9	1.1
NSC67090	3.6	1.3	2.8**	2.4	1.4	1.7
NSC676735	19.5	6.1	3.2*	19.1	14.6	1.3
NSC608465	3.4	1.1	3.0*	4.8	3.3	1.5
NSC13977	7.9	3.0	2.6*	7.7	5.2	1.5
NSC672035	51.9	53.6	1.0	-	-	
NSC73306	6.8	2.9	2.3**	5.3	3.9	1.4*
NSC17551	23.0	3.7	6.3**	23.5	10.8	2.2**

By summarizing the in vitro cytotoxicity data, we could successfully verify the non-cell line specific MDR-selective toxicity of 6 candidates (NSC297366, NSC57969, NSC676735, NSC608465, NSC13977, NSC17551). All of these compounds lost their MDR-selective toxicity in the presence of TQ. The other 7 compounds were hypertoxic only to certain MDR cell lines (thus, there were no compounds that were not hypertoxic to at least one of the four MDR cell lines). The most prominent of the validated hits was the 8-hydroxy-quinoline (8-OH-Q) analogue NSC297366, which produced the highest selectivity ratios in every case.

4.2.2.2. Investigation of the structural coherence of the MDR-selective compounds

To characterize the structural coherence of the MDR-selective compounds identified from DTP database, we performed a 2D structural clustering. Compounds with a certain degree of similarity were then designated as chemotypes. Our goal with the structural clustering was to further confirm the already known MDR-selective chemotypes (from [98]), and to identify additional MDR-selective toxicity associated clusters (objective #2C). The defined chemotypes are useful to find more interesting molecules from the DTP repository or from other structural databases of APIs, which are available for purchase, leading potentially to preliminary SAR studies related to P-gp mediated hypertoxicity, as in [98]. Structural clustering was performed involving all the 19 hits that we identified from the DTP repository released in 2010. The clustering was supplemented with MDR-selective control compounds, which derive also from the DTP database, but were identified and published earlier (Figure 30). The control compounds were NSC73306, NSC693871, NSC10580, NSC168468, NSC292408 and NSC713048, all of them were selectively effective against several P-gp expressing MDR cell lines [98].

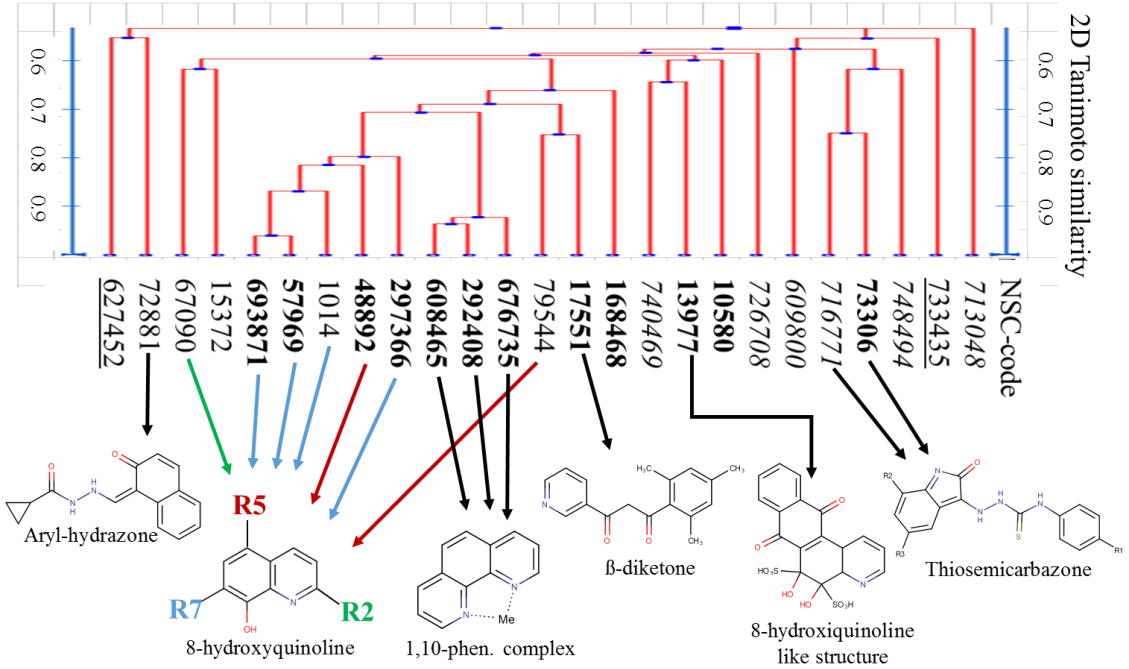

Figure 30. 2D Tanimoto Similarity of the 19 *in silico* hit compounds supplemented with MDR-selective compounds identified earlier from the DTP database [98] [140]. Compounds in italics were not available, thus not tested in vitro. Underlined compounds were tested but were not active against any of the cell lines. Compounds in bold showed robust MDR-selectivity. Arrows indicate the chemotype of the molecules (in the case of 8-hydroxyquinolines, color of the arrows indicates the respective moieties present on the core structure: green: R2-, red: R5-, blue: R7-substituents).

The MDR-selective compound set, identified from the DTP database, is abundant in 8-hydroxyquinoline (8-OH-Q) derivatives, there are six structures with this backbone. 8-OH-Qs substituted at the 5-, or 2-positions (NSC79544 and NSC48892, NSC67090) showed moderate SR values. However, certain 8-OH-Qs substituted at the 7-position seem to have higher potency (both higher selectivity and toxicity). In contrast to the less potent NSC1014, which has a bulkier residue with two aromatic rings at the 7-position, both of the two best performing hit compounds NSC57969 and NSC297366 consist only 1 ring at R7. Correspondingly, the control compound NSC693871 is structurally very similar to NSC57969, and it is also among the best performing MDR-selective molecules. The structure of NSC13977 (Alizarin Blue) contains a quinoidic system, and although it clustered separately, it resembles to a sulfonated 8-OH-Q condensed with an 1,4-naphtoquinone. Structures of 8-OH-Qs and NSC13977 are shown in Figure 31.

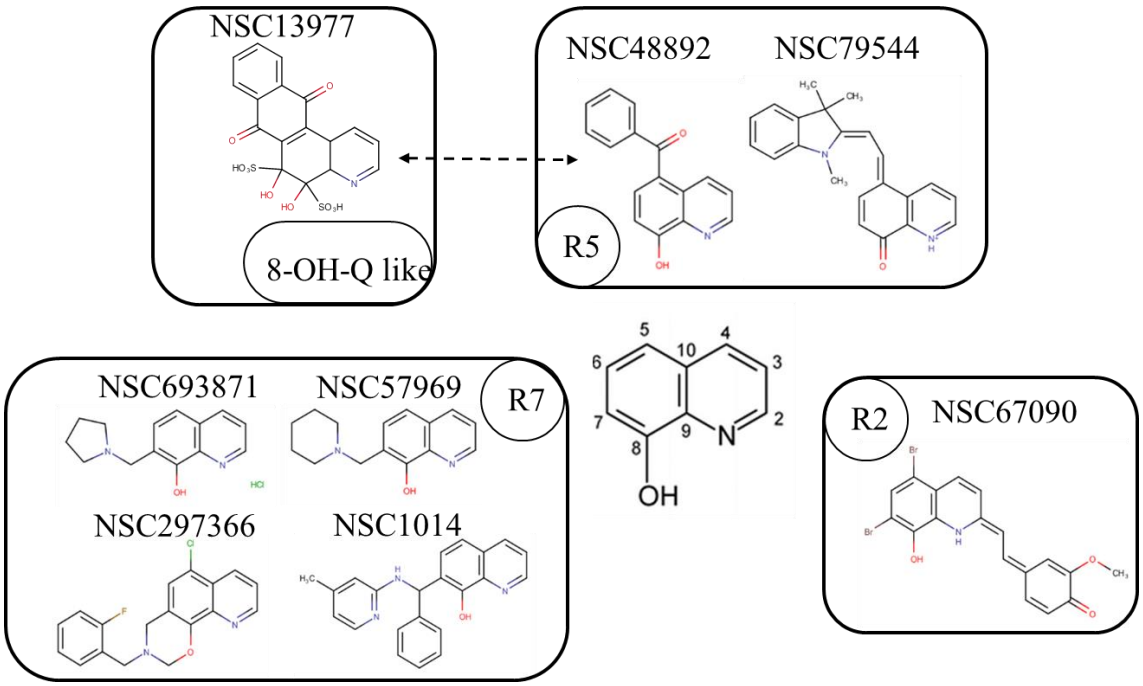

Figure 31. Structure and position numbering of the 8-OH-Q core. Structures of the 8-OH-Q derivatives are shown in the boxes according to the position of the residues (halogen atoms are not considered in this figure). NSC13977 is also sketched here, as it contains an 8-OH-Q substructure, where the aromaticity is disrupted, however with the additional connected aromatic ring system it resembles to NSC48892.

The MDR-selective toxicity of the 1,10-phenanthroline (1,10-phen) and its metal complexes was already revealed in two independent studies [98] [104]. Here, we

completed the list of MDR-selective 1,10-phens with a tin and a palladium complex, the NSC608465 and NSC676735, respectively (Figure 32). The 1,10-phen hits we identified exert robust, although moderate collateral sensitivity against MDR-cells with the highest SR of only 3.2 (NSC676735 against Mes-Sa over Dx5, Table 14).

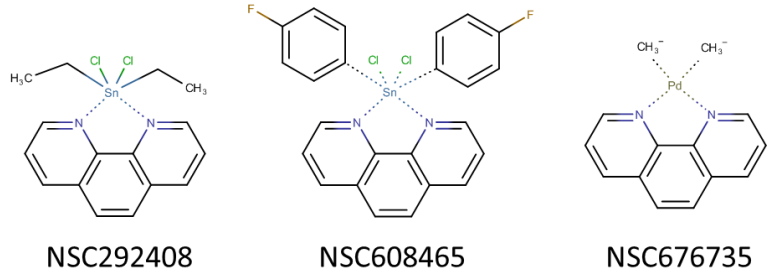

Figure 32. MDR-selective 1,10-phen complexes. NSC292408 was identified from the DTP database released in 2007, while NSC608465 and NSC676735 were found in the subsequent data mining from the DTP release in 2010.

NSC72881, a compound that seemed to show cell line specific collateral sensitivity was not clustered close to any compounds, although it resembles to the aryl-hydrazone tautomer NSC168468, which is a robust MDR-selective compound that was identified earlier (Figure 33/A). NSC17551 belongs to the group of ß-diketones, which chemotype was not associated to MDR-selectivity so far (Figure 33/B). The ß-isatin-thiosemicarbazone NSC716771, which is a close analogue of NSC73306 was not available, but its MDR-selectivity is known from the literature [100] (Figure 33/C).

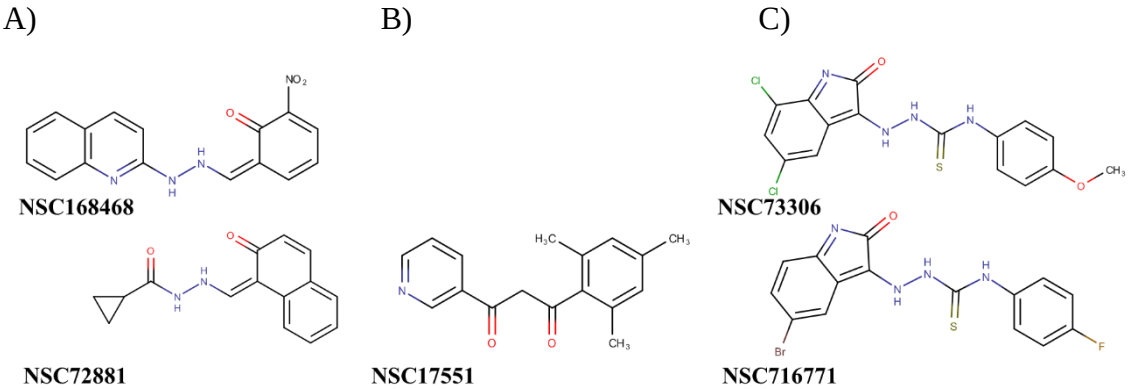

Figure 33. Structures of the MDR-selective A) arylhydrazones (NSC168468, NSC72881), B) ß-diketone (NSC17551) and C) ß-isatin TSCs (NSC73306, NSC716771).

The 4 non-available compounds are structurally diverse. NSC740469 consists a 1,4-naphtoquinone condensed to other aromatic rings, and a ß-diketone motif is also present in a tautomer form, which were present in the molecules NSC13977 and NSC17551, respectively. NSC748494, NSC726708 and the NSC609800 (which is similar to an isoflavone) are not related to the known chemotypes. Unfortunately, the putative MDR-selective toxicity of the 4 non-available compounds remains unknown (Figure 34).

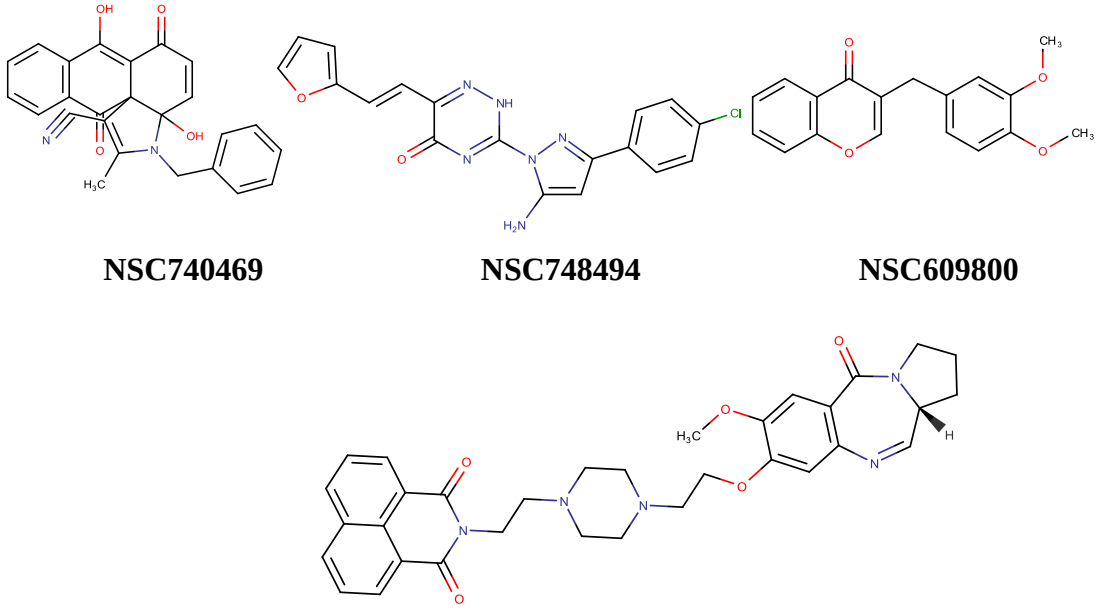

Figure 34. Non-available compounds from the in silico screening, which were not closely related to any identified MDR-selective chemotypes.

4.3. Screening of compound libraries focusing on flavonoid, TSC and 8-OH-quinoline chemotypes to explore collateral sensitivity

The establishment of the 3-step screening system created the possibility to test large amount of compounds. Based on the identified chemotypes, harboring distinct chemical features associated with MDR-selectivity, we compiled and purchased approx. 1800 compounds from commercial sources representing all the chemotypes, and 336 further structural analogues from the DTP repository were also acquired. Our compound library was enriched with additional molecules that we obtained via collaborations.

4.3.1. Primary screening of the compound collection

The investigation of the compounds (thus chemotypes) was initiated with a primary screening. 2160 molecules were tested in 10 µM and in 100 µM concentrations against Mes-Sa-mCherry and Dx5 mCherry cell lines to sort out non-toxic compounds. The

compounds were tested in 4 campaigns, firstly 756 molecules on 96 well plates, then 1404 compounds on 384 well plates in 3 parts.

Initially, when the first campaign was carried out, besides measuring the fluorescent signal of the surviving cells at 96 h, we obtained the fluorescent signal of the wells right after compound addition (which time point was considered as 0 h). This extra step served to identify inherently fluorescent molecules, as the outstanding emission of wells at this point could be addressed only to compound addition. As fluorescent molecules in the primary assay appeared as non-toxic compounds (high intensity refers to high amount of intact cells), this step was meant to reduce the number of false negatives. (Not shown here in details, but when fluorescent substances were re-tested with a counter assay, they possessed cytotoxic effect, e.g. NSC79544 was highly fluorescent, and was toxic to cells, which was revealed when MTT or PrestoBlue assays were applied, as shown in Tables 12-13-14. Similarly to fluorescent substances, such light absorbing compounds, which decrease the fluorescent signal, are also capable to interfere with the fluorescent protein based assay. As lower fluorescent signal level refers to lower cell number, this effect could produce false positive hits.

The 0 h fluorescent intensity measurement for the compounds, which were obtained from DTP and were tested in the primary screen on 96 well plates, are shown in Appendix 4. As in the 756 compound set, the number of fluorescent compounds was negligibly low, and we did not observe any initial decrease in the signal of mCherry, we stopped measuring fluorescence at 0 h, when we switched to 384 well plates, mostly to save the measurement time and the workload of the plate reader. (Moreover, perception of highly fluorescent compounds were possible also from the 96 h measurement data, as calculations returned impossibly high amount of cells).

The 96 h growth inhibition effect of the compounds measured on 384 well plates are shown in Figure 35. 38% of the compounds exerted less than 50 % GI at 100 μM against both Mes-Sa mCh and Dx5 mCh cell lines, thus were considered not toxic (NT). 5% of the compounds were selectively toxic against the parental line in at least 1 concentration (putative P-gp substrates) and 14% were killing the MDR cells preferably (putative collateral sensitivity eliciting agents). Another 14% of the compounds were toxic to both cell lines even at 10 μM.

A)

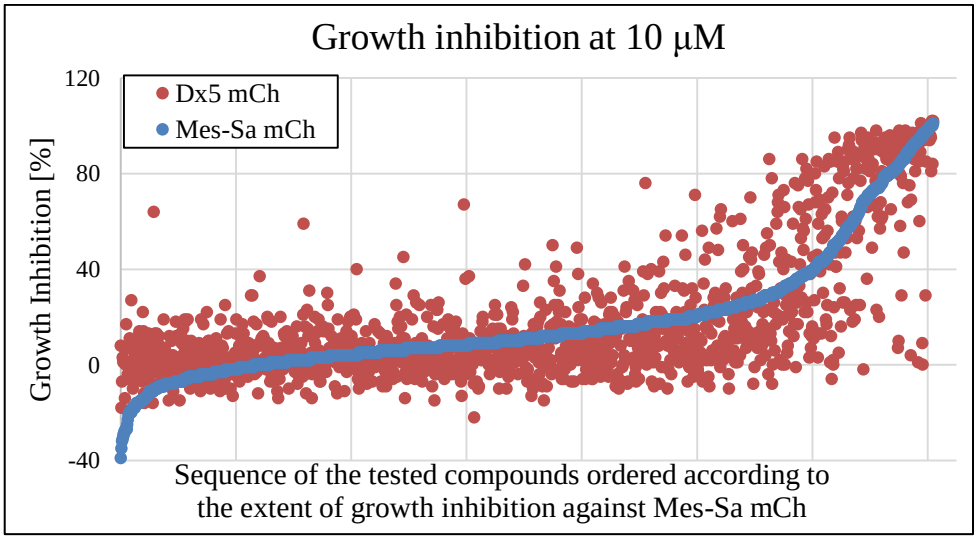

B)

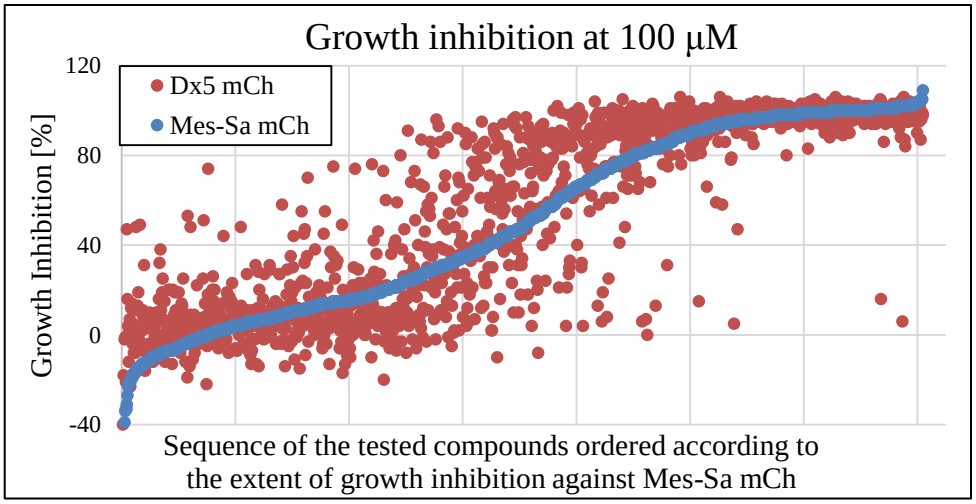

Figure 35. Growth inhibition (GI) effect of 1404 molecules tested in the primary screen on 384 well plates in A) 10 µM and in B) 100 µM drug concentrations. Each dot represents the percentage of GI exerted by a compound against a cell line. Blue dots (quasi blue line): GI values against Mes-Sa mCh cell line in ascending order, red dots: corresponding GI values against Dx5 mCh cell lines. 100 % refers to complete growth inhibition, thus effects of the most toxic substances are located in the top right corner of the graph.

4.3.2. Utilization of the screening platform to identify improved MDR-selective compounds of the 8-OH-Q chemotype

To find more potent MDR-selective agents, and to perform basic SAR studies within the designed chemical space, we intended to test the majority of the toxic compounds in a dose-dependent manner. The performed consecutive confirmatory and secondary screening is exemplified herein via the optimization of the 8-OH-Q compounds, to improve their MDR-selective potency. The library of the 8-OH-Qs were compiled from

vendors and from the DTP repository. In addition, we obtained compounds from two cooperating partners (Dr. Tibor Soós, MTA TTK; Dr. Ferenc Fülöp, SZTE) who synthesized analogues, which were not available from commercial sources. The congeners were designed of R2, R7 and R5 position substitutions (Figure 36).

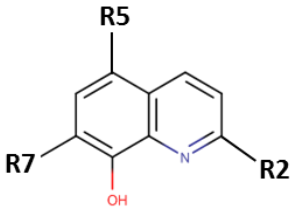

Figure 36. General formula of the compounds that are subject to the international patent application "MDR-reversing 8-hydroxy-quinoline derivatives". The core structure of the chemotype is 8-OH-Q, when R2, R5 and R7 are hydrogen atoms.

The confirmatory screening of 8-OH-Qs were conducted against the Mes-Sa mCh and Dx5 mCh cell lines on 384 well plates, where the molecules were tested in 9 concentration points. As apparent from Figure 37, there were compounds, which killed Dx5 preferably, but we found also molecules with equal toxicity to the parental and MDR cell lines, and potential P-gp substrates were also identified (some inactive compounds were designed on purpose to investigate the relevance of certain functionalities.

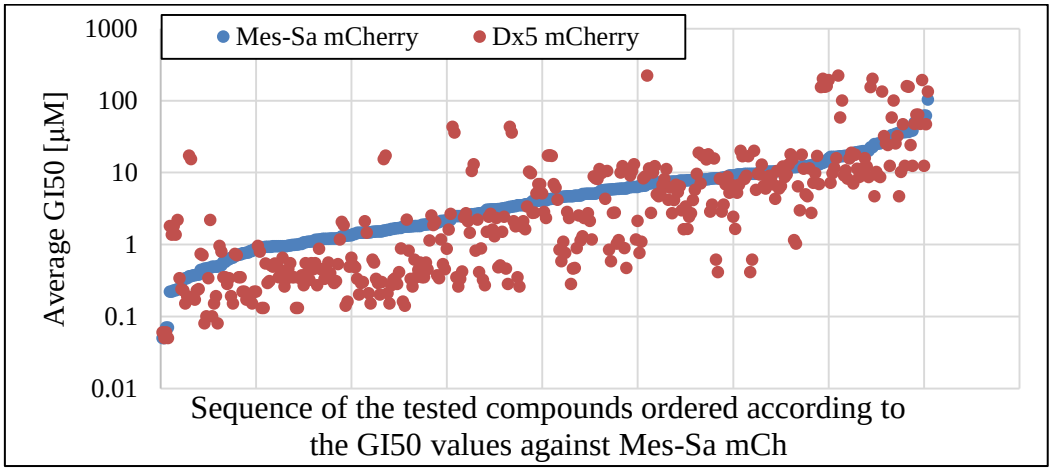

Figure 37. Confirmatory screening result of the 8-OH-Q library measured by the fluorescent protein based cytotoxicity assay. Growth inhibition effects of the tested molecules are presented as GI_{50} values, and are shown in blue for Mes-Sa mCh, and the corresponding GI_{50}s against Dx5 mCh in red. Each point represents the average GI_{50} values of a compound, which were plotted in an ascending order based on the GI_{50} values against Mes-Sa mCherry.

Those 8-OH-Qs, which showed a dose-dependent cytotoxicity (when GI_{50} values could be acquired) in the fluorescent protein based assay were passed to the secondary

screening, where drugs were tested on 96 well plates manually, and viability was assessed with PrestoBlue viability reagent, which served as a counter assay. The results for the non-fluorescent Mes-Sa and Dx5 cells are shown in Figure 38/A. Many compounds that we acquired via the collaborations, as a result of designed synthesis, entered directly to this step of testing, as primary and confirmatory screens were performed in campaigns, while synthesized compounds arrived disorderly in time. To investigate if the selective toxicity against Dx5 cells was conferred by the P-gp function, we repeated those experiments in the presence of 1 μM TQ, where drugs were possessing a significant selectivity ratio (Figure 38/B).

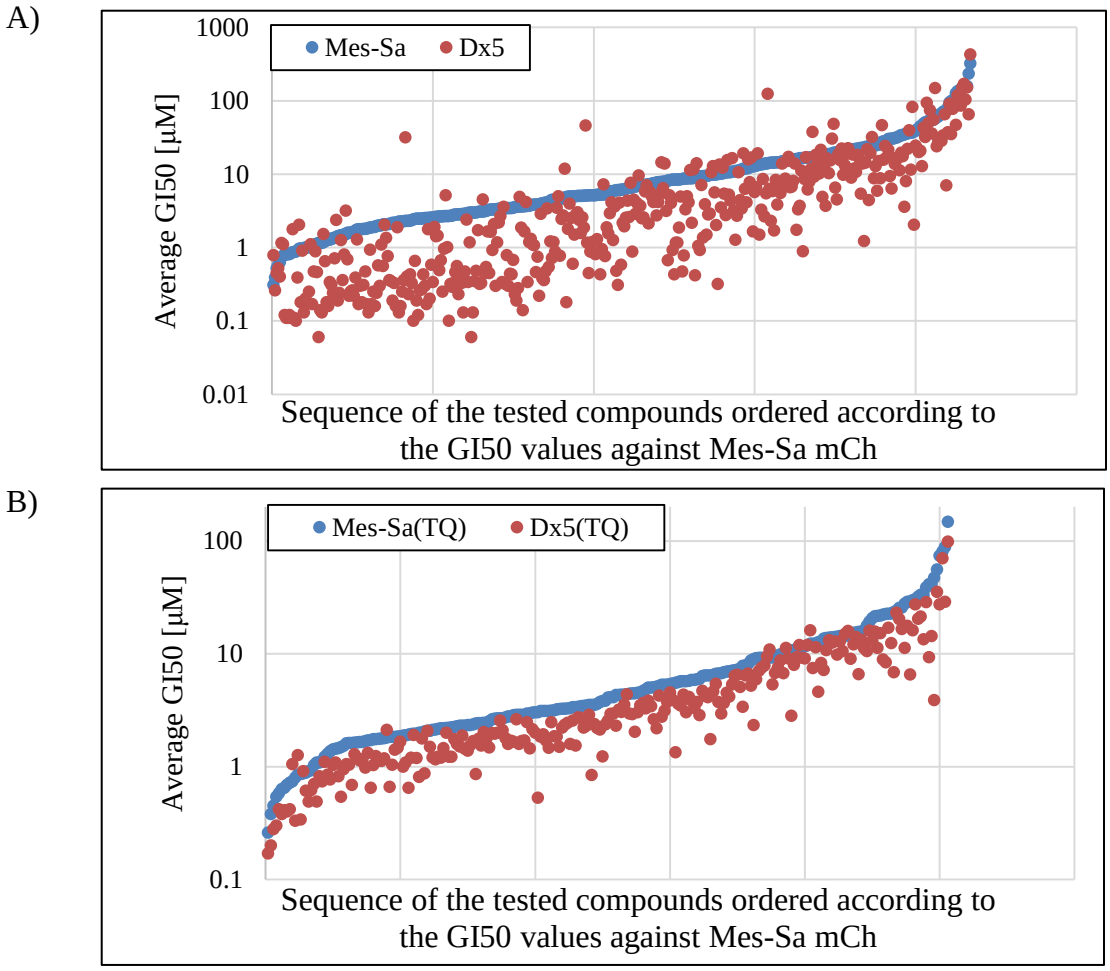

Figure 38. Cytotoxicity (IC_{50} in μM) of 8-OH-Qs against non-fluorescent Mes-Sa (blue) and Dx5 (orange) cells measured by PrestoBlue viability reagent in the (A) absence and (B) presence of 1 μM TQ, tested manually on 96 well plates. Each point represents the average IC_{50} value of a molecule, plotted in ascending order based on the IC_{50} values against the parental cell line.

As apparent from Figure 38/B, the preferential toxicity of the most 8-OH-Q analogues were conveyed by the function of P-gp, thus these compounds are verified as MDR-

selective agents. In the terms of secondary screening, the robustness of the MDR-selective cytotoxicity of a subset of molecules were tested against additional parental-MDR cell lines pairs. Results against A431 & A431-B1, KB-3-1 & KB-V1 and MDCK II & MDCK II B1 cell lines pairs are shown in Figure 39/A-B-C, respectively.

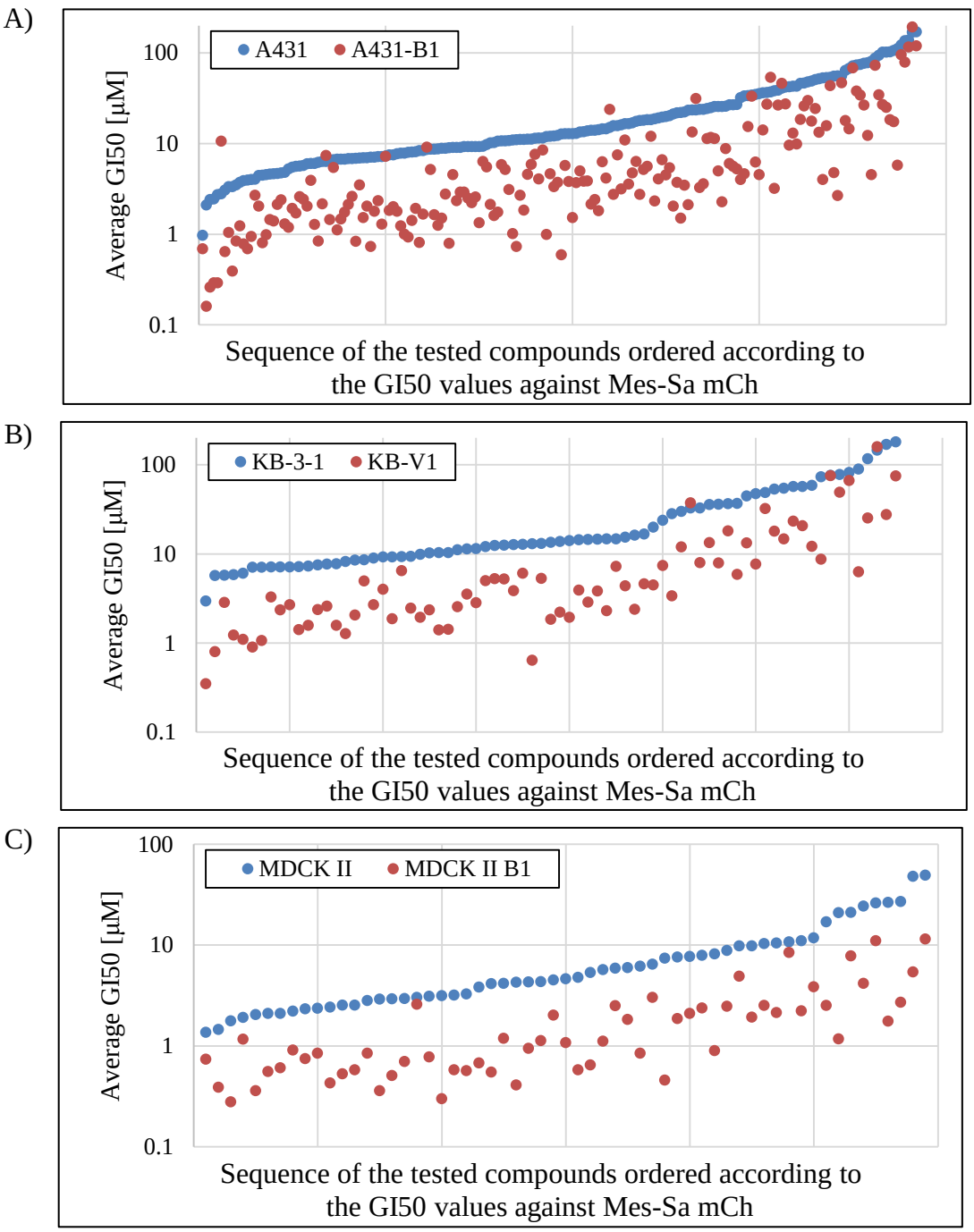

Figure 39. Cytotoxicity (IC_{50} in µM) of selected subsets of 8-OH-Qs measured by PrestoBlue viability reagent against (A) A431 cell lines, (B) KB-3-1 and KB-V1 cell lines, (C) MDCK II cell lines. Each point represents the average IC_{50} value of a drug, and data points are plotted in an ascending order of the IC_{50} values against the parental cell line.

Majority of the tested 8-OH-Q compound set elicited P-gp mediated MDR-selectivity against drug selected (Dx5, KB-V1) and against *MDR1* transfected (A431-B1, MDCK II B1) cell lines.

As a next step, we wanted to investigate, which structural modifications granted improved potency for our compounds during the optimization via designed synthesis. The comparison of only the selectivity ratios or the cytotoxicity would not give appropriate answer, as potency is the function of both. Thus, we introduced the activity index (AI) of the compounds as follows:

$AI = SR/IC_{50}MDR$.

The activity index assigns MDR-selective potency to the tested drugs, which can be compared to each other to find the best performing entities against a resistant cell line.

As cell lines have their inherent susceptibility towards xenobiotics in general, which might depend e.g. on their proliferation rate or on the mutations they harbor, we introduced also the normalized activity index (NAI), which characterizes the potency of MDR-selective agents in a way, that it is comparable between cell line pairs. The NAI was calculated as follows:

NAI = ("individual AI" – "average AI of compound set") / "sd of AIs of compound set".

As derived from the equation, NAI can be the basis to compare MDR-selective potency of drugs only when the same set of compounds were tested against all the cell lines in the investigation, as individual AIs are normalized to the statistics of the compound set (average and standard deviation of AIs), which would be distorted e.g. if for a cell line pair, only half of the compounds would be included in contrast to the other cell lines. If we include several other compounds in the set, the NAI will change for every compound. However, the interpretation of NAI remains the same. Drugs with a NAI of 0 are possessing the average potency in the set. Drugs with NAI < 0 are less potent, while drugs with NAI > 0 have a more pronounced MDR-selective effect compared to the average potency in the compound set. Thus, NAI can support the drug optimization by indicating possible cell line specific improvement of compounds, but most importantly we used it to identify the most potent analogues (Figure 40).

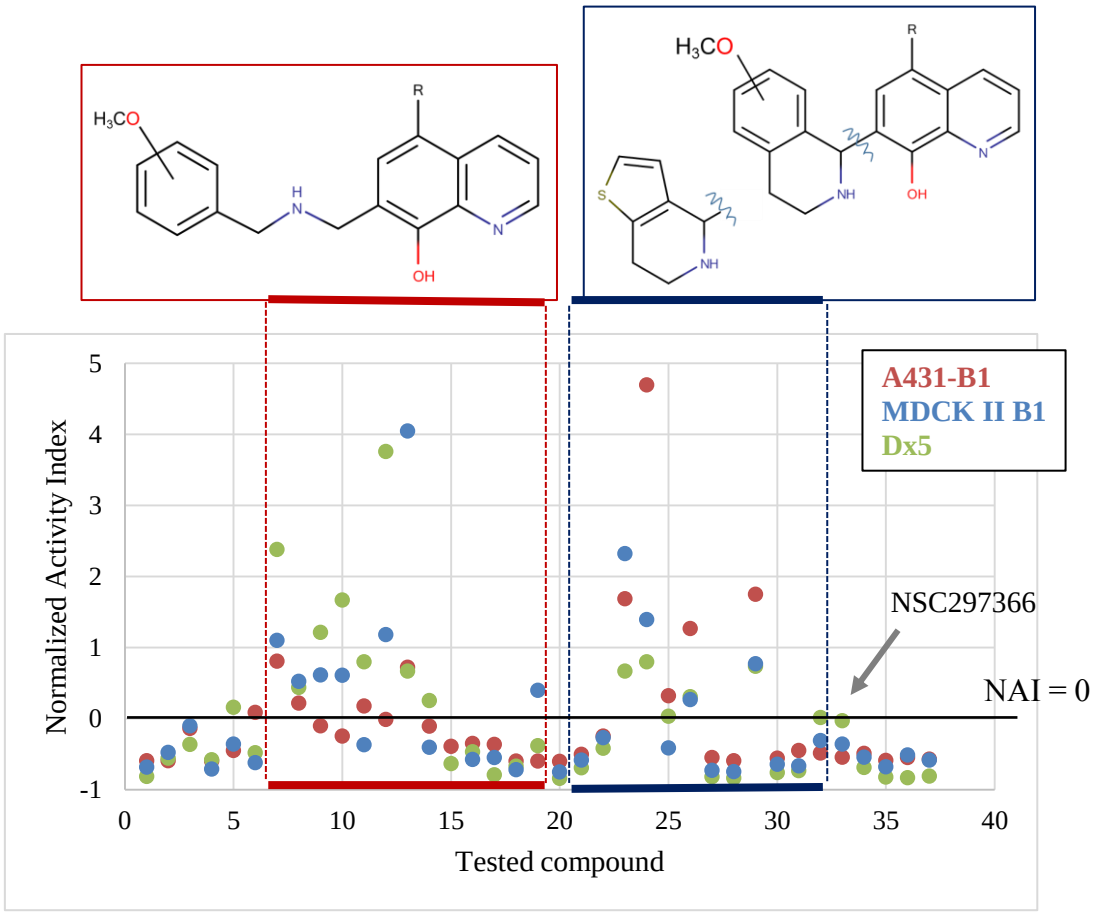

Figure 40. Normalized activity index (NAI) of a subset of 8-OH-Qs tested against A431 and MDCK II cell lines, and against Mes-Sa & Dx5 cell lines. Compounds in the red and blue boxes belong to subclusters of 8-OH-Qs depicted above them. Compounds on the right (compound 33 – 37) were identified through the systematic investigation of the DTP repository, of which the best performing NSC297366 is indicated, and followed by NSC57969, NSC48892, NSC693871 and NSC693872 in this sequence.

Based on NAI, the improvement of 8-OH-Qs through design and synthesis was successful, as NAI pattern was similar for all the 3 cell lines pairs. When analogues were tested against KB-3-1 and KB-V1, the NAI pattern was in concordance to the results shown in figure, but due to lack of data (only 60% of the compound subset was tested), we were not able to compare the potency against KB-V1 via NAI values properly. The successful optimization returned also slight differences between cell lines. Improvement against A431 cells was better when tetrahydro-isoquinoline moieties were present in R7, but against MDCK II cell lines and against Mes-Sa/Dx5 the methoxy-substituted benzil-amine containing molecules were performing better. Nevertheless, the previously identified NSC-compounds, which served as basis for compound optimization, all

returned a negative NAI, referring to "worse than average" MDR-selective effect among the investigated drugs.

4.3.3 Screening and testing a TSC library against resistant cancer

Thiosemicarbazones (TSCs) are known for their potential anticancer properties, moreover, certain TSC analogues are capable to provoke P-gp mediated MDR-selective cytotoxicity (see in 1.3.3 and in [152]). Here, we conducted a systematic testing of a medium sized focused library designed by Veronika F.S. Pape, a former PhD student in the lab. The compound library was designed by considering the current understanding of the relation between TSCs and MDR-selectivity/cytotoxicity. One of the reference points was the β-thiosemicarbazone NSC73306, as this compound (just as its close analogues) showed anticancer cytotoxicity, which was potentiated in the presence of functional P-gp. Arylhydrazones and benzothiazoles have been introduced to the focused library as well, as alternatives to thiosemicarbazones (Figure 41), since TSCs exhibit pharmacological side effects due to the putative liberation of H_2S during their metabolism. The rationale behind the chemical library design was to investigate the impact of metal chelation to cytotoxicity, particularly to MDR-selective cytotoxicity, as the increased proliferation of cancer cells results in an elevated demand for metal ions, which creates a vulnerability that can be exploited therapeutically. The size of the library was of 50 compounds.

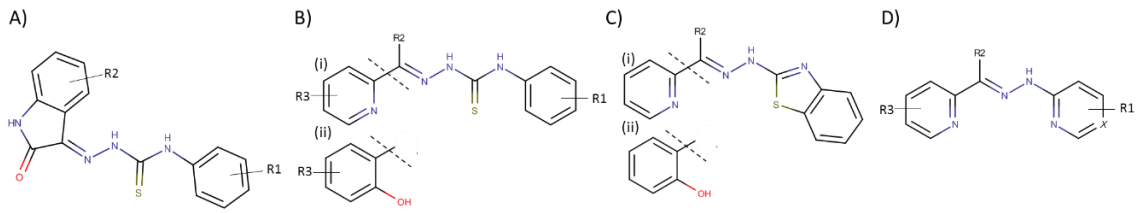

Figure 41. Focused library designed of A) ß-isatin TSCs; B) picolinylidene (i) and salicylidene (ii) TSCs; C) picolinylidene (i) and salicylidene (ii) hydrazino-benzothiazoles; D) arylhydrazones [153].

The compounds of the library were tested against 3 cell line pairs: Mes-Sa & Dx5, KB-3-1 & KB-V1 and A2780 & A2780adr, using the MTT reagent to determine the viability and calculate the IC_{50} values. I contributed to the cytotoxicity results by testing the growth inhibition of the members of this focused library additionally with the fluorescent protein based assay. For this purpose, I used the Mes-Sa mCherry and Dx5 mCherry cell lines,

and conducted the experiments on 384 well plates as a confirmatory screen. Primary screen was missed, as the toxicity of the compounds were already known from the MTT measurements.

To measure the cell mass by the detection of mCherry intensity of the surviving cells was necessary, as the compounds, presented in this focused library were considered as so called "PAINs" (pan assay interference compounds). PAINs, due to their chemical characteristics, interfere with several applied assays resulting in false hits. Chelators, present in this library are typically such frequent hitters, e.g. hydroxyl-phenylhydrazone compounds have been reported to frequently disturb several diverse in vitro assays [154] [155]. Therefore the cytotoxicity had to be confirmed with a counter assay, that works based on a different principle than MTT, and the reagent free fluorescent protein based assay was a suitable choice. Comparison of the MTT assay measured on Mes-Sa and Dx5 cells to the fluorescent protein based measurement gave a good correlation, supporting that the results are not false positives, no observable MTT assay interference had occurred (Figure 42). Although the mCherry based assay returned higher IC_{50} values, the two methods provided concordant results.

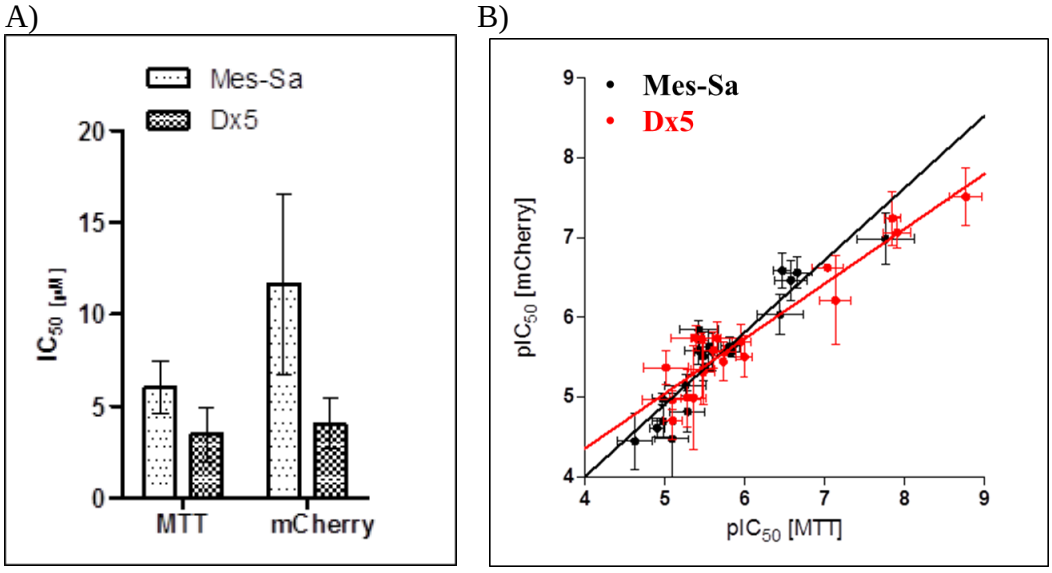

Figure 42. Comparison of toxicity of the compounds against Mes-Sa and Dx5 cell lines obtained either by MTT reagent or by the fluorescent protein based assay measuring the intensity of mCherry. A) IC_{50} values of the MDR-selective compound NSC73306 (1a; Figure 43). B) Correlation of pIC_{50} values for MTT and mCherry measurements. Pearson correlation was calculated to be 0.95 with an r^2 of 0.87 for Mes-Sa (black) and 0.62 with an r^2 of 0.91 for Dx5 (red). Panel B was taken from [153].

In terms of MDR-selectivity, only the NSC73306 like TSCs showed tariquidar sensitive hypertoxicity to MDR cells (compounds 1a-e; Figure 43). Collateral sensitivity was observed also for some other structures, although this hypertoxicity towards MDR cells was unaffected in the presence of P-gp inhibitor tariquidar, suggesting that hypersensitivity of the MDR cells cannot be exclusively linked to the activity of P-gp, and should be rather explained by off-target effects linked to other specific resistance mechanisms or the genetic drift of the selected cells.

A)

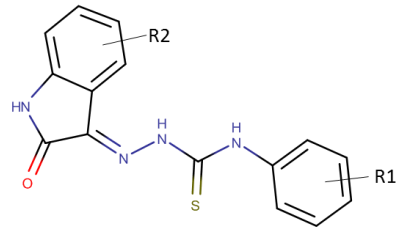

B)

	R1	R2
1a	4-OMe	H
1b	4-OMe	5-OCF_3
1c	4-Me	H
1d	4-NO_2	H
1e	3-CF_3	H

C)

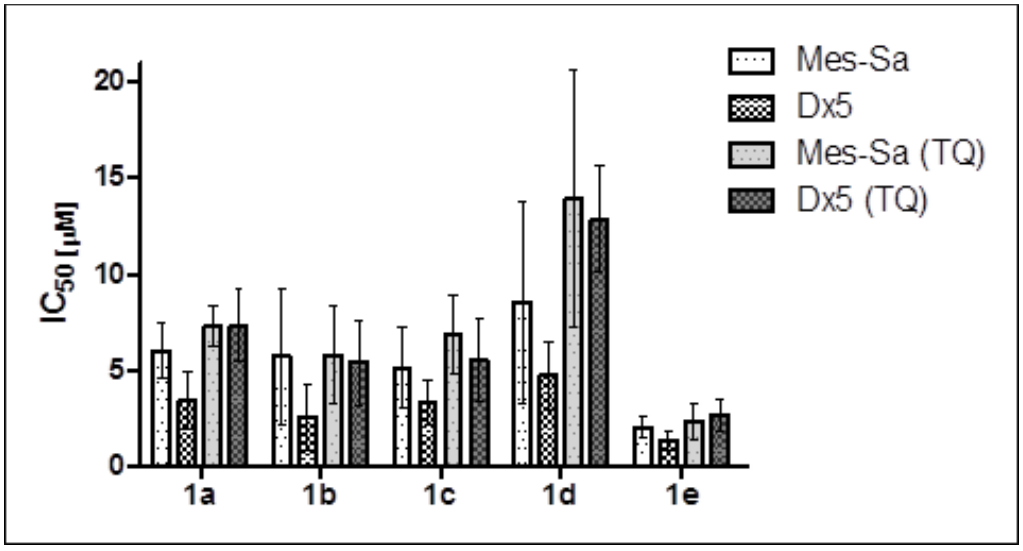

Figure 43. A) General formula of the MDR-selective ß-isatin-TSCs; B) NSC73306 (1a) and its analogues; C) GI_{50} values [µM] of the TSC analogues1a-1e measured against Mes-Sa mCherry and Dx5 mCherry cell lines in the absence and presence of tariquidar (TQ). ($P < 0.05$:*; $P < 0.01$:**; unpaired t-test). Panel B was taken from [153].

In terms of cytotoxicity (regardless of P-gp overexpression) of the tested chelator compounds, the donor atom set proved to be the most determinant factor. The library was designed to have chelators with ONS, NNS or NNN atom sets (Figure 44/A), which

provides different metal chelating affinities to the compounds. Chelator donor atom set determines the binding preference for different metal ions, and stabilizes different oxidation states of these ions. The different chelators might influence the redox properties of the ions as well. Superior cytotoxic activity of NNS and NNN chelators over ONS chelators was observed (Figure 44/B). Regarding to MDR-selectivity, only the ONS-containing ß-isatin TSCs showed P-gp mediated hypertoxicity, other ONS-containing TSCs did not provoke it. It seems, the chelation donor atom set itself is not enough to convey the hypertoxicity to P-gp overexpressing MDR cells.

A) B)

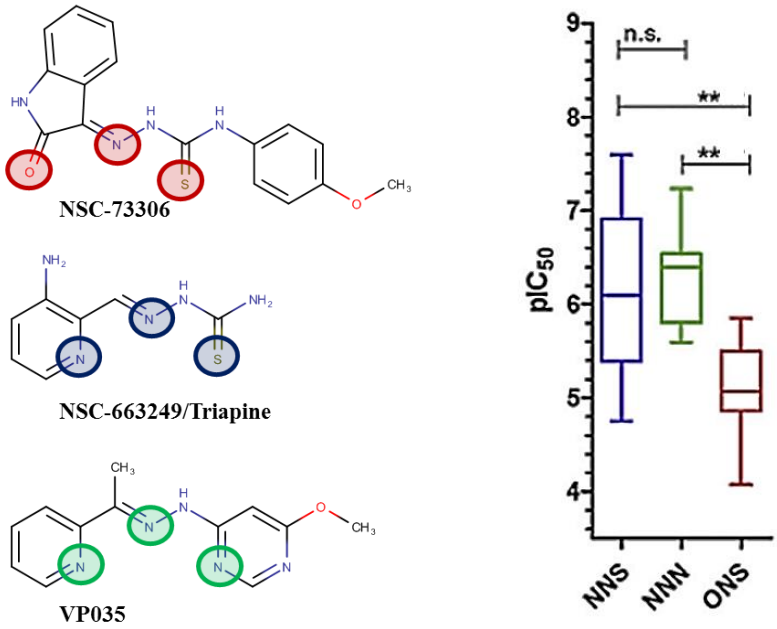

Figure 44. Cytotoxicity of the compounds based on the chelator donor atom set. A) Example compounds with ONS, NNS and NNN donor atom set, used in the design of the focused library. B) Comparison of overall toxicity data of ONS (red), NNS (blue) and NNN (green) chelators. Data from mCherry fluorescence measurements using Mes-Sa and Dx5 cells are shown (**p < 0.01; figures taken from [153]).

4.3.4. Screening and testing a medium sized compound library with flavonoids and thiosemicarbazones.

In collaboration with the group of Ahcène Boumendjel (Univ. Grenoble Alpes, Département de Pharmacochimie Moléculaire, Grenoble, France), we screened a set of 156 compounds in search for MDR-selective cytotoxicity. The library included mostly

flavonoid derivatives and thiosemicarbazones (Figure 45). The rationale behind this choice was the fact that flavonoid derivatives have been widely studied as potential candidates for cancer treatment and prevention [156] and a number of naturally occurring derivatives were reported to be effective against resistant tumors. Although the increased cytotoxicity to MDR cells were linked mostly to the MRP1 transporter (ABCC1; reviewed in [70]), there are a few examples, where MDR-selective toxicity was dedicated to the function of ABCB1. For example the desmosdumotin B flavonoids were reported to exhibit significant collateral sensitivity against P-gp expressing vincristine resistant cells [84] [85]. However, based on our detailed investigation, we revealed that desmosdumotins confer only a marginal effect, which was highly cell line specific (see in 4.2.1.2).

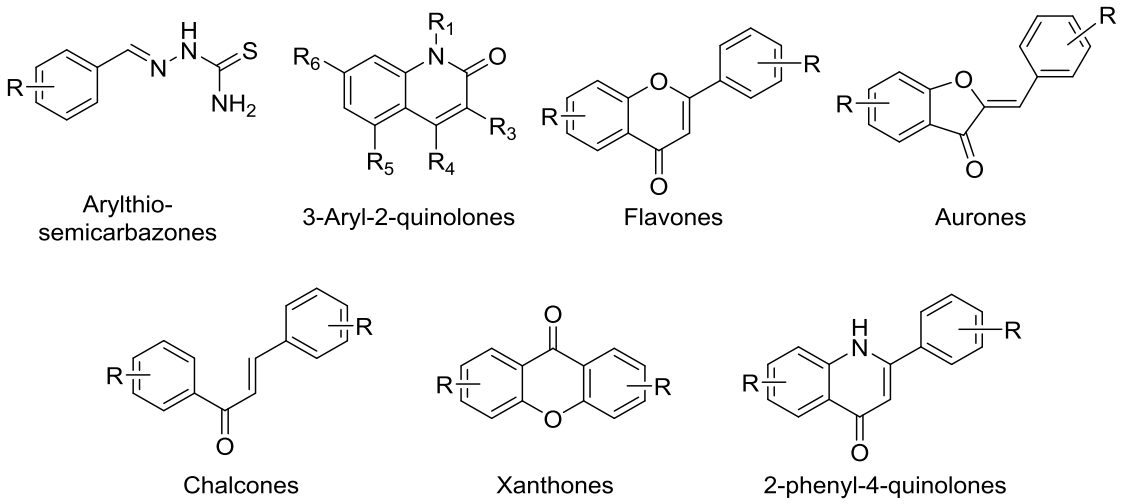

Figure 45. Main scaffolds of the 156 membered compound library.

To filter out not active and less toxic entities, we performed a primary screening. The primary screen of the compounds was conducted using the mCherry expressing variants of Mes-Sa and Dx5 cell lines on 96 well plates. Growth inhibition (GI) of the compounds was determined based on the fluorescence of the mCherry protein expressed by the cells reflecting to cell mass, and compounds were sorted based on growth inhibition. The two concentrations we used was 10 μM and 100 μM. Of the compounds tested, 13 were toxic at a concentration of 10 μM to both cell lines, 32 compounds were not toxic at all even at 100 μM, and 111 compounds were toxic at least against 1 of the cell lines at 100 μM.

In the next step, we serially diluted each interesting drug in 8 concentrations and performed an automated confirmatory screening on 96 well plates to obtain dose-response curves. At this step, we intended to demonstrate, that the compounds excert dose-dependent toxicity, thus IC_{50} values can be obtained. Therefore we decided to use the confirmatory screening only to obtain the right concentration interval, and to approximate IC_{50} values. The confirmatory data then served as an applicable input source for the secondary screen where we obtained accurate IC_{50} values from dose-response curves by PrestoBlue viability reagent as a counter assay, where we used non-fluorescent Mes-Sa and Dx5 cells. For the secondary experiments, we chose representative compounds from all chemotypes, in a way to include the 13 primarily toxic molecules. The result of the secondary screen was in concordance with the primary and confirmatory toxicity of the compounds: xanthones were the least toxic entities, while chalcones were the most toxic ones (Figure 46/A). Moreover, we have found some compounds with selective toxicity either to Mes-Sa or to Dx5 cells (Figure 46/B).

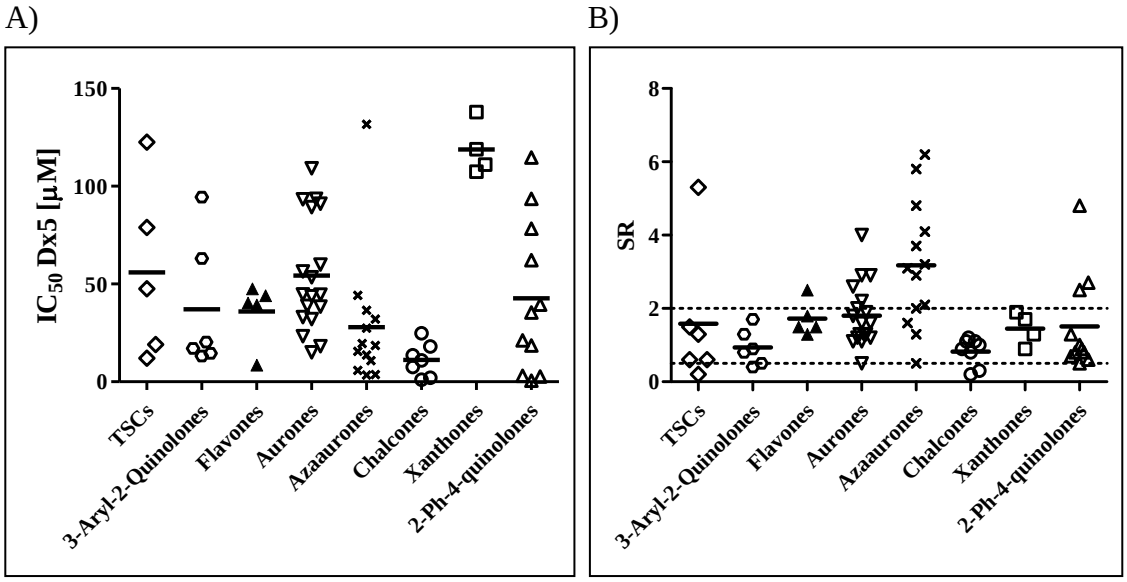

Figure 46. (A) Cytotoxicity of the tested compounds against Dx5 cell lines by the main scaffolds, measured by PrestoBlue reagent. (B) Selectivity ratio (SR) of compounds to Dx5 MDR cell line compared to Mes-Sa parental cell line (flavones are including the isoflavone genistein).

The 3-step screening system revealed that scaffolds derived from azaaurones are particularly the most promising agents from the aspect of selective toxicity towards the MDR cell line Dx5. In 10/13 cases the selectivity ratio (SR) of azaaurones were ≥ 2. We further investigated the azaaurone compounds to see if P-gp contributed to the MDR-

selective toxicity. We tested 4 azaaurones that were more toxic to Dx5 cells (CHB1-59, CHB1-43, CHB1-44, CHB1-41) and one that was more toxic to the Mes-Sa cell line (CHB1-63). In the presence of tariquidar the azaaurones, which killed Dx5 cells preferably became more toxic against both the parental and the MDR cell lines. Moreover these compounds kept their selective behavior, without remarkable change in the SR. In contrast, the presence of TQ did not influence the IC_{50} value of CHB1-63 against Mes-Sa, while the toxicity to Dx5 was significantly increased, suggesting strongly that this compound can be a substrate of ABCB1 (Table 15). The reason of the increment of CHB1-59, -43, -44 and -41 cytotoxicity against both cell lines in the presence of TQ is unknown, and mediated plausibly due to a yet undiscovered effect of the inhibitor.

Table 15. IC_{50} values (in μM) of azaaurone compounds in the presence and absence of the P-gp inhibitor tariquidar (TQ; 1 μM). SR stands for selectivity ratio and was considered significant if the IC_{50} values were statistically different (unpaired t-test, $P < 0.05$:*; $P < 0.01$:**).

Azaaurone	Mes-Sa	Dx5	SR	Mes-Sa(TQ)	Dx5(TQ)	SR(TQ)
CHB1-59	17.8 ± 4.1	3.7 ± 0.6	4.8**	3.2 ± 0.7	0.8 ± 0.2	4.0*
CHB1-43	9.4 ± 1.6	2.5 ± 0.2	3.7**	2.5 ± 0.3	0.6 ± 0.01	3.9*
CHB1-44	50.2 ± 10.0	18.5 ± 5.6	2.7**	16.9 ± 0.3	4.9 ± 0.4	3.5**
CHB1-41	17.1 ± 1.7	5.8 ± 1.3	3.0*	4.3 ± 0.4	1.1 ± 0.3	3.7*
CHB1-63	9.2 ± 2.3	19.5 ± 3.5	0.47*	9.6 ± 1.0	6.7 ± 0.7	1.4

To test the cell line specificity, some of the azaaurones were probed against another *in vitro* cell line based MDR model, where we compared the toxicity of A431 human epidermoid carcinoma cells to A431-B1 cell line, which expresses P-gp due to retroviral transduction of the human MDR1 gene (Table 16). The selectivity ratio of the azaaurones in this system was between 0.5 and 2, meaning that the compounds did not confer remarkable collateral selectivity nor resistance related to P-gp. Although we have observed a slight MDR-selective effect in the case of CHB1-59, which mean that P-gp might contributed to the selective toxicity, and A431-B1 cells showed a 1.5 fold resistance to CHB1-63 (a SR of 0.67 refers to1.5 fold resistance), which supports that this compound was extruded by P-gp.

Table 16. IC_{50} values (in μM) of azaaurone compounds against A431 cell lines. SR stands for selectivity ratio (P < 0.05:*; P < 0.01:**).

Azaaurone	A431	A431-B1	SR
CHB1-59	44.6 ± 6.9	27.0 ± 3.0	1.7**
CHB1-43	33.4 ± 5.5	45.9 ± 6.4	0.7
CHB1-44	76.1 ± 18.2	75.9 ± 26.0	1.0
CHB1-41	65.7 ± 3.3	57.4 ± 2.5	1.1
CHB1-63	10.3 ± 1.4	15.4 ± 2.2	0.67*

Based on the cytotoxicity tests with A431 and A431-B1 cell lines, and based on the experiments conducted in the presence of tariquidar, azaaurone compounds did not possess general P-gp mediated MDR-selectivity. We observed a marginal P-gp potentiated cytotoxic effect in the case of CHB1-59, and identified a P-gp substrate (CHB1-63) (Figure 47).

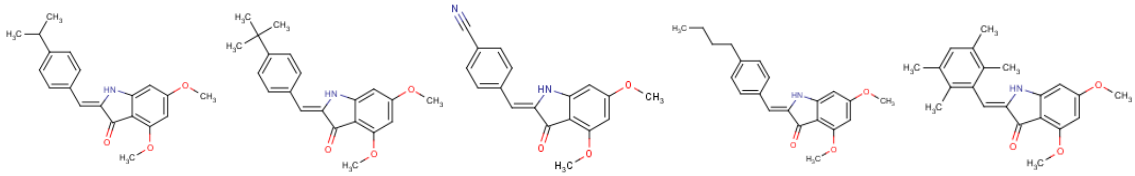

CHB1-41 CHB1-43 CHB1-44 CHB1-59 CHB1-63

Figure 47. Structure of selected azaaurone compounds, which were investigated in more details.

From the tested focused compound library, azaaurones were the most potent candidates, they showed hypertoxicity (up to 6-fold) against the doxorubicin selected, P-gp expressing Dx5 cell line. However, the selective effect was not influenced by the inhibition of P-gp, hence azaaurones were not targeting cells with functional P-gp in general, and can overcome MDR because of other cellular alterations, which seem to be cell line specific. Eventually, the borderline MDR-selective cytotoxicity of CHB1-59 might worth to be investigated in the future by synthesizing additional analogues.

The other flavonoid (and TSC) compounds in the library, which killed Dx5 cells preferably (Figure 46/B) were also tested in the presence of TQ, but none of them had a P-gp mediated preferential toxicity (data not shown).

4.3.5. Investigation of protoflavone compounds against MDR cancer

In the framework of a cooperation with Attila Hunyadi (SZTE, GYTK, Szeged), we had the possibility to investigate another focused library, comprised of the unique flavonoids called protoflavones. Protoflavones are rare flavonoids, found mostly in ferns, and some members are known from their anticancer properties [157]. Moreover, as Hunyadi and colleagues have reported, certain members can evoke a mild collateral sensitivity towards P-gp expressing MDR cell lines, which was linked to the decline in oxidative stress tolerating capacity of the cell lines that were previously long-term selected with a cytotoxic drug [158] [159]. The selective toxicity was suggested to be linked to substituents on the C6 position of the protoflavone core, as in the case of an *MDR1* transfected cell line, only compounds with C6-methyl moiety elicited a slight but significant collateral sensitivity, and the extent of the effect was only moderately influenced by the C1' substituents (Figure 47).

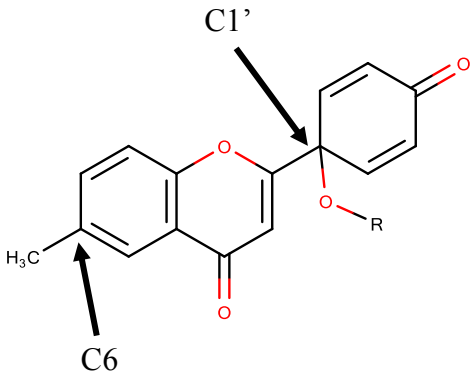

Compound	-R	SR
9	-H	1.63
10	-Methyl	1.37
11	-Ethyl	1.36
12	-Propyl	1.57
13	-Butyl	1.37
14	-Allyl	1.31
15	-Propargyl	1.48

Figure 47. Structure of protoflavones with mild selective toxicity (1.31-1.63 fold) against the P-gp overexpressing L5178B1 cell lines over the L5178 parental line [159]. Position C6 and C1' are highlighted. The protoflavone skeleton is defined as the compound when C6 harbors a H atom instead of the methyl-group, while R=H.

In the terms of the cooperation we intended to explore the effect of various substituents on the cytotoxicity of the protoflavones, particularly to explore the change in hypertoxicity to MDR cell lines. Therefore, protoflavones with distinct core structure and with various moieties on C6 and C1'-OR were included in the focused library. The library enclosed 52 protoflavones in total, of which we tested the cytotoxicity of 26 analogues against 4 parental-MDR cell line pairs.

These 26 analogues represent the derivatives of the naturally occurring protoapigenone and analogs of the synthetic WYC0209 identified as a potential lead in previous studies [160], and a 6-phenyl series of the core protoflavone structure (Figure 48). The compound compilation was supplemented with 6-methyl- and 6-pentyl-derivatives of the core protoflavone together with the naturally occurring protogenkwanone aiming to further explore SAR at C6.

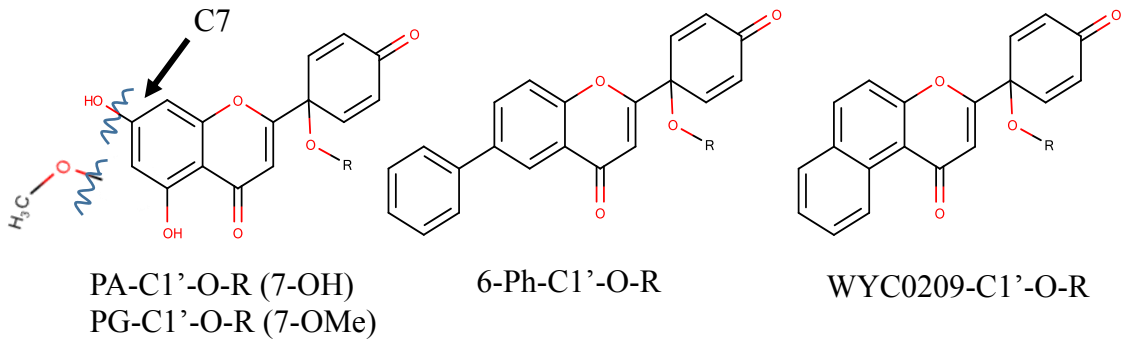

Figure 48. Structure of PA-C1'-O-R, 6-phenyl-protoflavon-C1'-O-R and WYC0209-C1'-O-R. Protogenkwanone (PG) is the 7-methoxy substituent of PA.

The assessment of the cytotoxic effect of the protoflavones was initiated with the first campaign of primary screening (see in 4.3.1.), where we included the 4 representative protoflavone compounds (where R = H based on Figure 48), which we received prior to the rest of the analogues. As these 4 compounds inhibited the growth of both Mes-Sa mCh and Dx5 mCh cell lines at 10 µM completely, we compiled a cell line panel, and tested a set of 26 analogues manually. The cell line panel we used was comprised of the Mes-Sa and Dx5 cell line pair, the KB-3-1 and KB-V1 cell line pair, and the A431 cell line with two ABC-transporter transfected variants, the A431-B1 and the A431-G2. Our results of the 26 analogues are summarized in Figure 49.

In general, protoflavones were toxic to every cancer cell line in the panel, and as it was expected from the primary screening, a majority of them showed an IC_{50} value below 10 µM (thus pIC_{50} above 5). Several compounds exerted different activity against parental and MDR cells, which was quantified based on the fraction of IC_{50} values obtained in P-gp negative vs. positive cells. Accordingly, SR < 0.5 indicated that the compound was subject to ABC transporter mediated resistance, whereas SR > 2 suggested that the ABC

transporter overexpressing cells demonstrated collateral sensitivity against the tested protoflavone derivative. Against the MDR cell line Dx5 only a few compounds showed a hypertoxicity approaching or even exceeding the SR of 2. Interestingly, all these compounds have an unsubstituted C1'-OH group, while C1'-OR analogues (where R ≠ H) were all less effective in killing Dx5 preferably over Mes-Sa. The results for KB-3-1 and KB-V1 were inconsistent from this aspect, C1'-OH structures were not showing higher CS to KB-V1 than the C1'-OR substituted analogues. However, most protoflavones provoked collateral sensitivity of the KB-V1 cell line.

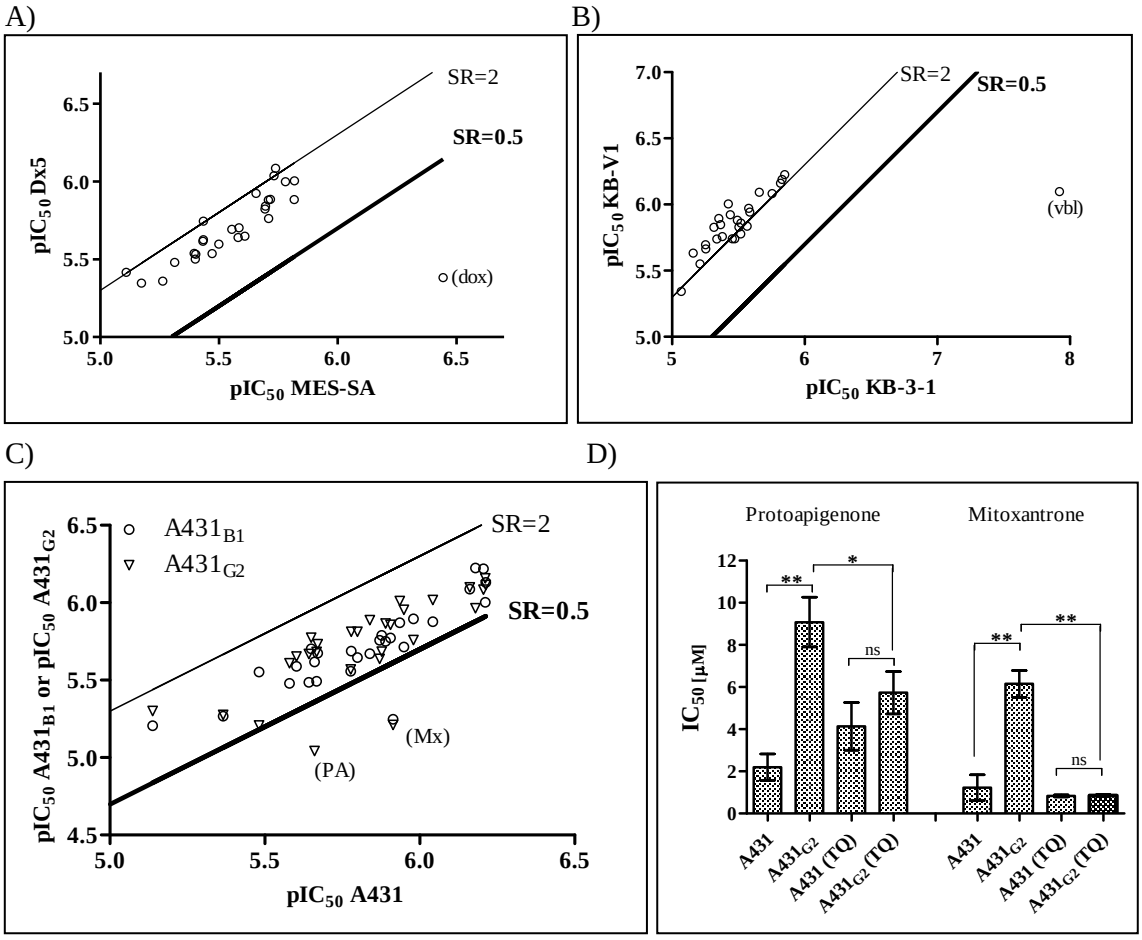

Figure 49. Cytotoxicity of a subset of 26 protoflavone analogues measured by PrestoBlue viability assay against (A) Mes-Sa and Dx5, against (B) KB-3-1 and KB-V1 cell lines and against (C) A431 parental, A431-B1 and A431-G2 cell lines. (D) IC50 values of protoapigenone and mitoxantrone in the absence and presence of ABCG2 inhibitor tariquidar. Dox: doxorubicin; Vbl: vinblastine, Mx: mitoxantrone; PA: protoapigenone; TQ: 1 µM tariquidar. SR: selectivity ratio, SR > 2 refers to collateral sensitivity, SR < 0.5 refers to drug resistance. P < 0.05:*; P < 0.01:**.

When we tested the protoflavones against A431, A431-B1 or A431-G2 cells, we observed no collateral sensitivity nor resistance exceeding the 2-fold threshold, except of protoapigenone (PA). Resistance of A431-G2 cells to protoapigenone was abolished in the presence of tariquidar, confirming that this compound was a subject of the efflux transport. Other protoapigenone C1'-OR analogues, especially C1'-O-iPro, seemed to have also a slight (but less than 2-fold) substrate manner (Figure 50), thus the affinity of protoapigenone derivatives to ABCG2 can be influenced at this position. Interestingly, protogenkwanone, which differs from PA only in its 7-methoxy group (Figure 48) was not recognized by ABCG2.

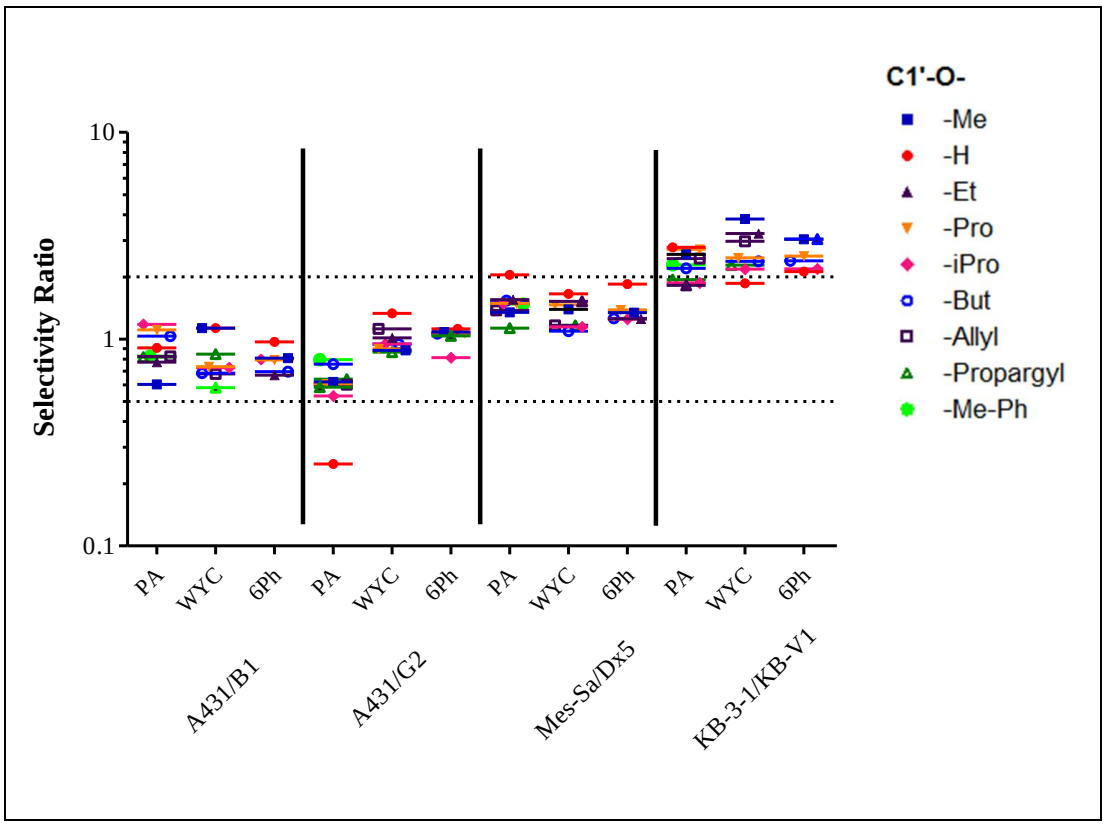

Figure 50. Selectivity ratio of the various C1'-OR protoapigenone (PA), WYC0209 (WYC) and 6-phenyl (6Ph) analogues against the cell line pairs.

As a summary of the systematic experiments with protoflavones, we observed a strong cytotoxic activity for most of the derivatives. In terms of the 6-substituents, cytotoxicity (and collateral sensitivity) was apparently independent of the moieties attached to C6, as the pattern differed from cell line to cell line. All compounds seemed to evade P-gp conferred multidrug resistance, which was tested against various *in vitro* models of parental – MDR cell lines pairs. Moreover, cell lines, which were created by long-term

selection in doxorubicin or vinblastine, suffered from a mild to strong degree of collateral sensitivity provoked by the protoflavones. However, in contrast to MDR-selective compounds, protoflavone derivatives did not target cells engineered to overexpress P-glycoprotein, suggesting that the increased toxicity observed in the MDR cells is not conferred by the efflux pump. Indeed, protoflavones were earlier reported to kill P-gp overexpressing cells preferentially due to the altered antioxidative capacity of the cells, which was acquired during drug selection [158]. We investigated also the effect of ABCG2 on cytotoxicity, where we identified the substrate nature of the naturally occurring protoapigenone.

5. Discussion

The multidrug resistance of tumor cells against chemotherapy mediated by the pathological overexpression of P-gp is still an unresolved problem in the clinics. In MDR tumors, P-gp is located in the plasma membrane of the malignant cells and protects them from the intracellular accumulation of xenobiotics through the active extrusion of a wide range of cytostatics or targeted drugs. Attempts in clinical trials to reverse drug accumulation of cancer cells by inhibiting the function of P-gp had failed due to pharmacokinetic side effects, or simply due to ineffectiveness. A novel approach to fight against MDR cancer is based on the phenomenon of collateral sensitivity, when tumor resistance is considered as a targetable trait. This phenomenon, known also as fitness cost, can be explained with the acquisition of such characteristics, which serve as a drawback in a different environment. Several collateral sensitivity provoking compounds were reported to kill P-gp overexpressing cancer cells *in vitro*. Some of them were linked to such cellular alterations, which were not influenced by P-gp overexpression. For example, in a study of Rickardson et al. [161] the library of pharmacologically active compounds ($LOPAC_{1266}$) was tested against the human myeloma cell line RPMI-8226 and its doxorubicin resistant P-gp positive phenotype RPMI-8226/Dox40. Some of the compounds, which belong to the cluster of glucocorticoid steroids killed the MDR cells preferentially. Subsequent analysis showed that the observed collateral sensitivity was linked to the upregulation of the glucocorticoid receptor at the cell surface, which facilitated an increased drug accumulation, while P-gp was not contributing to this effect. Other compounds, such as austocystin D and 2-deoxyglucose were also reported to kill P-gp overexpressing cells preferentially. However, in the case of austocystin D, the collateral sensitivity was derived from its selective activation by cytochrome P450 in MDR cells [76], while hypertoxicity of 2-DG was linked to the altered apoptotic pathway of the investigated MDR lines [74]. If such CS agents are applied and the cell line specific changes are targeted during treatment, P-gp overexpression might not be eliminated concurrently, thus MDR of the tumor would still be a hurdle of an effective treatment.

In other instances, collateral sensitivity of P-gp expressing cancer cells was linked to the function of P-gp. In some of these reported studies, the causal link between P-gp and hypersensitivity of MDR cells to CS agents were not examined thoroughly, thus we collected several substances to probe their robustness in killing MDR cells. We tested

verapamil, reversin121, TritonX-100, desmosdumotin B flavonoids, rotenone, KP772, Dp44mT and the Pluronic block copolymer P85 against a panel of parental & MDR cell line pairs in cytotoxicity assays. Unfortunately, except of KP772, none of the compounds elicited robust P-gp mediated selectivity in our hands (Tables 8-11; Figure 29).

Our inability to confirm the reported collateral sensitivity can possibly be explained by the fact that both the special cellular changes in the particular cell lines used in the studies and the function of P-gp contributed to the observed effect, but P-gp alone was not sufficient to confer CS. Another plausible explanation for the irreproducibility of the reported data is the difference in the degree of resistance of the applied MDR cell lines. While testing desmosdumotin B flavonoids against KB and KB-VIN cell lines, we used the same conditions (kanamycin and HEPES supplemented medium) for cell culturing and the same assay type (SRB) for cytotoxicity assays to exclude the possibility of any assay specific disturbance. Compared to the data in the original article [84], our IC_{50} values measured by SRB assay were similar for the parental KB cells, while a remarkable difference was seen when we compared the results of KB-VIN. These cells in our hands were less sensitive to desmosdumotins, but more sensitive to vincristine (Table 10). The IC_{50} for KB-VIN was 7 μg/ml (which is approx. 8.5 μM) based on the reference [84], whereas for us it was only 0.57 μM. As the level of P-gp is proportional to the resistance, and inversely related to MDR-selective toxicity [152], unreproducible data might linked to the extreme P-gp level of KB-VIN cells used in the original work. Similarly, when we examined the cytotoxicity of Dp44mT, we did not observe any lysosomal accumulation of P-gp, which might have occurred due to extreme level of transporter overexpression (Figure 29). Thus, the *in vivo* experiments, when KB-3-1 and KB-V1 xenografts were treated with Dp44mT in mice has to be interpreted with caution, particularly because xenografts are known for their limited utility, as compared to more realistic tumor models, the response of xenografts to drug treatment is more pronounced [162] [163]. When Richardson et al. treated the xenografted mice with Dp44mT, a more than 5-fold reduction was observed in the growth of the KB-V1 xenografts over KB-3-1 xenografts, albeit the KB-3-1 consisting tumor grew faster also when vehicle control was administered [103].

As indicated, when treated with KP772, MDR cells were killed by this drug to a greater extent as a consequence of functional P-gp expression (which was reproducible also in our hands). Thus, KP772 and other so called MDR-selective compounds are more

promising and more preferable drug candidates, as the source of their hypertoxicity is linked the function of P-gp, which is at the same time the causative factor of MDR to chemotherapeutics. KP772 was tested also *in vivo* against human DLD-1 colon carcinoma xenografts in mice [164]. Albeit it had a promising anticancer properties comparable to cisplatin and methotrexate treatment, no experiments were reported, when MDR tumors were treated.

Our research group used a systematic approach to identify P-gp potentiated MDR-selective agents in a previous study, which proved to be highly useful, and led to the identification of NSC73306 and other MDR-selective compounds from the NCI DTP drug repository [73] [98]. Later, as presented in this thesis, we repeated the consecutive *in silico* filtering and *in vitro* validation of the MDR-selective candidate drugs, and identified 6 compounds, which killed 4 P-gp positive cell lines preferentially over the parental counterparts, unless P-gp was inhibited (Tables 12-14). Hypertoxicity against MDR lines was observed both when long-term drug selected cell lines and when *MDR1* transfected cells were used. The best performing hit compound we identified was the 8-OH-Q analogue NSC297366, which was tested against additional cell line pairs, where we further demonstrated its robust effect. As apparent from Figure 51, NSC297366 provoked MDR-selectivity in every case, which was abrogated in the presence of the P-gp inhibitor TQ, regardless also of the cytotoxicity assay type we used.

Besides the 8-OH-Qs (especially NSC297366 and NSC57969), other structural congeners were also associated with MDR-selectivity. Of the compounds we identified in the repeated datamining from the DTP repository, we have found two 1,10-phenanthroline complexes (same chemotype as KP772), a diketone compound (NSC17551) and a compound which is a sulfonated 7,8-dihydroxy-quinoline condensed to a 1,4-naphtoquinone (NSC13977). We also identified a thiosemicarbazone compound NSC716771, which is a close analogue of NSC73306, although we were not able to purchase it and verify its MDR-selective cytotoxicity in our hands.

Despite the dissimilarity of the 2D structures of the identified MDR-selective chemotypes (Figure 30), an earlier drug activity pattern analysis by our research group revealed an association with metal chelation complexes [98], suggesting that metal binding is relevant in the mechanism of action of these agents. In fact, the identified MDR-selective

compounds and their structural congeners could chelate metal ions [98] [165] [166] [167], or were present already in a metal-bound form. The metal chelating coherency seemed to be valid also for the MDR-selective compounds we identified from the new release of the DTP repository, e.g. ß-diketones (chemotype of NSC17551) were already used as chelating agents in biological systems [168].

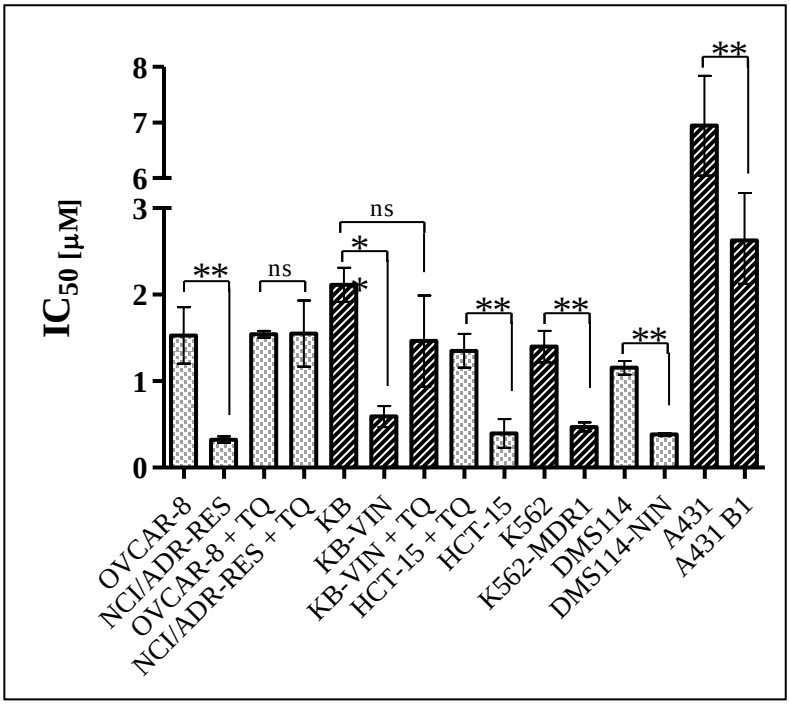

Figure 51. Robustness of the MDR-selective cytotoxicity of NSC297366. OVCAR-8 and NCI-ADR/RES cells were measured with the fluorescent protein based assay (based on DsRed2 and eGFP, respectively); KB cell lines were tested with SRB assay; other cell lines were tested with PrestoBlue viability reagent. Statistics: unpaired t-test, $P < 0.05$:*; $P < 0.01$:**. TQ: 1 μM tariquidar.

Based on the experiments with the 8-OH-Q core structure, which is a strong metal chelating agents, but cannot provoke P-gp mediated MDR-selectivity to any cell lines [151], we assume that metal ion coordination is necessary but not sufficient for the effect of MDR-selective compounds. However, details of the mechanism of action of selective toxicity remains elusive. As reviewed partly by our research group [70], it is possible that P-gp simply increases the intracellular accumulation of an MDR-selective compound. Alternatively, by extruding a physiological substrate, P-gp can unshield the molecular target of an MDR-selective compound. It is also possible, that the function of P-gp is necessary to activate the MDR-selective compound in a way to increase its cytotoxicity.

Finally, an MDR-selective compound might bind an intracellular component, and the complex that was formed is already recognized and effluxed by P-gp, resulting in the depletion of the ligand (putative mechanism are shown in Figure 52). The most common species believed to be depleted by P-gp, either directly or conveyed by the transporter, are ATP, GSH or metal ions.

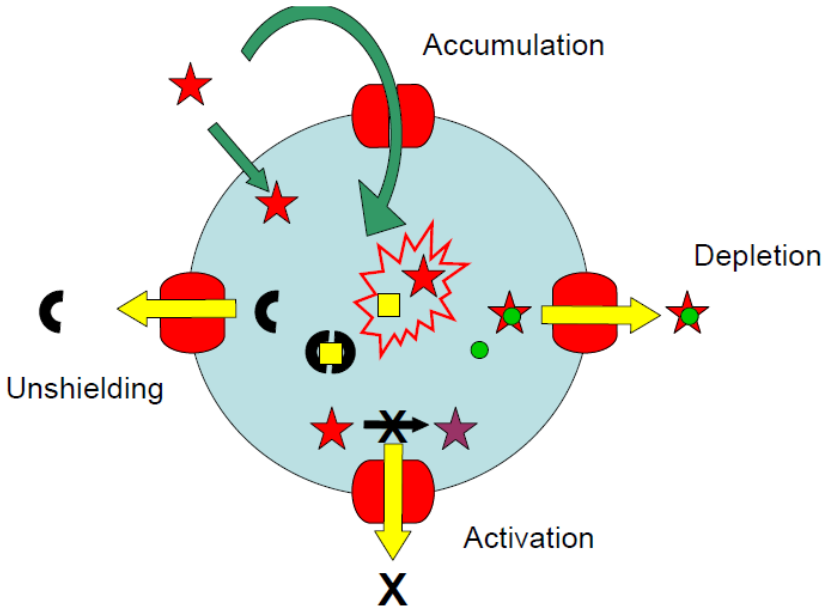

Figure 52. Putative mechanism of action of an MDR selective compound. (I) accumulation of MDR-selective compound (red star); (II) unshielding of molecular target (yellow square); (III) activation of MDR-selective compound linked to the efflux of compound '**X**'; (IV) depletion of endogenous substrate (green circle) [70].

MDR-selective compounds, besides the preferable killing of P-gp positive MDR cells possess a second unique feature: when P-gp expressing, drug resistant cancer cell lines were treated with non-toxic concentration of an MDR-selective compound, P-gp disappeared from the cell surface due to the decrease in the mRNA level transcribed from *MDR1* [152]. Moreover, the MDR-selective substances identified from the systematic DTP repository data mining (including KP772) induced the loss of P-gp already in response to one single, 5 day long, high dose treatment [151]. This so called P-gp phenotype switch seemed to be permanent, as the P-gp expression did not return after the MDR-selective agent was removed. In contrast, example compounds (e.g. verapamil) eliciting cell line specific collateral sensitivity and the non-selective 8-OH-Q core induced only partial or insignificant P-gp downregulation of Dx5 cells [151].

The aim of the research on MDR-selective compounds is to utilize them in future cancer treatment. There are several possibilities, how therapeutic modalities can benefit by the application of such molecules. If P-gp is already present and confers resistance to the tumor, MDR-selective compounds can be administered (alone or in combination with a chemotherapeutic agent) either to selectively eliminate the transporter expressing cells, or to downregulate the expression of P-gp, thus re-sensitizing the tumor to the applied chemotherapeutic agent. Alternatively, MDR-selective compounds can also be used to prevent the occurrence of MDR phenotype by administering them simultaneously, consecutively or prior to cytostatic or chemotherapeutical treatment. Unfortunately, there are no MDR-targeting therapies to date, because crucial *in vivo* proof-of-concept studies are still missing.

Therefore, we decided to perform a compound screening followed by preliminary lead optimization to find more potent MDR-selective agents, which could be used efficiently in *in vivo* experiments.

To have the capacity of testing a large amount of molecules, we established an automated, high throughput amenable screening platform. Cytotoxicity testing was designed in 3 consecutive screening steps, which provided more detailed information of the tested drugs in every step. The results of the 3 steps (I-III) indicated if compounds are cytotoxic (I, primary), gave confirmed dose-dependent response, preferably in an MDR-selective manner (II, confirmatory), and if the MDR-selectivity was robust across different parental & MDR models and across assay procedure types (III, secondary) (Figure 7).

The growth inhibition in the primary and confirmatory screens was measured by a fluorescent protein based cytotoxicity assay. This novel type of reagent free assay was based on the detection of fluorescent protein expression, as the fluorescent intensity was proportional to the cell number. We adapted and developed this type of assay based on publications, where fluorescent proteins were utilized in cytotoxicity measurements. The fluorescent protein based cytotoxicity assay was automated and was compatible with both 96 well and 384 well microplates. During the implementation of the assay, the special 2D growth characteristics of Mes-Sa mCherry and Dx5 mCherry cell lines was to be considered (Figures 19, 20, 25). Due to visible evaporation from the side wells by 144 h, assay optimization involved also the investigation of the edge (or side) effect, which is a

commonly encountered systemic error appearing because of physical or environmental variances of the wells within a plate [138], and the affected area of the plates were excluded from the cytotoxicity experiments (Figure 26/C). Moreover, the measurements were continuously checked for their reliability via calculating the Z'-factor of each microplate (Tables 3, 5, 6, 7; Figures 16, 24, 28), which reported on assay robustness. The fluorescent protein based assay was selected for screening purposes because the reagent free detection of cell viability grants cost effectiveness in long term, and because it is free of liquid handling, which is highly advantageous in automated processes, as pipetting is always a possible source of error. Moreover, as the detection of the fluorescent signal is not harmful to the cells ("quasi label free"), fluorescent intensity of wells can be measured even every day, thus following cell growth is also achievable if needed.

The primary compound screening was performed in campaigns to minimize the disturbing effect of external factors. Based on primary growth inhibition results, we excluded mostly only the non-toxic hits to narrow the number of compounds, which lead to a high hit ratio compared to the HTS performed by pharmaceutical companies, where hit ratio is ideally around 2%. However, our high hit ratio was designed on purpose, as we intended to use the cytotoxicity data of as many agents as possible, to perform detailed SAR studies on toxicity and on MDR-selectivity. Moreover, compound purchase was already designed in a way to include such compounds that were tailored to be inactive to prove the importance of certain structural elements that are absent or blocked in the modified molecules, thus non-toxicity was also a source of information.

In between the primary campaigns, the interesting molecules were tested in the confirmatory and secondary steps. The testing was based on designed focused libraries of chemotypes. The focused libraries we tested, and which were introduced in the frame of this thesis were (i) 8-hydroxy-quinolines, (ii) TSCs and analogues, (iii) TSCs and flavonoids including azaaurones and (iv) protoflavones.

The library of 8-hydroxyquinolines investigated herein was compiled based on a previous intellectual property search, and the results of the new chemical entities (NCE) were filed in as an international patent application "MDR-reversing 8-hydroxy-quinoline derivatives". The optimization of the 8-OH-Qs returned 2 potent subtypes, where R2 was substituted with a hydrogen, R5 with either a hydrogen or a halogen atom or with a nitro-

group, and R7 was constituted either from methoxy-benzylamines or tetrahydro-isoquinoline derivatives (Figures 36, 40; structures represented in Figure 52). The non-cell line-specific MDR-selective potency of the NCEs was quantified by the normalized activity index (NAI), which was calculated from both the selectivity ratio (SR) and the cytotoxicity of a compound. The best performing hit NSC297366 that we identified from the DTP repository possessed a NAI of negative values (-0.54, -0.02, -0.36 against A431 & A431-B1, Mes-Sa & Dx5 and MDCK II & MDCK II B1, respectively), while the best performing NCEs returned a NAI of 4.70, 3.76 and 4.05 for the same cell lines. (NAI is the interpretation, of the optimization, where NAI = 0 is the average improvement, while positive values show compounds with 'better than average' MDR-selective effect). *In vivo* experiments with the optimized 8-OH-Qs are already under elaboration, preliminary results are expected in the near future.

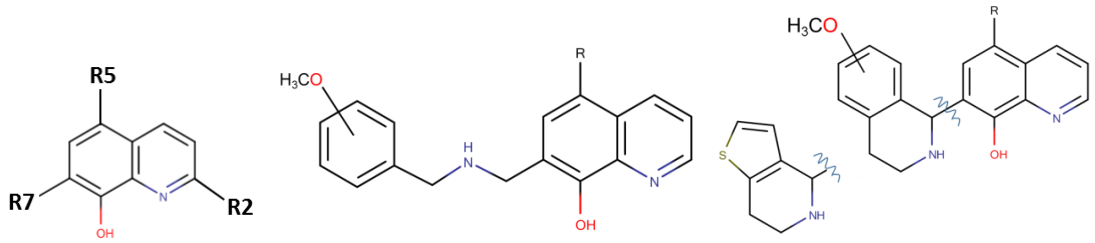

Figure 52. General formula of the 8-hydroxyquinoline derivatives, which were the subject of the patent application "MDR-reversing 8-hydroxy-quinoline derivatives", and the structure of the most potent compounds as a result of optimization.

Although thiosemicarbazones (TSCs) are known for their potential MDR-targeting properties [73][100][101], when a focused library of TSCs, hydrazino-benzothiazoles and aryl-hydrazones were tested, we unfortunately did not identified more potent compounds in terms of MDR-selectivity. However some of the compounds shown relatively high level of collateral sensitivity against Dx5 cells, but this preferential effect was not linked to the function of P-gp. Nevertheless, with the study [153], we provided new insights of the relation of cytotoxicity and metal chelation, which was particularly important, as chelators are often considered as pan assay interference compound (PAINSs), and it was also a task for us to demonstrate the cytotoxicity of such compounds with a reagent free assay, as MTT (or PrestoBlue) might react with redox active metal complexes.

It has to mentioned here, that the issue of PAINs is a recurring problem when the

cytotoxicity of chelators are discussed in publications, as automated algorithms of the scientific journals recognize PAIN-like structures, and the submitted manuscript will be rejected without any substantive review. To exemplify that the identified MDR-selective agents are not false positive results due to the redox cycling of non-toxic compounds, we probed a set of 80 compounds, including e.g. 8-OH-Qs, TSCs, ß-diketones and arylhydrazones, and we compared the GI_{50} data measured against Mes-Sa mCh and Dx5 mCh after 144 h incubation (confirmatory screen was performed on 384 well plates) to the IC_{50} values obtained from PrestoBlue viability measurements at 72 h (against non-fluorescent Mes-Sa and Dx5).

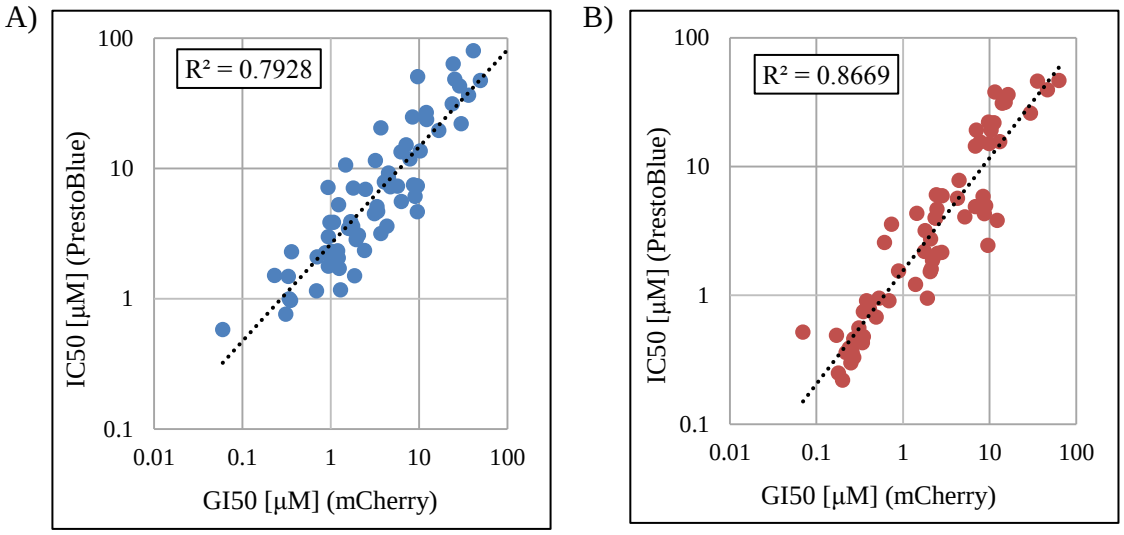

Figure 53. Correlation of fluorescent protein based detection of growth inhibition and PrestoBlue viability measurement against (A) Mes-Sa mCherry and Mes-Sa cell lines, and (B) against Dx5 mCherry and against Dx5 cell lines.

The correlation (Figure 53/A and B) demonstrated that fluorescent protein based measurement data was in concordance with the conventional PrestoBlue viability measurement, thus the PAIN issue did not interfere with our results. Not shown here, but we demonstrated the MDR-selective cytotoxicity of NSC57969 also by measuring apoptosis with Annexin V and propidium-iodide staining [151].

We probed also several flavonoids to test their putative MDR-selectivity. As seen, desmosdumotin B analogues worked cell line specifically. Similarly, distinct subtypes of protoflavones (protoapigenone, WYC0209 and 6-phenyl-protoflavone analogues) elicited collateral sensitivity only against drug-selected cell lines, which was not

influenced by the presence of P-gp (Figures 49 and 50). This behavior was further evinced by Hunyadi and colleagues, when they tested the 26 analogues as a part of a 52 membered protoflavone compound library against 2 additional cell line pairs (L5178 and $L5178_{B1}$, and MCF-7 and $MCF\text{-}7_{Dox}$, Figure 54/A and 54/B, respectively) [169].

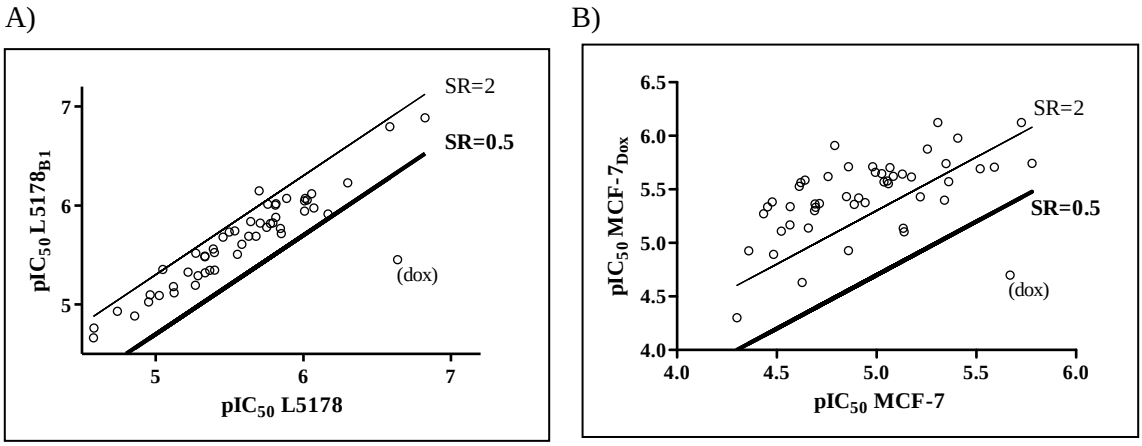

Figure 54. Cytotoxicity (pIC_{50}) of 52 protoflavone analogues measured by MTT against (A) L5178 and $L5178_{B1}$ and against (B) MCF-7 and $MCF\text{-}7_{Dox}$ cell lines, performed by Attila Hunyadi and colleagues. Dox: doxorubicin; SR: selectivity ratio, SR > 2 refers to collateral sensitivity, SR < 0.5 refers to drug resistance. $P < 0.05$:*; $P < 0.01$:**.

The tested analogues, of which some returned an IC_{50} value below 1 μM against L5178 or A431 cell line variants, were equally toxic to L5178 and MDR1 transfected $L5178_{B1}$ cell lines (SRs were below 2), indicating, that the compounds can overcome MDR, although the contribution of P-gp in this phenomenon is not remarkable. On the contrary, many compounds showed hypertoxicity to $MCF\text{-}7_{dox}$ cells compared to the parental MCF-7, with SR values exceeding 5 in the case of 12 compounds. Thus, tested protoflavones were not MDR-selective compounds, although their potent cytotoxicity, even if ABCB1 or ABCG2 transporters are present, can be exploited in an anticancer therapy, as P-gp mediated multidrug resistance was overcome.

When we tested the flavonoid library containing 3-aryl-2-quinolones, flavones, aurones, azaaurones, chalcones, xanthones and azaflavones, the most relevant hits were the aurones, especially azaaurones. These compounds seemed to be even more interesting candidates, as an *in silico* hit from the DTP repository, NSC43320 belongs also to aurones, and it was eliciting collateral sensitivity against KB-V1 cells over KB-3-1 [98]. When azaaurones were probed, we observed collateral sensitivity against Dx5 cells of

several analogues. To explore, if the preferential toxicity was conveyed by functional P-gp, we repeated the experiments with co-incubating tariquidar and selected azaaurones. Surprisingly, non-toxic concentration of TQ exerted an increase in azaaurone cytotoxicity, while the SRs remained significant (Table 15). Thus, we probed the selected analogues also against A431 and *MDR1* transfected A431-B1, and we demonstrated the slight (1.7-fold), but significant MDR-selective cytotoxicity of the analogue CHB1-59 (Table 16).

The compound compilation, which we purchased and already tested in the primary screening (Figure 35) contains the congeners of more chemotypes than presented in this thesis. However, the additional chemotypes are still under continuous *in vitro* investigations in confirmatory and secondary screening steps, and a few manuscripts will probably be submitted in the near future.

Our screening results were characterized also from a statistical point of view by monitoring assay robustness via the Z'-factor. As the fluorescent protein based cytotoxicity assay is not used commonly in the literature, we could compare our Z'-factors only to fluorescent protein measurements based on different principles, introduced in point 1.4.4. In the study of Rao et al., the high content screening was performed on 384 well plates with Z'-factors of 0.50 and 0.54 for eGFP and mCherry, respectively [131]. In the study of Kenny et al., where a fluorescent laser scanning microplate cytometer was applied, the Z'-factors varied between 0.4–0.7 on 384 and 1536 well formats (Figure 55, [133]). In comparison, our Z'-factors were generally better for mCherry, eGFP and mOrange fluorescent proteins (Tables 5, 6, 7; Figures 16, 24, 28), reaching the maximal average value of 0.87 in the case of Dx5 eGFP measurement on 384 well plates after 144h incubation time.

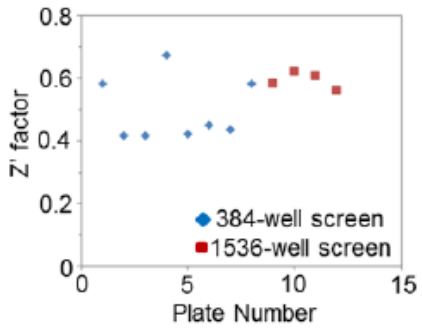

Figure 55. Z'-factors values from [133] performed on 384 well and 1536 well plates.

6. Conclusions

1. I established and characterized a fluorescent protein based cytotoxicity assay, and proved that it is amenable to screen putative MDR-selective substances in a higher throughput.

2. I found that reported compounds do not possess robust MDR-selective activity, and the provoked collateral sensitivity was linked to other factors than functional P-gp.

3. I extended the systematic datamining of the NCI DTP drug repository. This analysis has led to the identification of robust MDR-selective compounds.

4. I performed structural clustering of the known MDR-selective compounds in order to associate 2D structures (chemotypes) to the observed effect.

5. By screening the cytotoxicity of 2160 compounds, which were purchased based on the chemotypes that were associated with MDR-selective cytotoxicity, I facilitated the generation of lead (or lead like) compounds.

6. I contributed to the understanding of essential structure-activity relationship of 8-hydroxy-quinolines, which led to the development of more, highly active compounds. The most potent, so far unknown analogues were the basis of the international patent application “MDR-reversing 8-hydroxy-quinoline derivatives”.

7. I investigated the MDR-selective cytotoxicity of structural congeners of thiosemicarbazones and flavonoids (particularly protoflavones and azaaurones).

7. Summary

Due to inherent or acquired therapy resistance, cancer remains a deadly disease. One of the cellular factors contributing to the simultaneous resistance of tumors to multiple treatments is associated to the overexpression of ABC transporters (multidrug resistance, MDR). P-glycoprotein (ABCB1/P-gp) confers MDR to cancer cells by keeping the concentration of cytotoxic agents below a cell-killing threshold. Whereas transporter inhibition did not achieve clinical success, MDR-selective compounds preferentially targeting P-gp expressing cancer cells represent a new and promising approach for the resolution of cancer MDR.

The overall aim of my doctoral work was to establish a screening platform for the identification of more potent MDR-selective analogs. I found that compounds reported in the literature to possess MDR-selective toxicity were in fact not robustly toxic to a panel of MDR cell lines, suggesting that their activity is limited to specific cellular alterations not related to P-glycoprotein. In contrast, our analysis of the NCI60 database identified several MDR-selective compounds, whose toxicity is potentiated, rather than attenuated by P-gp, irrespectively of the particular cell model. *In silico* and *in vitro* characterization of these compounds lead to the identification of highly active molecules, clustering into distinct chemotypes associated with MDR-selectivity. Focused libraries built around the molecular scaffolds were obtained, and their toxicity was characterized in a dedicated screening platform. Therefore, I established an automated screening system amenable to high-throughput based on a reagent free cytotoxicity assay measuring the growth inhibition of fluorescent protein expressing cell lines.

In the primary screening campaign I tested the cytotoxicity of 2160 compounds against a parental and an MDR cell line. 4 focused compound libraries were then assayed in consecutive confirmatory and/or secondary screening tests, characterizing dose-dependent cytotoxicity, cell line specificity and the contribution of P-gp to cytotoxicity. Testing and limited optimization of the 8-hydroxy-quinoline scaffold resulted in analogs with significantly increased toxicity and MDR-selectivity, leading to an international patent application. By testing thiosemicarbazones, protoflavones and flavonoids, we observed crucial relationships between structure and activity, which were reported in 2 publications, and an additional manuscript is already under preparation.

Összefoglalás

A malignus tumorok eredményes kezelésének egyik fő korlátja a kezelés során rendszerint kialakuló multidrog rezisztencia (MDR), ami sokszor az ABC-transzporterek fokozott sejtfelszíni expressziójához köthető. A P-glikoprotein (ABCB1/P-gp) efflux funkciójának köszönhetően megvédheti a rákos sejteket az alkalmazott kemoterápiás szerektől. Az MDR leküzdésére fejlesztett transzporter gátlók klinikailag hatástalannak bizonyultak, azonban az ún. MDR-szelektív vegyületek alkalmazásával lehetőség nyílt egy újszerű, kifejezetten az MDR tumorokat célzó kemoterápia fejlesztésére, mivel bizonyos vegyületek a P-glikoprotein funkciójának függvényében hatékonyabban képesek elpusztítani az MDR tumorsejteket.

A doktori munkám során a jelenleg ismert MDR-szelektív vegyületeknél hatékonyabb analógok azonosítása céljából kialakítottam egy molekulaszűrési eljárást. A szakirodalomban publikált, P-glikoproteint kifejező sejtvonalakat szelektíven támadó vegyületek tesztelésekor azt tapasztaltam, hogy a megnövekedett toxicitás a transzporter funkciójától függetlenül, sejtvonal specifikusan jelentkezett. Ezzel ellentétben, a kutatócsoportunk szisztematikus *in silico* és *in vitro* megközelítéssel az NCI60 adatbázisából sikeresen azonosított számos olyan molekulát, melyek citotoxicitását kifejezetten fokozta a P-gp funkciója. A validált MDR-szelektív vegyületeket szerkezetük alapján kemotípusokba soroltuk, és fókuszált vegyület-könyvtárakat állítottunk össze, hogy minél hatásosabb vezérmolekula jelölteket találhassunk. A molekulák szűrésérét egy nagy áteresztőképességű rendszeren keresztül valósítottam meg, melyhez bevezettem egy reagensmentes, fluoreszcens fehérje expresszión alapuló citotoxicitási esszét.

Az elsődleges szűrés során 2160 vegyület toxikusságát teszteltem le egy parentális és egy MDR sejtvonalon. Ezt követően a megerősítő és másodlagos tesztek során 4 fókuszált vegyületkönyvtárat teszteltük le, hogy meggyőződjünk a dózis-függő szelektív toxicitások sejtvonal specifikusságáról és P-gp függéséről. A 8-hidroxi-kinolinok tesztelésének és limitált optimalizációjának eredményeként olyan analógokat találtunk, amelyek toxikussága és MDR-szelektivitása szignifikáns mértékben megnövekedett, így egy nemzetközi szabadalmi beadványt nyújtottunk be. A tioszemikarbazonok, protoflavonok és flavonoidok tesztelésének eredményeként alapvető szerkezet-hatás összefüggéseket figyeltünk meg, melyeket 2 tudományos közleményben publikáltunk, illetve kézirat formájában egy harmadik tanulmány is készülőben van.

8. Bibliography

[1] http://www.who.int/mediacentre/factsheets/fs297/en/

[2] http://eco.iarc.fr/EUCAN/Default.aspx

[3] http://ec.europa.eu/eurostat/

[4] Bonadonna G, Veronesi U, Brambilla C, Ferrari L, Luini A, Greco M, Bartoli C, Coopmans de Yoldi G, Zucali R, Rilke F. (1990) Primary chemotherapy to avoid mastectomy in tumors with diameters of three centimeters or more. J Natl Cancer Inst, 82(19): 1539-1545.

[5] Fisher B, Brown A, Mamounas E, Wieand S, Robidoux A, Margolese RG, Cruz AB Jr, Fisher ER, Wickerham DL, Wolmark N, DeCillis A, Hoehn JL, Lees AW, Dimitrov NV. (1997) Effect of preoperative chemotherapy on local-regional disease in women with operable breast cancer: findings from National Surgical Adjuvant Breast and Bowel Project B-18. J Clin Oncol, 15(7): 2483-2493.

[6] Witjes JA, Compérat E, Cowan NC, De Santis M, Gakis G, Lebret T, Ribal MJ, Van der Heijden AG, Sherif A. (2014) EAU guidelines on muscle-invasive and metastatic bladder cancer: summary of the 2013 guidelines. Eur Urol, 65(4): 778-792.

[7] Balog J, Sasi-Szabó L, Kinross J, Lewis MR, Muirhead LJ, Veselkov K, Mirnezami R, Dezső B, Damjanovich L, Darzi A, Nicholson JK, Takáts Z. (2013) Intraoperative tissue identification using rapid evaporative ionization mass spectrometry. Sci Transl Med, 5(194): 194ra93.

[8] Kuruvilla J, Assouline S, Hodgson D, MacDonald D, Stewart D, Christofides A, Komolova M, Connors J. (2015) A Canadian Evidence-Based Guideline for the First-Line Treatment of Follicular Lymphoma: Joint Consensus of the Lymphoma Canada Scientific Advisory Board. Clinical Lymphoma Myeloma and Leukemia, 15(2): 59-74.

[9] Cao L, Cai G, Xu F, Yang Z, Yu X, Ma J, Zhang Q, Wu J, Guo X, Chen J. (2016) Trastuzumab improves locoregional control in HER2-positive breast cancer patients following adjuvant radiotherapy. Medicine (Baltimore), 95(32): e4230.

[10] Achkar T, Tarhini AA. The use of immunotherapy in the treatment of melanoma. J Hematol Oncol, 10(1): 88.

[11] Bhuva N, Li, SP, Maher J. (2012) Living With and Beyond Cancer: New

Challenges. Topics in cancer survivorship. Editor: Mohan R. Mount Vernon Cancer Centre, Northwood, Middlesex, UK, 1-12.

[12] Pecorino L. (2012) Molecular biology of cancer – mechanisms, targets, and therapeutics. Chapter I – Introduction. Oxford University Press, Oxford, 2-20.

[13] Hanahan D, Weinberg RA. (2000) The hallmarks of cancer. Cell, 100(1): 57-70.

[14] Hanahan D, Weinberg RA. (2011) Hallmarks of cancer: the next generation. Cell, 144(5): 646-674.

[15] Housman G, Byler S, Heerboth S, Lapinska K, Longacre M, Snyder N, Sarkar S. (2014) Drug resistance in cancer: an overview. Cancers (Basel), 6(3): 1769-1792.

[16] Brown R., Curry E., Magnani L.,Wilhelm-Benartzi C.S., Borley J. (2014) Poised epigenetic states and acquired drug resistance in cancer. Nat Rev Cancer, 14(11): 747-753.

[17] Tomlinson IP, Novelli MR, Bodmer WF. (1996) The mutation rate and cancer. Proc Natl Acad Sci USA, 93(25): 14800-14803.

[18] De Sousa E Melo F, Vermeulen L, Fessler E, Medema JP. (2013) Cancer heterogeneity – a multifaceted view. EMBO Rep, 14(8):686-695.

[19] Kandoth C, McLellan MD, Vandin F, Ye K, Niu B, Lu C, Xie M, Zhang Q, McMichael JF, Wyczalkowski MA, Leiserson MDM, Miller CA, Welch JS, Walter MJ, Wendl MC, Ley TJ, Wilson RK, Raphael BJ, Ding L. (2013) Mutational landscape and significance across 12 major cancer types. Nature, 502(7471):333-339.

[20] Adey A, Burton JN, Kitzman JO, Hiatt JB, Lewis AP, Martin BK, Qiu R, Lee C, Shendure J. (2013) The haplotype-resolved genome and epigenome of the aneuploid HeLa cancer cell line. Nature, 500(7461):207-211.

[21] Landry JJ, Pyl PT, Rausch T, Zichner T, Tekkedil MM, Stütz AM, Jauch A, Aiyar RS, Pau G, Delhomme N, Gagneur J, Korbel JO, Huber W, Steinmetz LM. (2013) The genomic and transcriptomic landscape of a HeLa cell line. G3 (Bethesda), 3(8):1213-1224.

[22] Barretina J, Caponigro G, Stransky N, Venkatesan K, Margolin AA, Kim S, Wilson CJ, Lehár J, Kryukov GV, Sonkin D, Reddy A, Liu M, Murray L, Berger MF, Monahan JE, Morais P, Meltzer J, Korejwa A, Jané-Valbuena J, Mapa FA, Thibault J, Bric-Furlong E, Raman P, Shipway A, Engels IH, Cheng J, Yu GK, Yu J, Aspesi

P Jr, de Silva M, Jagtap K, Jones MD, Wang L, Hatton C, Palescandolo E, Gupta S, Mahan S, Sougnez C, Onofrio RC, Liefeld T, MacConaill L, Winckler W, Reich M, Li N, Mesirov JP, Gabriel SB, Getz G, Ardlie K, Chan V, Myer VE, Weber BL, Porter J, Warmuth M, Finan P, Harris JL, Meyerson M, Golub TR, Morrissey MP, Sellers WR, Schlegel R, Garraway LA. (2012) The Cancer Cell Line Encyclopedia enables predictive modelling of anticancer drug sensitivity. Nature, 483(7391): 603-607.

[23] Garnett MJ, Edelman EJ, Heidorn SJ, Greenman CD, Dastur A, Lau KW, Greninger P, Thompson IR, Luo X, Soares J, Liu Q, Iorio F, Surdez D, Chen L, Milano RJ, Bignell GR, Tam AT, Davies H, Stevenson JA, Barthorpe S, Lutz SR, Kogera F, Lawrence K, McLaren-Douglas A, Mitropoulos X, Mironenko T, Thi H, Richardson L, Zhou W, Jewitt F, Zhang T, O'Brien P, Boisvert JL, Price S, Hur W, Yang W, Deng X, Butler A, Choi HG, Chang JW, Baselga J, Stamenkovic I, Engelman JA, Sharma SV, Delattre O, Saez-Rodriguez J, Gray NS, Settleman J, Futreal PA, Haber DA, Stratton MR, Ramaswamy S, McDermott U, Benes CH. (2012) Systematic identification of genomic markers of drug sensitivity in cancer cells. Nature, 483(7391):570-575.

[24] Ehrlich M. (2002) DNA methylation in cancer: too much, but also too little. Oncogene, 21(35):5400-5413.

[25] Baylin SB, Jones PA. (2011) A decade of exploring the cancer epigenome-biological and translational implications. Nat Rev Cancer, 11: 726–734.

[26] Aparicio S, Caldas C. (2013) The implications of clonal genome evolution for cancer medicine. N Engl J Med, 368: 842–851.

[27] Greaves M, Maley CC. (2012) Clonal evolution in cancer. Nature, 481:306–313.

[28] Salonga D, Danenberg KD, Johnson M, Metzger R, Groshen S, Tsao-wei DD, Lenz HJ, Leichman CG, Leichman L, Diasio RB, Danenberg PV. (2000) Colorectal tumors responding to 5-fluorouracil have low gene expression levels of dihydropyrimidine dehydrogenase, thymidylate synthase, and thymidine phosphorylase. Clin Cancer Res, 6:1322-1327.

[29] Shimizu T, Nakagawa Y, Takahashi N, Hashimoto S. (2016) Thymidylate synthase gene amplification predicts pemetrexed resistance in patients with advanced non-small cell lung cancer. Clin Transl Oncol, 18:107-112.

[30] Watson RG, Muhale F, Thorne LB, Yu J, O'Neil BH, Hoskins JM, Meyers MO, Deal AM, Ibrahim JG, Hudson ML, Walko CM, Mcleod HL, Auman JT. (2010) Amplification of thymidylate synthetase in metastatic colorectal cancer patients pretreated with 5-fluorouracil-based chemotherapy. Eur J Cancer, 46:3358-3364.

[31] Wang TL, Diaz LA Jr, Romans K, Bardelli A, Saha S, Galizia G, Choti M, Donehower R, Parmigiani G, Shih Ie M, Lacobuzio-Donahue C, Kinzler KW, Vogelstein B, Lengauer C, Velculescu VE. (2004) Digital karyotyping identifies thymidylate synthase amplification as a mechanism of resistance to 5-fluorouracil in metastatic colorectal cancer patients. Proc Natl Acad Sci USA, 101:3089-3094.

[32] Gorre ME, Sawyers CL. (2002) Molecular mechanisms of resistance to STI571 in chronic myeloid leukemia. Curr Opin Hematol, 9:303-307.

[33] Roche-Lestienne C, Laï JL, Darré S, Facon T, Preudhomme C. (2003) A mutation conferring resistance to imatinib at the time of diagnosis of chronic myelogenous leukemia. N Engl J Med, 348:2265–2266.

[34] Russo M, Siravegna G, Blaszkowsky LS, Corti G, Crisafulli G, Ahronian LG, Mussolin B, Kwak EL, Buscarino M, Lazzari L, Valtorta E, Truini M, Jessop NA, Robinson HE, Hong TS, Mino-Kenudson M, Di Nicolantonio F, Thabet A, Sartore-Bianchi A, Siena S, Iafrate AJ, Bardelli A, Corcoran RB. (2016) Tumor heterogeneity and lesion-specific response to targeted therapy in colorectal cancer. Cancer Discov, 6(2):147–153.

[35] Gottesman MM. (2002) Mechanisms of cancer drug resistance. Annu Rev Med, 53:615-627.

[36] Fojo T. (2007) Multiple paths to a drug resistance phenotype: Mutations, translocations, deletions and amplification of coding genes or promoter regions, epigenetic changes and microRNAs. Drug Resistance Updates, 10:59-67.

[37] Szakács G, Paterson JK, Ludwig JA, Booth-Genthe C, Gottesman MM. (2006) Targeting multidrug resistance in cancer. Nat Rev Drug Discov, 5(3):219-234.

[38] Dano, K. (1973) Active outward transport of daunomycin in resistant Ehrlich ascites tumor cells. Biochim Biophys Acta, 323(3):466-483.

[39] Allikmets R, Schriml LM, Hutchinson A, Romano-Spica V, Dean M. (1998) A human placenta-specific ATP-binding cassette gene (ABCP) on chromosome 4q22 that is involved in multidrug resistance. Cancer Res, 58(23):5337-5339.

[40] Doyle LA, Yang W, Abruzzo LV, Krogmann T, Gao Y, Rishi AK, Ross DD. (1998) A multidrug resistance transporter from human MCF-7 breast cancer cells. Proc. Natl. Acad. Sci. U.S.A, 95(26):15665-15670.

[41] Miyake K, Mickley L, Litman T, Zhan Z, Robey R, Cristensen B, Brangi M, Greenberger L, Dean M, Fojo T, Bates SE. (1999) Molecular cloning of cDNAs which are highly overexpressed in mitoxantrone-resistant cells: demonstration of homology to ABC transport genes. Cancer Res, 59(1):8-13.

[42] Cole SP, Bhardwaj G, Gerlach JH, Mackie JE, Grant CE, Almquist KC, Stewart AJ, Kurz EU, Duncan AM, Deeley RG. (1992) Overexpression of a transporter gene in a multidrug-resistant human lung cancer cell line. Science, 258(5088): 1650-1654.

[43] Rottenberg S, Nygren AO, Pajic M, van Leeuwen FW, van der Heijden I, van de Wetering K, Liu X, de Visser KE, Gilhuijs KG, van Tellingen O, Schouten JP, Jonkers J, Borst P. (2007) Selective induction of chemotherapy resistance of mammary tumors in a conditional mouse model for hereditary breast cancer. Proc Natl Acad Sci USA, 104(29) : 12117-12122.

[44] Rottenberg S, Borst P. (2012) Drug resistance in the mouse cancer clinic. Drug Resist Updat, 15(1-2):81-89.

[45] Goldstein LJ, Galski H, Fojo A, Willingham M, Lai SL, Gazdar A, Pirker R, Green A, Crist W, Brodeur GM. (1989) Expression of a multidrug resistance gene in human cancers. J. Natl. Cancer Inst, 81(2):116-124.

[46] Sarkadi B, Homolya L, Szakács G, Váradi A. (2006) Human Multidrug Resistance ABCB and ABCG Transporters: Participation in a Chemoimmunity Defense System. Physiol Rev, 86(4):1179-1236.

[47] Schinkel AH, Smit JJ, van Tellingen O, Beijnen JH, Wagenaar E, van Deemter L, Mol CA, van der Valk MA, Robanus-Maandag EC, te Riele HP. (1994) Disruption of the mouse *mdr1a* P-glycoprotein gene leads to a deficiency in the blood– brain barrier and to increased sensitivity to drugs. Cell, 77(4):491-502.

[48] Cooray HC, Blackmore CG, Maskell L, Barrand MA. (2002) Localisation of breast cancer resistance protein in microvessel endothelium of human brain. Neuroreport, 13(16):2059-2063.

[49] Eisenblätter T, Galla HJ. (2002) A new multidrug resistance protein at the blood–

brain barrier. Biochem Biophys Res Commun, 293(4):1273-1278.

[50] Szakács G, Váradi A, Özvegy-Laczka C, Sarkadi B. (2008) The role of ABC transporters in drug absorption, distribution, metabolism, excretion and toxicity (ADME–Tox). Drug Discov Today, 13(9-10):379-393.

[51] Chen CJ, Chin JE, Ueda K, Clark DP, Pastan I, Gottesman MM, Roninson IB. (1986) Internal duplication and homology with bacterial transport proteins in the mdr1 (P-glycoprotein) gene from multidrug-resistant human cells. Cell, 47(3):381-389.

[52] Gottesman MM, Pastan I, Ambudkar SV. (1996) P-glycoprotein and multidrug resistance. Curr Opin Genet Dev, 6(5):610-617.

[53] Verhalen B, Dastvan R, Thangapandian S, Peskova Y, Koteiche HA, Nakamoto RK, Tajkhorshid E, Mchaourab HS. (2017) Energy Transduction and Alternating Access of the Mammalian ABC Transporter P-glycoprotein. Nature, 543(7647): 738-741.

[54] Liu M, Hou T, Feng Z, Li Y. (2013) The flexibility of P-glycoprotein for its poly-specific drug binding from molecular dynamics simulations. J Biomol Struct Dyn, 31(6):612-629.

[55] Juliano RL, Ling V. (1976) A surface glycoprotein modulating drug permeability in Chinese hamster ovary cell mutants. Biochim Biophys Acta, 455(1):152-162.

[56] Eckford PD, Sharom FJ. (2009) ABC Efflux Pump-Based Resistance to Chemotherapy Drugs. Chem Rev, 109(7):2989-3011.

[57] Cripe LD, Uno H, Paietta EM, Litzow MR, Ketterling RP, Bennett JM, Rowe JM, Lazarus HM, Luger S, Tallman MS. (2010) Zosuquidar, a novel modulator of P-glycoprotein, does not improve the outcome of older patients with newly diagnosed acute myeloid leukemia: a randomized, placebo-controlled trial of the Eastern Cooperative Oncology Group 3999. Blood, 116(20):4077-4085.

[58] Wu CP, Calcagno AM, Ambudkar SV. (2008) Reversal of ABC drug transporter-mediated multidrug resistance in cancer cells: Evaluation of current strategies. Curr Mol Pharmacol, 1(2):93-105.

[59] Fang L, Zhang G, Li C, Zheng X, Zhu L, Xiao JJ, Szakacs G, Nadas J, Chan KK, Wang PG, Sun D. (2006) Discovery of a Daunorubicin Analogue That Exhibits Potent Antitumor Activity and Overcomes P-gp-Mediated Drug Resistance. J Med

Chem, 49(3):932-941.

[60] Yoshikawa M, Ikegami Y, Hayasaka S, Ishii K, Ito A, Sano K, Suzuki T, Togawa T, Yoshida H, Soda H, Oka M, Kohno S, Sawada S, Ishikawa T, Tanabe S. (2004) Novel camptothecin analogues that circumvent ABCG2-associated drug resistance in human tumor cells. Int J Cancer, 110(6):921-927.

[61] Füredi A, Szebényi K, Tóth S, Cserepes M, Hámori L, Nagy V, Karai E, Vajdovich P, Imre T, Szabó P, Szüts D, Tóvári J, Szakács G. (2017) Pegylated liposomal formulation of doxorubicin overcomes drug resistance in a genetically engineered mouse model of breast cancer. J Control Release, 261:287-296.

[62] Krishna R, Mayer LD. (1997) Liposomal doxorubicin circumvents PSC 833-free drug interactions, resulting in effective therapy of multidrug-resistant solid tumors. Cancer Res, 57(23):5246-5253.

[63] Szybalski W, Bryson V. (1952) Genetic Studies on Microbial Cross Resistance to Toxic Agents. I. Cross Resistance of Escherichia coli to Fifteen Antibiotics. J. Bacteriol, 64:489-499.

[64] Ascher KR, Kocher C. (1954) Enhanced susceptibility of a highly resistant strain of houseflies to ingestion of potassium bromide. Experientia, 10(11):465-467.

[65] Ascher KR. (1960) A review on resistance-induced enhanced susceptibility in insects, with some notes on similar phenomena (especially "collateral sensitivity") in microorganisms. Arzneimittel-Forschung, 10:450-461.

[66] Rank GH, Bech-Hansen NT. (1973) Single nuclear gene inherited cross resistance and collateral sensitivity to 17 inhibitors of mitochondrial function in S. cerevisiae. Mol Gen Genet, 126(2):93-102.

[67] Jeffers TK, Challey JR. (1973) Collateral sensitivity to 4-hydroxyquinolines in Eimeria acervulina strains resistant to meticlorpindol. J Parasitol, 59(4):624-630.

[68] Vaughn KC, Marks MD, Weeks DP. (1987) A Dinitroaniline-Resistant Mutant of *Eleusine indica* Exhibits Cross-Resistance and Supersensitivity to Antimicrotubule Herbicides and Drugs. Plant Physiol, 83(4):956-964.

[69] Law LW. (1951) Resistance in leukemic cells to a guanine analog, 8-azaguanine. Proc Soc Exp Biol Med, 78(2):499-502.

[70] Szakács G, Hall MD, Gottesman MM, Boumendjel A, Kachadourian R, Day BJ, Baubichon-Cortay H, Di Pietro A. (2014) Targeting the Achilles Heel of Multidrug-

Resistant Cancer by Exploiting the Fitness Cost of Resistance. Chem Rev, 114(11): 5753-5774.

[71] Pluchino KM, Hall MD, Goldsborough AS, Callaghan R, Gottesman MM. (2012) Collateral sensitivity as a strategy against cancer multidrug resistance. Drug Resist Updat, 15(1-2):98-105.

[72] Hall MD, Handley MD, Gottesman MM. (2009) Is resistance useless? Multidrug resistance and collateral sensitivity. Trends Pharmacol Sci, 30(10):546-556.

[73] Szakács G, Annereau JP, Lababidi S, Shankavaram U, Arciello A, Bussey KJ, Reinhold W, Guo Y, Kruh GD, Reimers M, Weinstein JN, Gottesman MM. (2004) Predicting drug sensitivity and resistance: profiling ABC transporter genes in cancer cells. Cancer Cell, 6(2):129-137.

[74] Bell SE, Quinn DM, Kellett GL, Warr JR. (1998) 2-Deoxy-D-glucose preferentially kills multidrug-resistant human KB carcinoma cell lines by apoptosis. Br J Cancer, 78(11):1464-1470.

[75] Ireland CM, Aalbersberg W, Andersen RJ, Ayral-Kaloustain S, Berlinck RGS, Bernan V, Carter G, Churchill ACL, Clardy J, Concepcion GP, De Silva ED, Discafani C, Fojo T, Frost P, Gibson D, Greenberger LM, Greenstein M, Harper MK, Mallon R, Loganzo F, Nunes M, Poruchynsky MS, Zask A. (2003) Anticancer agents from unique natural product sources. Pharm. Biol, 41:15–38.

[76] Marks KM, Park ES, Arefolov A, Russo K, Ishihara K, Ring JE, Clardy J, Clarke AS, Pelish HE. (2011) The selectivity of austocystin D arises from cell-line-specific drug activation by cytochrome P450 enzymes. J Nat Prod, 74(4):567-573.

[77] Stow MW, Warr JR. (1991) Amplification and expression of mdr genes and flanking sequences in verapamil hypersensitive hamster cell lines. Biochim Biophys Acta, 1092(1):7-14.

[78] Warr JR, Brewer F, Anderson M, Fergusson J. (1986) Verapamil hypersensitivity of vincristine resistant Chinese hamster ovary cell lines. Cell Biol Int Rep, 10(5):389-399.

[79] Warr JR, Quinn D, Elend M, Fenton JA. (1995) Gain and loss of hypersensitivity to resistance modifiers in multidrug resistant Chinese hamster ovary cells. Cancer Lett, 98(1):115-120.

[80] Laberge RM, Ambadipudi R, Georges E. (2009) P-glycoprotein (ABCB1)

modulates collateral sensitivity of a multidrug resistant cell line to verapamil. Arch Biochem Biophys, 491(1-2):53-60.

[81] Muller C, Bailly JD, Goubin F, Laredo J, Jaffrézou JP, Bordier C, Laurent G. (1994) Verapamil decreases P-glycoprotein expression in multidrug-resistant human leukemic cell lines. Int J Cancer, 56(5):749-754.

[82] Loe DW, Sharom FJ. (1993) Interaction of multidrug-resistant Chinese hamster ovary cells with amphiphiles. Br J Cancer, 68(2):342-351.

[83] Sharom FJ, Yu X, Lu P, Liu R, Chu JW, Szabó K, Müller M, Hose CD, Monks A, Váradi A, Seprődi J, Sarkadi B. (1999) Interaction of the P-glycoprotein multidrug transporter (MDR1) with high affinity peptide chemosensitizers in isolated membranes, reconstituted systems, and intact cells. Biochem Pharmacol, 58(4):571-586.

[84] Nakagawa-Goto K, Bastow KF, Chen TH, Morris-Natschke SL, Lee KH. (2008) Antitumor agents 260. New desmosdumotin B analogues with improved in vitro anticancer activity. J Med Chem, 51(11):3297-3303.

[85] Nakagawa-Goto K, Chang PC, Lai CY, Hung HY, Chen TH, Wu PC, Zhu H, Sedykh A, Bastow KF, Lee KH. (2010) Antitumor agents 280. Multidrug resistance-selective desmosdumotin B analogues. J Med Chem, 53(18):6699-6705.

[86] Kuo TC, Chiang PC, Yu CC, Nakagawa-Goto K, Bastow KF, Lee KH, Guh JH. (2011) A unique P-glycoprotein interacting agent displays anticancer activity against hepatocellular carcinoma through inhibition of GRP78 and mTOR pathways. Biochem Pharmacol, 81(9):1136-1144.

[87] Pauli-Magnus C, Kroetz DL. (2004) Functional implications of genetic polymorphisms in the multidrug resistance gene MDR1 (ABCB1). Pharm Res, 21(6): 904-913.

[88] Kabanov AV, Batrakova EV, Alakhov VY. (2003) An essential relationship between ATP depletion and chemosensitizing activity of Pluronic block copolymers. J Control Release, 91(1-2):75-83.

[89] Sharma AK, Zhang L, Li S, Kelly DL, Alakhov VY, Batrakova EV, Kabanov AV. (2008) Prevention of MDR development in leukemia cells by micelle-forming polymeric surfactant. J Control Release, 131(3):220-227.

[90] Alakhova DY, Rapoport NY, Batrakova EV, Timoshin AA, Li S, Nicholls D,

Alakhov VY, Kabanov AV. (2010) Differential metabolic responses to pluronic in MDR and non-MDR cells: a novel pathway for chemosensitization of drug resistant cancers. J Control Release, 142(1):89-100.

[91] https://dtp.cancer.gov/default.htm

[92] https://dtp.cancer.gov/discovery_development/nci-60/

[93] Heidi Ledford. (2016) US cancer institute to overhaul tumour cell lines. Nature, 530:391.

[94] https://wiki.nci.nih.gov/display/NCIDTPdata/NCI-60+Growth+Inhibition+Data

[95] Reinhold WC, Sunshine M, Liu H, Varma S, Kohn KW, Morris J, Doroshow J, Pommier Y. (2012) CellMiner: A Web-Based Suite of Genomic and Pharmacologic Tools to Explore Transcript and Drug Patterns in the NCI-60 Cell Line Set. Cancer Res, 72(14):3499-3511.

[96] Scherf U, Ross DT, Waltham M, Smith LH, Lee JK, Tanabe L, Kohn KW, Reinhold WC, Myers TG, Andrews DT, Scudiero DA, Eisen MB, Sausville EA, Pommier Y, Botstein D, Brown PO, Weinstein JN. (2000) A gene expression database for the molecular pharmacology of cancer. Nat Genet, 24(3):236-244.

[97] Reiner A, Yekutieli D, Benjamini Y. (2003) Identifying differentially expressed genes using false discovery rate controlling procedures. Bioinformatics, 19(3): 368-375.

[98] Türk D, Hall MD, Chu BF, Ludwig JA, Fales HM, Gottesman MM, Szakács G. (2009) Identification of compounds selectively killing multidrug-resistant cancer cells. Cancer Res, 69(21):8293-8301.

[99] Heffeter P, Pape VFS, Enyedy ÉA, Keppler BK, Szakacs G, Kowol CR. (2018) Anticancer Thiosemicarbazones: Chemical Properties, Interaction with Iron Metabolism, and Resistance Development. Antioxid Redox Signal (E-pub, ahead of print).

[100] Hall MD, Salam NK, Hellawell JL, Fales HM, Kensler CB, Ludwig JA, Szakács G, Hibbs DE, Gottesman MM. (2009) Synthesis, activity, and pharmacophore development for isatin-beta-thiosemicarbazones with selective activity toward multidrug-resistant cells. J Med Chem, 52(10):3191-3204.

[101] Hall MD, Brimacombe KR, Varonka MS, Pluchino KM, Monda JK, Li J, Walsh MJ, Boxer MB, Warren TH, Fales HM, Gottesman MM. (2011) Synthesis and

structure-activity evaluation of isatin-β-thiosemicarbazones with improved selective activity toward multidrug-resistant cells expressing P-glycoprotein. J Med Chem, 54(16): 5878-5889.

[102] Whitnall M, Howard J, Ponka P, Richardson DR. (2006) A class of iron chelators with a wide spectrum of potent antitumor activity that overcomes resistance to chemotherapeutics. Proc Natl Acad Sci USA, 103(40):14901-14906.

[103] Jansson PJ, Yamagishi T, Arvind A, Seebacher N, Gutierrez E, Stacy A, Maleki S, Sharp D, Sahni S, Richardson DR. (2015) Di-2-pyridylketone 4,4-dimethyl-3-thiosemicarbazone (Dp44mT) overcomes multidrug resistance by a novel mechanism involving the hijacking of lysosomal P-glycoprotein (Pgp). J Biol Chem, 290(15):9588-9603.

[104] Heffeter P, Jakupec MA, Körner W, Chiba P, Pirker C, Dornetshuber R, Elbling L, Sutterlüty H, Micksche M, Keppler BK, Berger W. (2007) Multidrug-resistant cancer cells are preferential targets of the new antineoplastic lanthanum compound KP772 (FFC24). Biochem Pharmacol, 73(12):1873-1886.

[105] Michelini E, Cevenini L, Mezzanotte L, Coppa A, Roda A. (2010) Cell-based assays: fuelling drug discovery. Anal Bioanal Chem, 398(1):227-238.

[106] Moore K, Rees S. (2001) Cell-based versus isolated target screening: how lucky do you feel? J Biomol Screen, 6(2):69-74.

[107] Walters WP, Murcko MA. (2002) Prediction of 'drug-likeness'. Adv Drug Deliv Rev, 31;54(3):255-271.

[108] Hughes JP, Rees S, Kalindjian SB, Philpott KL. (2011) Principles of early drug discovery. Br J Pharmacol, 162(6):1239-1249.

[109] Visegrády A. (2011) Kémiai kiindulópont keresése nagy áteresztőképességű szűréssel. A gyógyszerkutatás kémiája. Editor: Keserű GyM. Akadémiai Kiadó, Budapest, 212-232.

[110] Crouch SPM, Slater KJ. (2001) High-throughput cytotoxicity screening: hit and miss. Drug Discovery Today, 6(12):48-53.

[111] Slater K. (2001) Cytotoxicity tests for high-throughput drug discovery. Curr Opin Biotechnol, 12(1):70-74.

[112] Pereira DA, Williams JA. (2007) Origin and evolution of high throughput screening. Br J Pharmacol, 152(1):53-61.

[113] Sivaraman Dandapani S, Rosse G, Southall N, Salvino JM, Thomas CJ. (2012) Selecting, Acquiring, and Using Small Molecule Libraries for High-Throughput Screening. Curr Protoc Chem Biol, 4:177-191.

[114] Swinney DC, Anthony J. (2011) How were new medicines discovered? Nat Rev Drug Discov, 10(7):507-519.

[115] Eder J, Sedrani R, Wiesmann C. (2014) The discovery of first-in-class drugs: origins and evolution. Nat Rev Drug Discov, 13(8):577-587.

[116] Terstappen GC, Schlüpen C, Raggiaschi R, Gaviraghi G. (2007) Target deconvolution strategies in drug discovery. Nat Rev Drug Discov, 6(11):891-903.

[117] Macarron R, Banks MN, Bojanic D, Burns DJ, Cirovic DA, Garyantes T, Green DV, Hertzberg RP, Janzen WP, Paslay JW, Schopfer U, Sittampalam GS. (2011) Impact of high-throughput screening in biomedical research. Nat Rev Drug Discov, 10(3):188-195.

[118] Niles AL, Moravec RA, Riss TL. (2009) In vitro viability and cytotoxicity testing and same-well multi-parametric combinations for high throughput screening. Curr Chem Genomics, 3:33-41.

[119] Sundberg S. (2000) High-throughput and ultra-high-throughput screening: solution- and cell-based approaches. Curr Opin Biotechnol, 11:47-53.

[120] Skehan P, Storeng R, Scudiero D, Monks A, McMahon J, Vistica D, Warren JT, Bokesch H, Kenney S, Boyd MR. (1990) New colorimetric cytotoxicity assay for anticancer-drug screening. J Natl Cancer Inst, 82(13):1107-1112.

[121] Mosmann T. (1983) Rapid colorimetric assay for cellular growth and survival: application to proliferation and cytotoxicity assays. J Immunol Methods, 65(1-2): 55-63.

[122] https://dtp.cancer.gov/discovery_development/nci-60/methodology.htm

[123] Goodwin CJ, Holt SJ, Downes S, Marshall NJ. (1995) Microculture tetrazolium assays: a comparison between two new tetrazolium salts, XTT and MTS. J Immunol Methods, 179(1):95-103.

[124] Ahmed SA, Gogal RM Jr, Walsh JE. (1994) A new rapid and simple non-radioactive assay to monitor and determine the proliferation of lymphocytes: an alternative to [3H]thymidine incorporation assay. J Immunol Methods, 170(2): 211-224.

[125] Crouch SP, Kozlowski R, Slater KJ, Fletcher J. (1993) The use of ATP bioluminescence as a measure of cell proliferation and cytotoxicity. J Immunol Methods, 160(1):81-88.

[126] Zumpe C, Bachmann CL, Metzger AU, Wiedemann N. (2010) Comparison of potency assays using different read-out systems and their suitability for quality control. J Immunol Methods, 360(1-2):129-140.

[127] Squarito RC, Connor JP, Buller RE. (1995) Comparison of a novel redox dye cell growth assay to the ATP bioluminescence assay. Gynecol Oncol, 58(1):101-105.

[128] Steff AM, Fortin M, Arguin C, Hugo P. (2001) Detection of a decrease in green fluorescent protein fluorescence for the monitoring of cell death: an assay amenable to high-throughput screening technologies. Cytometry, 45(4):237-243.

[129] Torrance CJ, Agrawal V, Vogelstein B, Kinzler KW. (2001) Use of isogenic human cancer cells for high-throughput screening and drug discovery. Nat Biotechnol, 19(10):940-945.

[130] Rosado A, Zanella F, Garcia B, Carnero A, Link W. (2008) A dual-color fluorescence-based platform to identify selective inhibitors of Akt signaling. PLoS One, 3(3): e1823.

[131] Rao TD, Rosales N, Spriggs DR. (2011) Dual-fluorescence isogenic high-content screening for MUC16/CA125 selective agents. Mol Cancer Ther, 10(10):1939-1948.

[132] Brimacombe KR, Hall MD, Auld DS, Inglese J, Austin CP, Gottesman MM, Fung KL. (2009) A dual-fluorescence high-throughput cell line system for probing multidrug resistance. Assay Drug Dev Technol, 7(3):233-249.

[133] Kenny HA, Lal-Nag M, White EA, Shen M, Chiang CY, Mitra AK, Zhang Y, Curtis M, Schryver EM, Bettis S, Jadhav A, Boxer MB, Li Z, Ferrer M, Lengyel E. (2015) Quantitative high throughput screening using a primary human three-dimensional organotypic culture predicts in vivo efficacy. Nat Commun, 6:6220.

[134] Zhang JH, Chung TD, Oldenburg KR. (1999) A Simple Statistical Parameter for Use in Evaluation and Validation of High Throughput Screening Assays. J Biomol Screen, 4(2):67-73.

[135] Sui Y, Wu Z. (2007) Alternative statistical parameter for high-throughput screening assay quality assessment. J Biomol Screen, 12(2):229-234.

[136] Zhang JH, Wu X, Sills MA. (2005) Probing the Primary Screening Efficiency by Multiple Replicate Testing: A Quantitative Analysis of Hit Confirmation and False Screening Results of a Biochemical Assay, 10(7):695-704.

[137] Malo N, Hanley JA, Cerquozzi S, Pelletier J, Nadon R. (2006) Statistical practice in high-throughput screening data analysis. Nat Biotechnol, 24(2):167-175.

[138] Zhang Z, Guan N, Li T, Mais DE, Wang M. (2012) Quality control of cell-based high-throughput drug screening. Acta Pharmaceutica Sinica B, 2(5):429-438.

[139] Hart FA, Laming FP. (1964) Complexes of 1,10-phenanthroline with lanthanide chlorides and thiocyanates. J Inorg Nucl Chem, 26:579–585.

[140] https://pubchem.ncbi.nlm.nih.gov/assay/assay.cgi?p=clustering

[141] Elkind NB, Szentpétery Z, Apáti A, Laczka C, Várady G, Ujhelly O, Szabó K, Homolya L, Váradi A, Buday L, Kéri G, Német K, Sarkadi B. (2005) Multidrug transporter ABCG2 prevents tumor cell death induced by the epidermal growth factor receptor inhibitor Iressa (ZD1839, Gefitinib). Cancer Res, 65(5):1770-1777.

[142] Nerada Z, Hegyi Z, Szepesi Á, Tóth S, Hegedüs C, Várady G, Matula Z, Homolya L, Sarkadi B, Telbisz Á. (2016) Application of fluorescent dye substrates for functional characterization of ABC multidrug transporters at a single cell level. Cytometry A, 89(9):826-834.

[143] Pape VFS, Türk D, Szabó P, Wiese M, Enyedy EA, Szakács G. (2015) Synthesis and characterization of the anticancer and metal binding properties of novel pyrimidinylhydrazone derivatives. J Inorg Biochem, 144:18-30.

[144] Holló Z, Homolya L, Davis CW, Sarkadi B. (1994) Calcein accumulation as a fluorometric functional assay of the multidrug transporter. Biochim Biophys Acta, 1191(2): 384-388.

[145] Shaner NC, Campbell RE, Steinbach PA, Giepmans BN, Palmer AE, Tsien RY. (2004) Improved monomeric red, orange and yellow fluorescent proteins derived from Discosoma sp. red fluorescent protein. Nat Biotechnol, 22(12):1567-1572.

[146] Shaner NC, Lin MZ, McKeown MR, Steinbach PA, Hazelwood KL, Davidson MW, Tsien RY. (2008) Improving the photostability of bright monomeric orange and red fluorescent proteins. Nat Methods, 5(6):545-551.

[147] Yang TT, Cheng L, Kain SR. (1996) Optimized codon usage and chromophore mutations provide enhanced sensitivity with the green fluorescent protein. Nucleic

Acids Res, 24(22):4592-4593.

[148] Wesolowska O, Paprocka M, Kozlak J, Motohashi N, Dus D, Michalak K. (2005) Human sarcoma cell lines MES-SA and MES-SA/Dx5 as a model for multidrug resistance modulators screening. Anticancer Res, 25(1A):383-389.

[149] Yamagishi T, Sahni S, Sharp DM, Arvind A, Jansson PJ, Richardson DR. (2013) P-glycoprotein mediates drug resistance via a novel mechanism involving lysosomal sequestration. J Biol Chem, 288:31761–31771.

[150] Paterson JK, Gottesman MM. (2007) P-glycoprotein is not present in mitochondrial membranes. Exp Cell Res, 313:3100–3105.

[151] Füredi A, Tóth S, Szebényi K, Pape VF, Türk D, Kucsma N, Cervenak L, Tóvári J, Szakács G. (2017) Identification and Validation of Compounds Selectively Killing Resistant Cancer: Delineating Cell Line–Specific Effects from P-Glycoprotein–Induced Toxicity. Mol Cancer Ther, 16(1):45-56.

[152] Ludwig JA, Szakács G, Martin SE, Chu BF, Cardarelli C, Sauna ZE, Caplen NJ, Fales HM, Ambudkar SV, Weinstein JN, Gottesman MM. (2006) Selective toxicity of NSC73306 in MDR1-positive cells as a new strategy to circumvent multidrug resistance in cancer. Cancer Res, 66(9):4808-4815.

[153] Pape VF, Tóth S, Füredi A, Szebényi K, Lovrics A, Szabó P, Wiese M, Szakács G. (2016) Design, synthesis and biological evaluation of thiosemicarbazones, hydrazinobenzothiazoles and arylhydrazones as anticancer agents with a potential to overcome multidrug resistance. Eur J Med Chem, 117:335-354.

[154] Baell JB, Holloway GA. (2010) New substructure filters for removal of pan assay interference compounds (PAINS) from screening libraries and for their exclusion in bioassays. J Med Chem, 53(7):2719-2740.

[155] Baell J, Walters MA. (2014) Chemistry: Chemical con artists foil drug discovery. Nature, 513(7519):481-483.

[156] Batra P, Sharma AK. (2013) Anti-cancer potential of flavonoids: recent trends and future perspectives. 3 Biotech, 3(6):439-459.

[157] Lin AS, Chang FR, Wu CC, Liaw CC, Wu YC. (2005) New Cytotoxic Flavonoids from Thelypteris torresiana. Planta Med, 71: 867-870.

[158] Stanković T, Dankó B, Martins A, Dragoj M, Stojković S, Isaković A, Wang HC, Wu YC, Hunyadi A, Pešić M. (2015) Lower antioxidative capacity of multidrug-

resistant cancer cells confers collateral sensitivity to protoflavone derivatives. Cancer Chemother Pharmacol, 76(3):555-565.

[159] Dankó B, Martins A, Chuang DW, Wang HC, Amaral L, Molnár J, Chang FR, Wu YC, Hunyadi A. (2012) In vitro cytotoxic activity of novel protoflavone analogs - selectivity towards a multidrug resistant cancer cell line. Anticancer Res, 32(7): 2863-2869.

[160] Wang HC, Lee AY, Chou WC, Wu CC, Tseng CN, Liu KY, Lin WL, Chang FR, Chuang DW, Hunyadi A, Wu YC. (2012) Inhibition of ATR-dependent signaling by protoapigenone and its derivative sensitizes cancer cells to interstrand cross-link-generating agents in vitro and in vivo. Mol Cancer Ther, 11(7):1443–1453.

[161] Rickardson L, Fryknäs M, Haglund C, Lövborg H, Nygren P, Gustafsson MG, Isaksson A, Larsson R. (2006) Screening of an annotated compound library for drug activity in a resistant myeloma cell line. Cancer Chemother Pharmacol, 58(6): 749-758.

[162] Kelland LR. (2004) Of mice and men: values and liabilities of the athymic nude mouse model in anticancer drug development. Eur J Cancer, 40(6):827-836.

[163] Kerbel RS. (2003) Human tumor xenografts as predictive preclinical models for anticancer drug activity in humans: better than commonly perceived-but they can be improved. Cancer Biol Ther, 2(4 Suppl 1):S134-139.

[164] Heffeter P, Jakupec MA, Körner W, Wild S, von Keyserlingk NG, Elbling L, Zorbas H, Korynevska A, Knasmüller S, Sutterlüty H, Micksche M, Keppler BK, Berger W. (2006) Anticancer activity of the lanthanum compound [tris(1,10-phenanthroline) lanthanum(III)] trithiocyanate (KP772; FFC24) Biochem Pharmacol, 71:426–440.

[165] Antholine W, Knight J, Whelan H, Petering DH. (1997) Studies of the reaction of 2-formylpyridine thiosemicarbazone and its iron and copper complexes with biological systems. Mol Pharmacol, 13:89–98.

[166] Hall IH, Lackey CB, Kistler TD, Durham RW Jr, Jouad EM, Khan M, Thanh XD, Djebbar-Sid S, Benali-Baitich O, Bouet GM. (2000) Cytotoxicity of copper and cobalt complexes of furfural semicarbazone and thiosemicarbazone derivatives in murine and human tumor cell lines. Pharmazie, 55(12):937–941.

[167] Prachayasittikul V, Prachayasittikul S, Ruchirawat S, Prachayasittikul V. (2013) 8-

Hydroxyquinolines: a review of their metal chelating properties and medicinal applications. Drug Des Devel Ther, 7:1157-1178.

[168] J. Sheikh, H. Junieja, V. Ingle, T.B. Hadda. (2013) Synthesis and in vitro biology of Co(II), Ni(II), Cu(II) and Zinc(II) complexes of functionalized beta-diketone bearing energy buried potential antibacterial and antiviral O,O pharmacophore sites. J. Saudi Chem. Soc, 17:269.

[169] Dankó B, Tóth S, Martins A, Vágvölgyi M, Kúsz N, Molnár J, Chang FR, Wu YC, Szakács G, Hunyadi A. (2017) Synthesis and SAR Study of Anticancer Protoflavone Derivatives: Investigation of Cytotoxicity and Interaction with ABCB1 and ABCG2 Multidrug Efflux Transporters. ChemMedChem, 12(11): 850-859.

9. Publication list

9.1. Publications related to the thesis

Füredi A, **Tóth S**, Szebényi K, Pape VF, Türk D, Kucsma N, Cervenak L, Tóvári J, Szakács G. (2017) Identification and Validation of Compounds Selectively Killing Resistant Cancer: Delineating Cell Line–Specific Effects from P-Glycoprotein–Induced Toxicity. Mol Cancer Ther, 16(1):45-56.

Dankó B, **Tóth S**, Martins A, Vágvölgyi M, Kúsz N, Molnár J, Chang FR, Wu YC, Szakács G, Hunyadi A. (2017) Synthesis and SAR Study of Anticancer Protoflavone Derivatives: Investigation of Cytotoxicity and Interaction with ABCB1 and ABCG2 Multidrug Efflux Transporters. ChemMedChem, 12(11):850-859.

Pape VF, **Tóth S**, Füredi A, Szebényi K, Lovrics A, Szabó P, Wiese M, Szakács G. (2016) Design, synthesis and biological evaluation of thiosemicarbazones, hydrazinobenzothiazoles and arylhydrazones as anticancer agents with a potential to overcome multidrug resistance. Eur J Med Chem, 117:335-354.

Dormán G, Ferenczi-Palkó R, Pape VF, **Tóth S**, Füredi A, Türk D, Soós T, Szakács G. MDR-reversing 8-hydroxy-quinoline derivatives. International patent application; application no.: pct-hu2017-050009.

Tóth S, Szepesi Á, Sarkadi B, Német K, Di Pietro A, Szakács G, Boumendjel A. Aurones inducing collateral sensitivity against multidrug resistant cells overexpressing P-glycoprotein. (In preparation).

9.2. Further publications not related to the thesis

Enyedi KN, **Tóth S**, Szakács G, Mező G. (2017) NGR-peptide-drug conjugates with dual targeting properties. PLoS One, 12(6):e0178632.

Nerada Z, Hegyi Z, Szepesi Á, **Tóth S**, Hegedüs C, Várady G, Matula Z, Homolya L, Sarkadi B, Telbisz Á. (2016) Application of fluorescent dye substrates for functional characterization of ABC multidrug transporters at a single cell level. Cytometry A, 89(9):826-834.

Füredi A, **Tóth S**, Hámori L, Nagy V, Tóvári J, Szakács G. (2015) Relevance of animal models in the development of compounds targeting multidrug resistant cancer. Hungarian Oncology, 59:338-345.

Füredi A, Szebényi K, **Tóth S**, Cserepes M, Hámori L, Nagy V, Karai E, Vajdovich P, Imre T, Szabó P, Szüts D, Tóvári J, Szakács G. (2017) Pegylated liposomal formulation of doxorubicin overcomes drug resistance in a genetically engineered mouse model of breast cancer. J Control Release, 261:287-296.

Tripodi AAP, Enyedi KN, Schlosser G, **Tóth S**, Szakács G, Mező G. (2018) Development of novel cyclic NGR peptide–daunomycin conjugates with dual targeting property. Beilstein J Org Chem, 14:911-918.

Temesszentandrási-Ambrus C, **Tóth S**, Verma R, Bánhegyi P, Szabadkai I, Baska F, Szántai-Kis C, Hartkoorn RC, Lingerfelt MA, Sarkadi B, Szakács G, Őrfi L, Nagaraja V, Ekins S, Telbisz Á. (2018) Characterization of new, efficient Mycobacterium tuberculosis topoisomerase-I inhibitors and their interaction with human ABC multidrug transporters. PLoS One, 13(9):e0202749.

10. Acknowledgements

I am highly grateful to Dr. Gergely Szakács, my boss and supervisor, for his continous support over my masters and PhD years, which I spent in his research group. I feel, I really learned from him the ‘ins and outs’ of the scientific work.

Special thanks to Dr. András Füredi, the pioneer PhD student in the lab, who is always available for a fruitful discussion about any topic including our research, life, or even about the science of space programs.

I am thankful to Kriszta Mohos to manage the everyday life of the lab, thus keeping us away from boring formalities, and that she encouraged me when I was moderately enthusiastic about work. I am grately thankful to Nóra Kucsma, who showed me most of the lab techniquies I used with endless patient. I am also grateful to Dr. Dóra Türk and Dóra Szegő, who helped me in planning experiments, to Dr. Veronika F.S. Pape, who helped me to improve my chemistry knowledge, and who baked very delicious cakes from time to time. I am thankful for my ‘students’ Eszter Kanta, Tímea Windt and Gergő Barta, teaching was a good way also to learn. The laboratory would have collapsed several times without the help of our assistants Rozália Soós, Elvira Komlós, and especially Ibolya Kurkó, whom I worked with over the PhD years.

My kind appreciation is expressed to Dr. Marianna Kovács and Dr. György Dormán, who were my mentors in the establishment of the HTS amenable system.

I wish to express many appreciation also to my many collegues in the Institute of Enzymology, whom I met and worked with during my thesis years, especially to the people in the ‘FACS lab’ and ‘virus lab’.

I am extremely thankful to my family and friends, who stood beside me, and supported me in many ways to facilitate to accomplish the present thesis.

Supplementary Information

Appendix 1. Mortality rate of all cancer per 100 thousand inhabitants in 2013.

Country	Mortality rate	Country	Mortality rate
Hungary	352	Germany	256
Croatia	334	Norway	253
Slovakia	327	Italy	251
Slovenia	315	Greece	250
Denmark	302	Austria	250
Latvia	301	Liechtenstein	248
Serbia	298	Bulgaria	246
Poland	292	Luxembourg	244
Estonia	291	Portugal	243
Czech Republic	290	Spain	239
Ireland	286	Sweden	237
Netherlands	284	Malta	230
United Kingdom	280	Switzerland	224
Lithuania	273	Finland	223
Romania	270	Cyprus	202
Belgium	260	Turkey	186

Appendix 2. Example plate maps for testing cytotoxicity on 384 well plates.

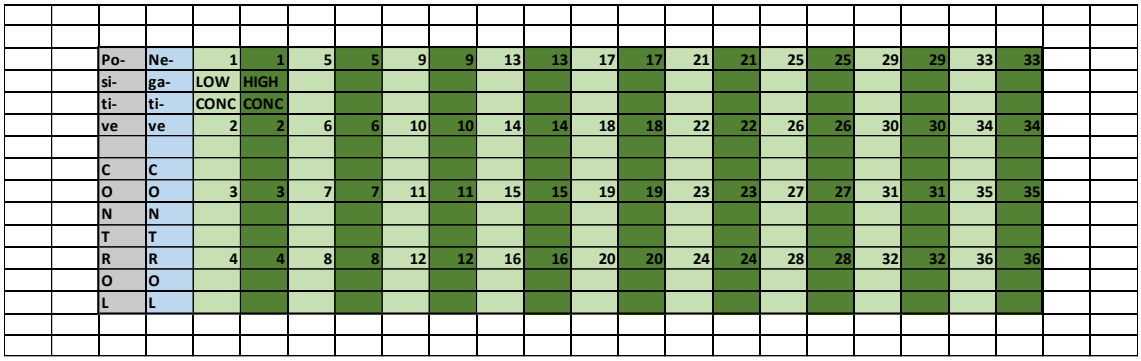

Locations of the 36 molecules on the 384 well plate during primary screening. Cells were seeded prior to drug pipetting. Light green: 10 μM, dark green: 100 μM concentrations of the tested drugs; grey: positive control (0% viability), blue: negative control (100% viability).

	Po-	1	1	1	1	1	1	1	1	1	Ne-	5	5	5	5	5	5	5	5	5	Ne-		
	si-										ga-										ga-		
	ti-										ti-										ti-		
	ve	2	2	2	2	2	2	2	2	2	ve	6									ve		
	C										C										C		
	O	3									O	7									O		
	N										N										N		
	T										T										T		
	R	4									R	8									R		
	O										O										O		
	L										L										L		

Locations of the 9 dilution points of the 8 compounds on the 384 well plate in a secondary screening plate map. Cells were seeded prior to drug pipetting. Compounds 1-4 and 5-8 were normalized to the adjacent negative controls (3 parallels each). Darker green refers to higher test compound concentrations (marked only for compound 1); grey: positive control, blue: negative control.

Appendix 3. Automatic data evaluation vs. evaluation of individual measurement by the GraphPad Prism software.

Comparison of the pGI_{50} values that were obtained by both techniques, we subtracted the one calculated automatically by our custom program from the other that was determined via Prism. The differences were in general low, especially for Dx5 cell line. The observed differences can partly emerge from the elimination of outlier data points, which is a built-in function in the Prism software, and was used during data evaluation, and partly due to 'problematic' dose-response data, where the sigmoidal shape was defective.

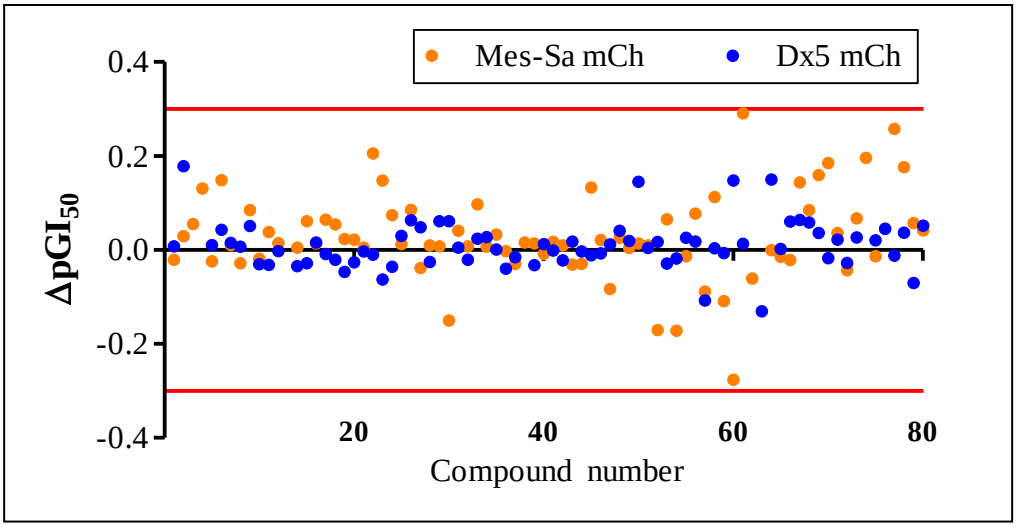

The differences of pGI_{50} values of 80 compounds calculated by subtracting the automatically evaluated data from manual pGI_{50} determination with the GraphPad Prism

software. The cytotoxicity was obtained from a confirmatory screening with 144 h incubation time against Mes-Sa mCherry (orange) and Dx5 mCherry (blue) cell lines. The red lines refer to 2-fold difference in GI_{50} (which is approx. ± 0.3 in pGI_{50}).

Appendix 4. Identification of fluorescent compounds by measuring the plates set for cytotoxicity right after compound addition, in order to decrease false negative hits.

A)

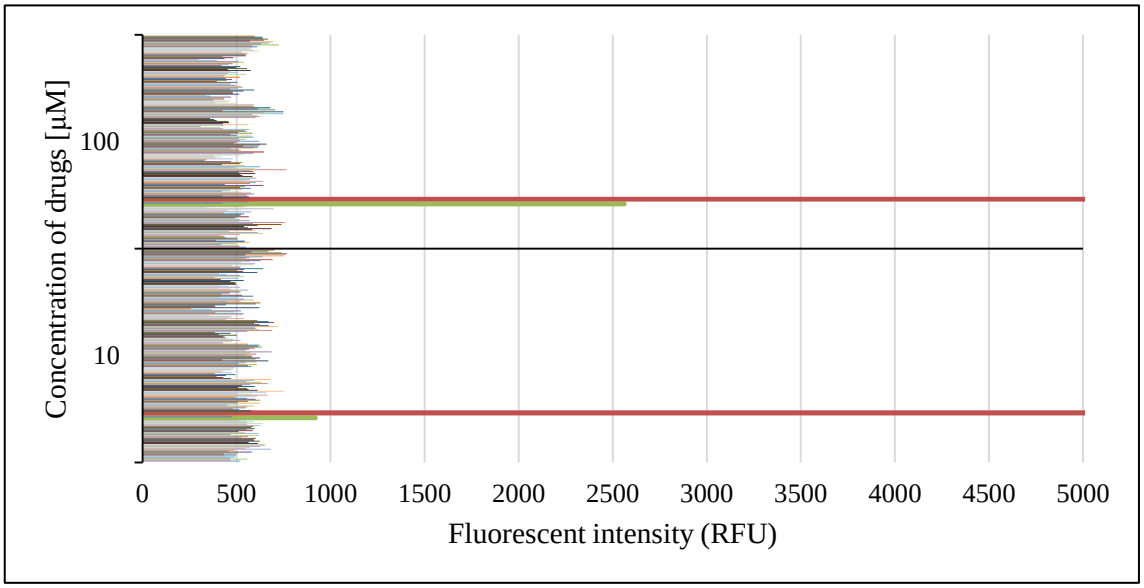

B)

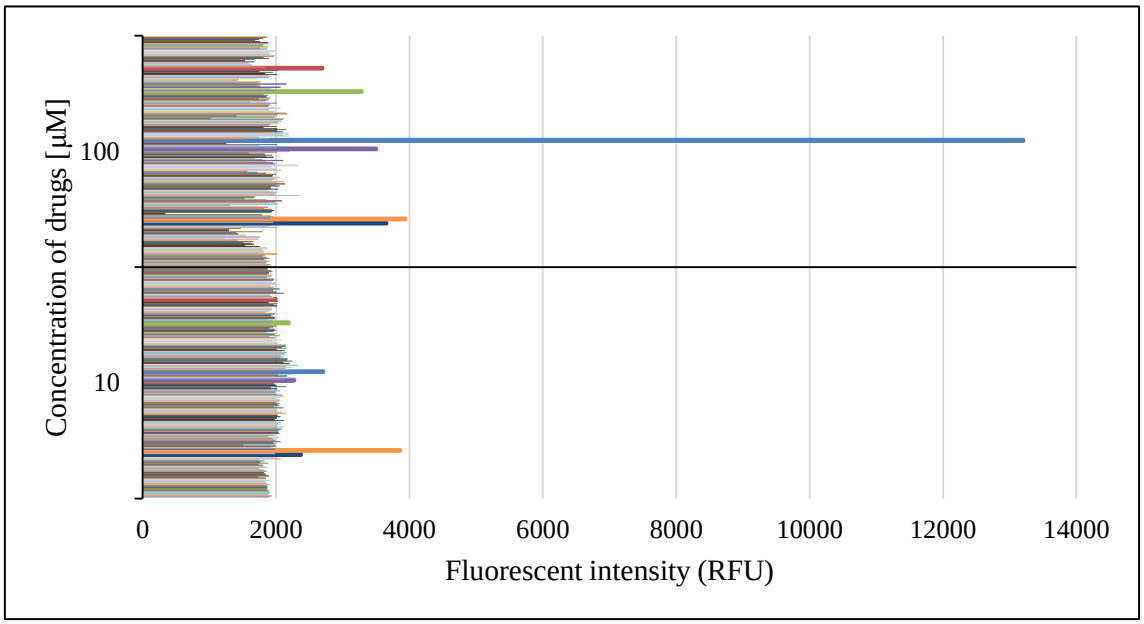

Fluorescent intensity of the wells, measured right after compounds were added to the cells (0 h measurement). The volume of the culture medium and the amount of the cells were equal in every well, thus outlying fluorescent intensities can be addressed only to

compounds, which are fluorescent by nature. 0 h measurements shown in panel A were acquired in the mCherry channel, while panel B shows compound fluorescence in the eGFP channel to have a broader overlook, and to utilize the results, when experiments with eGFP expressing cell lines are planned. On panel A, the upper limit of the fluorescent intensity on the X-axis was set to 5000, to visualize the lower RFU values, although the intensity of the most fluorescent compound was above 80 000 units.

Appendix 5. Automated seeding is not harmful to the cell lines.

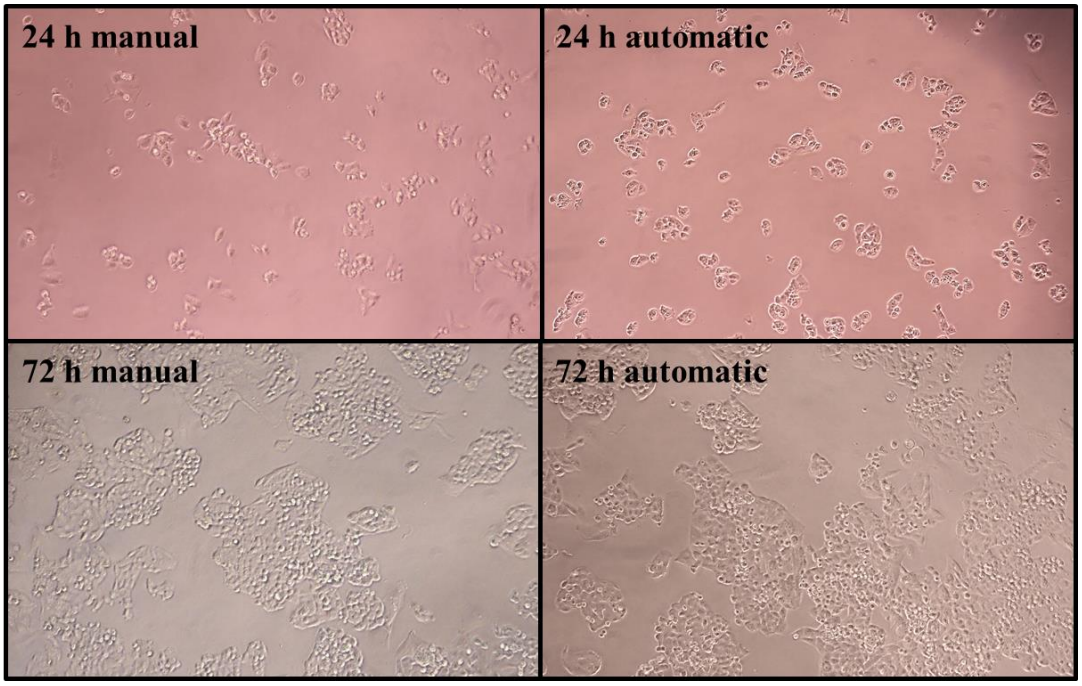

Mes-Sa cells were attached to the bottom of the well 24 h post seeding, and no floating cells were observed. The confluency of the wells were identical after 72 h incubation.

Appendix 6. Pearson's coefficients for the in silico hits.

Compound	Pearson's coeff.	Compound	Pearson's coeff.
NSC1014	0.433	NSC608465	0.441
NSC13977	0.481	NSC609800	0.401
NSC15372	0.421	NSC627452	0.405
NSC17551	0.481	NSC672035	0.409
NSC48892	0.500	NSC676735	0.452
NSC57969	0.684	NSC726708	0.405
NSC67090	0.416	NSC733435	0.407
NSC72881	0.407	NSC740469	0.507
NSC79544	0.717	NSC748494	0.538
NSC297366	0.461		